ELECTRIC FIELD INDUCED SPECTRA OF H_2 AND D_2

WILLIAM JOSEPH BOYD III

UNIVERSITY OF TENNESSEE
MOLECULAR SPECTROSCOPY
LABORATORY

1974

THE UNIVERSITY OF TENNESSEE
Knoxville, Tennessee

ELECTRIC FIELD INDUCED SPECTRA OF H_2 AND D_2

A Dissertation

Presented to

the Graduate Council of

The University of Tennessee

In Partial Fulfillment

of the Requirements for the Degree

Doctor of Philosophy

---

by

William Joseph Boyd, III

June 1974

ACKNOWLEDGMENTS

The author wishes to acknowledge the assistance of the members of his committee in the formulation and execution of the problem presented. Thanks is extended to the staff of the University of Tennessee Molecular Spectroscopy Laboratory and in particular to Gerald McElyea and Tom Moore for their able assistance. The excellent work and suggestions of the staff of the Physics Department Instrument Shop and in particular Mr. Ray Mink were appreciated.

The author wishes to thank Mr. Donald E. Jennings for help with the spectrometer and many useful theoretical discussions, and also Mr. George W. Halsey for considerable help with the Fortran programming used in the data analysis. The financial support of NASA grant NGL 43-001-006 was appreciated.

A special acknowledgment is extended to the author's parents and especially to his wife Jeanne for their concern and encouragement through the progress of this work.

ABSTRACT

The electric field induced absorption lines of H_2 and D_2 have been studied. The frequencies of four Q-branch lines of H_2 and five Q-branch lines of D_2 have been measured as a function of density, and their shifts were observed to be in the linear region. The individual slopes and extrapolated zero density frequency of each line is determined. The frequencies of the lines were determined to be independent of the electric field intensity within experimental error. The polarizability of H_2 has been measured using the integrated intensity of the $Q_1(0)$ and $S_1(1)$, H_2 absorption line.

A highly automated technique for determining the response function of the spectrometer using digitally recorded data is presented. The same techniques are used for manipulating data which is to be deconvoluted and converted to absorption coefficient curves. For the $Q_1(0)$ and $Q_1(1)$ lines of H_2 the halfwidths were measured as a function of electric field intensity at constant pressure. The half widths were observed not to be a function of the field intensity within experimental error. The half widths of these same lines were measured at several densities and compared to previously measured widths.

Technical and operational details of several pieces of equipment built for this experiment, and equipment built for the five-meter Littrow spectrometer used for the experiment, are described. These include the Stark cell, a high voltage power supply, two carbon rod furnaces and their power supplies, one of which has been automated. Also included

are a high pressure gas filling system, the Stark cell fore optics and flushing cover. For the spectrometer, a detector pumping system, light chopper, remotely operated beam switching mirror and detector switching mirror have been built. The modifications of the spectrometer optics to accept the Stark cell are discussed.

An attempt to study the electric field induced spectra of N_2 was made. The unresolved Q-branch was observed but was too weak for any quanitative measurements. An unsuccessful attempt to form HD through a catalitic reaction of H_2 and D_2 is discussed.

TABLE OF CONTENTS

LIST OF TABLES

TABLES PAGE

LIST OF FIGURES

FIGURE PAGE

FIGURE PAGE

CHAPTER I

INTRODUCTION

Diatomic molecules such as H_2, D_2 and N_2 provide good subjects for study since their simplicity provides an excellent proving ground for molecular models and theories. Unfortunately such homonuclear diatomic molecules are normally infrared inactive due to their symmetry which places the center of positive and negative charge at the same position. By means of an externally applied electric field it is possible to distort the symmetry of these molecules slightly, not enough to perturb the energy levels of the molecule to any observable degree, but enough to induce a slight separation of positive and negative charge and therefore a small dipole moment through which transitions can occur. This technique works also with molecules with extremely small electric dipoles such as HD for which the electric dipole spectrum is practically unobservable.

In electric field induced work the sample gas is introduced into a high pressure cell containing a pair of condenser plates with a high potential between them and with highly reflective surfaces. Light is transmitted through the gas between the plates by multiple reflections from the condenser surfaces. The sample gas is used at high pressures both to increase the number of absorbers in the path

and also to increase the electric field which can be maintained between the plates without electrical breakdown.

This work contains the theory of electric field induced spectra as applied to diatomic molecules. In Section 2.1 the energy levels for the diatomic molecule is an electric field are rederived. The selection rules for electric field induced spectra are rederived in Section 2.2. They are $\Delta V = 0,1,2---$ and $\Delta J = 0,\pm 2$ for the vibrational and rotational quantum numbers respectively. The rotational selection rules are different from those found ordinarily in electric dipole transitions for diatomic molecules, and are identical to Raman selection rules. This difference arises from the fact that an external electric field applied in a certain direction induces a double angular dependence in the dipole moment integrals calculated for the electric dipole. This is the same angular dependence found in the dipole moment integrals calculated for the Raman effect and of course leads to the same selection rules. The selection rules are derived as one of the steps used in the determination of the strength factors which are also calculated in Section 2.2. Section 2.4 calculates the Boltzmann weighting factors which are necessary to the determination of the integrated intensity. The expression for the integrated intensity contains the nonzero polarizability matrix elements through the strength factors so the integrated absorption is used to calculate the polarizability of the H_2 molecule as discussed in Section 4.6. The intensity of a line is also dependent on the orientation of the polarization vector of the incident radiation with respect to the direction of the electric

through the calculated strength factors, so that a polarizer must be used to eliminate one of the polarization directions when intensity measurements are being made.

Since the gas is used at high pressures a shift in the line positions is introduced. For this reason the absorption line positions should be measured at several pressures whenever possible in order to extrapolate their positions back to zero pressure. This was done for the Q-branch lines of both D_2 and H_2 as discussed in Section 4.3 and 4.4. A linear extrapolation was sufficiently accurate for the pressure range used in this experiment.

The absorption lines are broadened by the high pressures used. For light molecules such as H_2 and D_2 this broadening is not as great as for heavier molecules such as N_2. Section 4.7 and subsequent sections discuss the experimental procedure for the measurement of line widths including the determination of the response function of the spectrometer and the deconvolution process for removing the influence of the spectrometer on the spectral line profile.

The dipole moment induced in the molecule is proportional to the applied electric field intensity. Since the intensity of a line is proportional to the square of the dipole moment, the line intensity is proportional to the electric field intensity squared. High electric fields are therefore important and for intensity work, the field must be measured as accurately as possible. Chapter III contains a thorough description of the Stark cell and all associated equipment used in the experiment.

CHAPTER II

THEORY OF ELECTRIC FIELD INDUCED SPECTRA

2.1 Energy Levels of Diatomic Molecules in an Electric Field

The energy levels of diatomic molecules are to a first approximation, the sum of the vibrational and rotational energies of the molecule. Transitions which take place between quantized energy levels are characterized by a change in the vibrational quantum number v and the rotational quantum number J. The spectral absorption lines resulting from these transitions consist of a series of rotational lines for each vibrational transition. It is found that the rotational energy depends on the vibrational state so according to Dunham (1), the molecular energy T can be expressed as

$$T(v,J) = G(v) + F_v(J) \ .$$

where G is the vibrational energy and F the rotational energy. In order to obtain the energy levels, it is first necessary to derive the wave equation for the vibrating-rotating molecule. If we use the Born-Oppenheimer approximation we can separate the energies of the electrons from the energies of the nuclei. In the following only the nuclei are considered.

If we place a diatomic molecule in a coordinate system fixed at the center of mass of the molecule whose component nuclei are m_1 and m_2, as shown in the following figure, then the kinetic energy is given quite simply by equation (1).

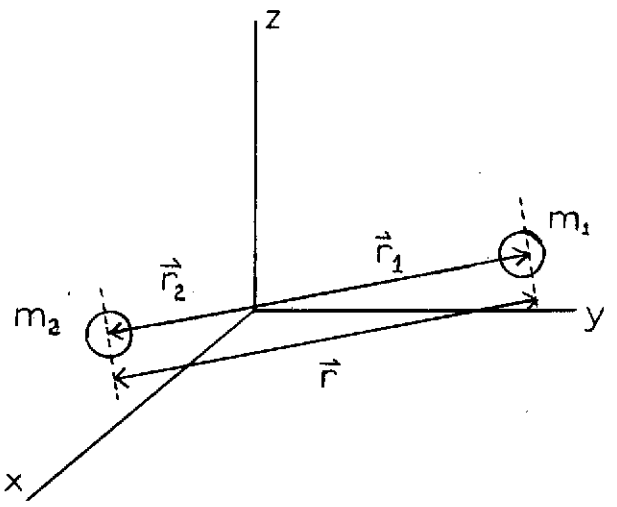

$$2T = m_1\dot{\vec{r}}_1^2 + m_2\dot{\vec{r}}_2^2 \ . \qquad (1)$$

The center of mass condition and the definition of the vector $\vec{r}$ can be used to derive a one body problem from the given two body problem. They are

$$m_1\vec{r}_1 + m_2\vec{r}_2 = 0 \text{ and}$$

$$\vec{r}_1 - \vec{r}_2 = \vec{r} \ .$$

From the equations above we can show that

$$\vec{r}_1 = \left(\frac{m_2}{m_1+m_2}\right)\vec{r} \text{ and}$$

$$\vec{r}_2 = \left(\frac{-m_1}{m_1+m_2}\right)\vec{r}.$$

If we now substitute these equations into equation (1), the following one body problem results.

$$2T = \left(\frac{m_1 m_2}{m_1+m_2}\right) \dot{r}^2 .$$

If we define the reduced mass μ as

$$\mu = \frac{m_1 m_2}{m_1+m_2} ,$$

then

$$T = \frac{1}{2} \mu \dot{r}^2 = \frac{p^2}{2\mu} .$$

The Hamiltonian for the system is then

$$H = \frac{p^2}{2\mu} + V(r) ,$$

where $V(r)$ is the potential in which the nuclei move. Therefore Schroedinger's time independent equation is

$$- \frac{\hbar^2}{2\mu} \nabla^2 U(r,\theta,\phi) + V(r)u(r,\theta,\phi) = EU(r,\theta,\phi) . \qquad (2)$$

We can assume as usual that the wave equation $U(r,\theta,\phi)$ is approximately the product of three wave functions, each depending on one variable only, so that

$$U(r,\theta,\phi) = R(r)\Theta(\theta)\Phi(\phi) . \qquad (3)$$

Combining equations (2) and (3) and using the form of ∇^2 in spherical coordinates then

$$\frac{-\hbar^2}{2\mu}\left[\frac{1}{r^2}\frac{\partial}{\partial r}\left(r^2\frac{\partial}{\partial r}\right)+\frac{1}{r^2\sin^2\theta}\frac{\partial}{\partial\theta}\left(\sin\theta\frac{\partial}{\partial\theta}\right)+\frac{1}{r^2\sin^2\theta}\frac{\partial^2}{\partial\phi^2}\right]R\Theta\Phi$$

$$+ VR\Theta\Phi = ER\Theta\Phi \ .$$

If we multiply by $\frac{r^2\sin^2\theta}{R\Theta\Phi}$ we find the ϕ dependent part of the equation separates and yields with a separation constant of $-m^2$, the usual azimuthal wave equation

$$\Phi(\phi) = e^{im\phi} \ . \tag{4}$$

We are left with

$$\frac{-\hbar^2}{2\mu}\left[\frac{\sin^2\theta}{R}\frac{\partial}{\partial r}\left(r^2\frac{\partial}{\partial r}\right)R+\frac{\sin\theta}{\Theta}\frac{\partial}{\partial\theta}\left(\sin\theta\frac{\partial}{\partial\theta}\right)\Theta-m^2\right]$$

$$+ Vr^2\sin^2\theta = Er^2\sin^2\theta \ .$$

If we divide by $\sin^2\theta$ the θ dependent part of the equation separates and yields with a separation constant of $-J(J+1)$, the associated Legendre equation. The solution to this equation is the associated Legendre polynomials, usually written as

$$\Theta(\theta) = P_J^m(\cos\theta) \ . \tag{5}$$

The remaining part of the wave equation depends on R only and is

$$\frac{1}{r^2}\frac{d}{dr}\left(r^2\frac{dR}{dr}\right)+\left[\frac{-J(J+1)}{r^2}+\frac{8\pi^2\mu}{h^2}\left\{E-V(r)\right\}\right]R = 0 \ . \tag{6}$$

The details of the solution of this equation are presented by Pauling and Wilson (2). The most important parts of their treatment are outlined in the following.

Since the potential is appreciably anharmonic, we can use the Morse potential given by

$$V(r) = D\left\{1 - e^{-a(r-r_e)}\right\}^2$$

where D is the disassociation energy and a is a constant characteristic of the molecule in question. The constant r_e is an equilibrium internuclear distance corresponding to the minimum of the potential function. The Morse potential of a typical diatomic molecule is shown in Figure 1. We would like to cast equation (6) in the form of the radial equation of the hydrogen atom whose solution we already know. This equation is

$$L'' + \left\{\frac{2(\ell+1)}{\rho} - 1\right\}L' + \left\{\frac{\lambda-(\ell+1)}{\rho}\right\} L = 0 \ ,$$

where $\lambda-\ell-1$ must be an integer value in order for solutions to exist. To this end we let

$$R(r) = \frac{1}{r} S(r) \ ,$$

$$x = e^{-a(r-r_e)} \text{ and}$$

$$A = \frac{J(J+1)h^2}{8\pi^2\mu r e^2} \ . \qquad (7)$$

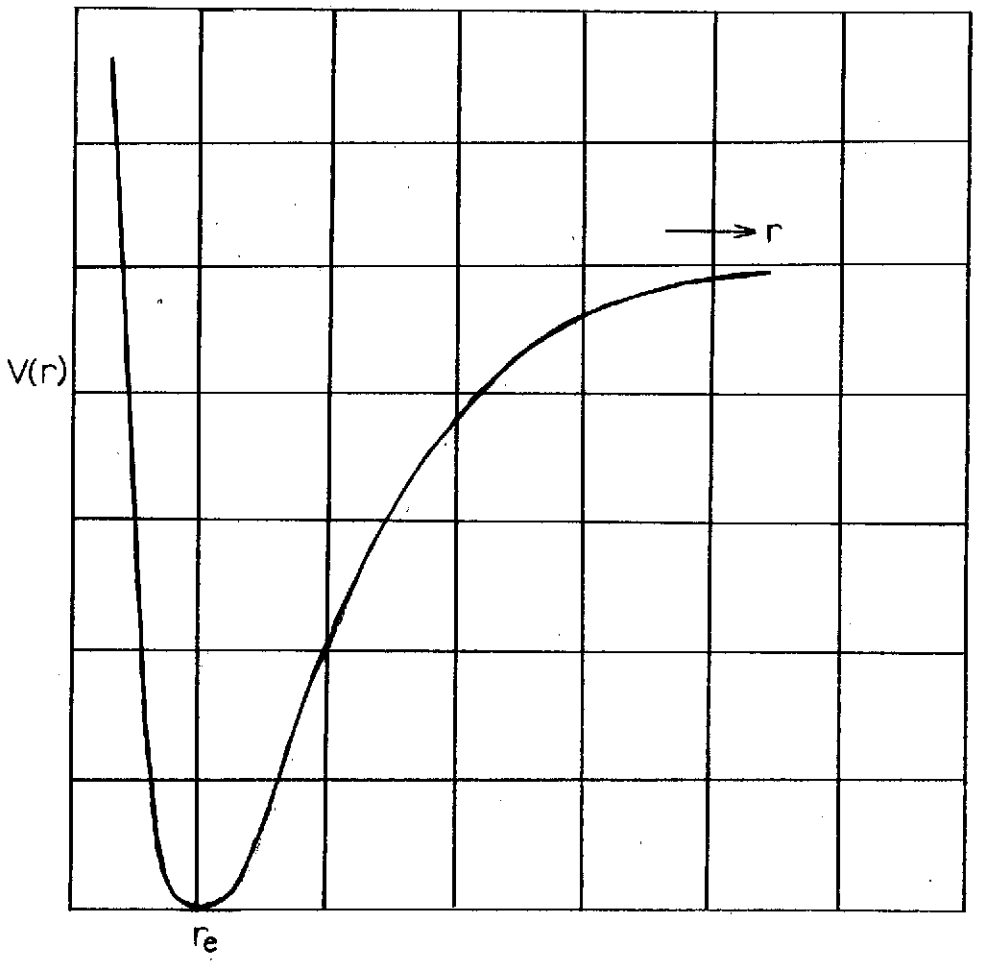

Figure 1. Morse Potential Function

Equation (6) becomes

$$\frac{d^2S}{dr^2} + \frac{8\pi^2\mu}{h^2}\left[-A\left(\frac{r_e}{r}\right)^2 + E - D(1-x)^2\right]S = 0 \ . \tag{8}$$

We can finish changing the variable in equation (8) to x by noting that

$$\frac{d^2S}{dr^2} = a^2x^2\frac{d^2S}{dx^2} + a^2x\frac{ds}{dx} \quad \text{and}$$

$$\left(\frac{r_e}{r}\right)^2 = \left(1 - \frac{\ln x}{ar_e}\right)^{-2} \ . \tag{9}$$

The latter equation can be expanded in a Taylor series in x-1. The first three terms are

$$\left(\frac{r_e}{r}\right)^2 = 1 + \frac{2}{ar_e}(x-1) + \left(\frac{3}{a^2r^2_e} - \frac{1}{ar_e}\right)(x-1)^2 \ .$$

Therefore

$$A\left(\frac{r_e}{r}\right)^2 = C_0 + C_1X + C_2X^2 \ , \tag{10}$$

where

$$C_0 = A\left(1 - \frac{3}{ar_e} + \frac{3}{a^2r_e^2}\right) \ , \tag{11}$$

$$C_1 = A\left(\frac{4}{ar_e} - \frac{6}{a^2r_e^2}\right) \quad \text{and} \tag{12}$$

$$C_2 = A\left(-\frac{1}{ar_e} + \frac{3}{a^2r_e^2}\right) . \tag{13}$$

Now substituting equation (9) and (10) into equation (8) we obtain

$$\frac{d^2S}{dx^2} + \frac{1}{x}\frac{dS}{dx} + \frac{8\pi^2\mu}{a^2h^2}\left[\frac{E-D-C_0}{x^2} + \frac{2D-C_1}{x} - D - C_2\right]S = 0 . \tag{14}$$

Comparing the hydrogen atom equation to our equation above we let

$$S(x) = e^{-\alpha y}\, y^{\beta}\, F(y) \text{ and} \tag{15}$$

$$y = \gamma x . \tag{16}$$

where α, β and γ are arbitrary constants which can be manipulated to change the form of (14). We can assign the following constants to terms in equation (14) to make the choice of the values of α, β and γ easier in later steps.

$$b^2 = \frac{8\pi^2\mu}{a^2h^2}(D + C_0 - E) ; \tag{17}$$

$$d^2 = \frac{8\pi^2\mu}{a^2h^2}(D + C_2) ; \tag{18}$$

$$e = \frac{8\pi^2\mu}{a^2h^2}(2D - C_1) . \tag{19}$$

When equations (15) through (19) are put into (14) the result is

$$\frac{d^2F}{dy^2} + \frac{dF}{dy}\left[\left(\frac{2B+1}{y}\right) - 2\alpha\right] + F\left[\left(\frac{\beta^2-b^2}{y^2}\right) + \left(\frac{e/\gamma-2\alpha B-\alpha}{y}\right)\right.$$

$$+ (\alpha^2 - d^2/\gamma^2) \Big] = 0 \ . \tag{20}$$

Comparing this equation to the hydrogen atom wave equation, we can make the following assignments to α, β and γ to change the arguments in equation (20) so that they have the same form.

$$\beta = b; \ \gamma = d/\alpha; \ \alpha = 1/2 \ . \tag{21}$$

Equation (20) becomes

$$\frac{d^2F}{dy^2} + \frac{dF}{dy}\left[\frac{(f+1)}{y} - 1\right] + \frac{Fv}{y} = 0 \ , \tag{22}$$

where

$$v = \frac{e}{2d} - \frac{1}{2}(f+1) \text{ and} \tag{23}$$

$$f = 2b \ . \tag{24}$$

In order for a solution to (22) to exist it is necessary to have v an integer as is the case of the hydrogen atom. To solve for the energy we must make use of equations (7), (11), (12), (13), (17), (18), (19), (23) and (24). We can solve (17) for E and substitute in (18), (19), (23) and (24). After simplification the result is

$$E = D + C_0\left[D\left(1 - \frac{C_1}{2D}\right)^2\left(1 + \frac{C_2}{D}\right)^{-1} - \frac{ah}{2\pi}\sqrt{\frac{2D}{\mu}}\left(1 - \frac{C_1}{2D}\right)\right.$$

$$\left.\left(1 + \frac{C_2}{D}\right)^{-1/2}\left(v + \frac{1}{2}\right) + \frac{a^2h^2}{8\pi^2\mu}\left(v + \frac{1}{2}\right)^2\right].$$

The terms involving C_1/D and C_2/D can be expanded keeping only squared terms or less. The equation for E then becomes

$$E = C_0 + C_1 + C_2 - \frac{1}{D}\left(\frac{C_1^2}{4} + C_1C_2 + C_2^2\right) + \frac{ah}{2\pi}\sqrt{\frac{2D}{\mu}}$$
$$\left[1 - \frac{1}{2D}(C_1 + C_2) + \frac{1}{4D^2}\left(C_1C_2 + \frac{3C_2^2}{2}\right)\right]\left(v + \frac{1}{2}\right)$$
$$- \frac{a^2h^2}{8\pi^2\mu}\left(v + \frac{1}{2}\right)^2 .$$

After putting in (11), (12) and (13) and dividing by hc then

$$\frac{E}{hc} = \frac{A}{hc} - \frac{A^2}{Da^2r_e^2hc} + \frac{a}{2\pi C}\sqrt{\frac{2D}{\mu}}\left(v + \frac{1}{2}\right) - \frac{a}{2\pi c}\sqrt{\frac{2D}{\mu}}$$
$$\left(\frac{1}{ar_e} - \frac{1}{a^2r_e^2}\right)\frac{3A}{2D}\left(v + \frac{1}{2}\right) - \frac{a}{2\pi c}\sqrt{\frac{2D}{\mu}}\frac{5A^2}{8D^2a^2r_e^2}\left(v + \frac{1}{2}\right)$$
$$- \frac{a^2h}{8\pi^2\mu}\left(v + \frac{1}{2}\right)^2 .$$

If we put in (3) and let

$$\omega_e = \frac{a}{2\pi c}\sqrt{\frac{2D}{\mu}} \quad \text{and}$$

$$\chi_e = \frac{h\omega_e c}{4D} ,$$

then

$$\frac{E}{hc} = \omega_e\left(v + \frac{1}{2}\right) - \omega_e\chi_e\left(v + \frac{1}{2}\right)^2 + \frac{h}{8\pi^2\mu r_e^2 c}\,J(J+1)$$

$$- \omega_e \left(\frac{1}{ar_e} - \frac{1}{a^2 r_e^2}\right) \frac{3h^2}{16\pi^2 \mu r_e^2 D} \left(v + \frac{1}{2}\right) J(J+1)$$

$$- \frac{h^3}{64\pi^4 \mu^2 r_e^6 D a^2 c} J^2 (J+1)^2 \ .$$

If we let

$$B_e = \frac{h}{8\pi^2 I_e c} \ ;$$

$$\alpha_e = \frac{3h^2}{16\pi^2 I_e D} \left(\frac{1}{ar_e} - \frac{1}{a^2 r_e^2}\right) \ ;$$

$$D_e = \frac{h^3}{128\pi^6 \omega_e^2 I_e^3 c^3} \ ;$$

$$\beta_e = \frac{5\omega_e h^4}{512\pi^4 I_e^3 D a^2} \quad \text{and}$$

$$I_e = \mu r_e^2 ;$$

then

$$\frac{E}{hc} = \omega_e \left(v + \frac{1}{2}\right) - \omega_e \chi_e \left(v + \frac{1}{2}\right)^2 + \beta_e J(J+1) -$$

$$\alpha_e \left(v + \frac{1}{2}\right) J(J+1) - D_e J^2 (J+1)^2 - \beta_e \left(v + \frac{1}{2}\right) J^2 (J+1)^2 \ .$$

Collecting terms we find that

$$\frac{E}{hc} = \omega_e \left(v + \frac{1}{2}\right) - \omega_e \chi_e \left(v + \frac{1}{2}\right)^2 + \omega_e y_e \left(v + \frac{1}{2}\right)^3 + \text{---}$$

$$+ J(J+1)\left[B_e - \alpha_e\left(v + \frac{1}{2}\right) + \gamma_e\left(v + \frac{1}{2}\right)^2 + \cdots\right]$$

$$+ J^2(J+1)^2\left[D_e + \beta_e\left(v + \frac{1}{2}\right) + \delta_e\left(v + \frac{1}{2}\right)^2 + \cdots\right]$$

$$+ J^3(J+1)^3\left[H_e + \cdots\right],$$

where some higher order terms not kept in previous expansions have been added. If we define

$$B_v = B_e - \alpha_e\left(v + \frac{1}{2}\right) + \gamma_e\left(v + \frac{1}{2}\right)^2 + \cdots,$$

$$D_v = D_e + \beta_e\left(v + \frac{1}{2}\right) + \delta_e\left(v + \frac{1}{2}\right)^2 + \cdots,$$

$$H_v = H_e + \cdots \text{ and}$$

$$\nu_{v\to v'} = \omega_e\left(v + \frac{1}{2}\right) - \omega_e\chi_e\left(v + \frac{1}{2}\right)^2 + \omega_e y_e\left(v + \frac{1}{2}\right)^3 + \cdots,$$

where the subscript v denotes the vibrational dependence of the rotational constant, then

$$\frac{E}{hc} = \nu_{v\to v'} + B_v J(J+1) - D_v J^2(J+1)^2 + H_v J^3(J+1)^3. \qquad (25)$$

This expression yields the term values for the diatomic energy levels. If the allowed rotational and vibrational selection rules are substituted into the equation above, we obtain the allowed absorption transitions for the rotational branches within a vibrational transition. The selection rules for electric field induced spectra are derived in

Section 2.2 and are

$$\Delta v = 0,\ 1,\ 2\ \text{--}\ \text{and}\ \Delta J = 0, \pm 2\ , \tag{26}$$

where Δv and ΔJ are changes in the vibrational and rotational quantum number respectively. The $\Delta J = 0$ transitions correspond to the Q branch; the $\Delta J = +2$ to the S branch and $\Delta J = -2$ to the 0 branch. The general formula for the frequencies in units of cm^{-1} of the three branches are therefore, combining equations (25) and (26)

$$Q_v(J) = \nu_{v\to v'} + (B_{v'}-B_v)J(J+1) - (D_{v'}-D_v)J^2(J+1)^2$$
$$+ (H_{v'}-H_v)J^3(J+1)^3\ ,$$

$$O_v(J) = \nu_{v\to v'} + B_{v'}(J-2)(J-1) - B_vJ(J+1) - D_{v'}(J-2)^2(J-1)^2$$
$$+ D_vJ^2(J+1)^2 + H_{v'}(J-2)^3(J-1)^3 - H_vJ^3(J+1)^3,$$

$$S_v(J) = \nu_{v\to v'} + B_{v'}(J+2)(J+3) - B_vJ(J+1) - D_{v'}(J+2)^2(J+3)^2$$
$$+ D_vJ^2(J+1)^2 + H_{v'}(J+2)^3(J+3)^3 - H_vJ^3(J+1)^3\ .$$

Here v is the initial (lower) vibrational state and v' is the final (upper) vibrational state. The J values are initial rotational states. Table I shows the first several transitions for specific J values, for the pure rotational spectral lines ($\Delta v=0$) and the fundamental spectrum ($\Delta v=1$). The transitions in each branch are represented by a symbol which characterizes that specific transition. For example $S_2(3)$

TABLE I

ELECTRIC FIELD INDUCED TRANSITIONS

Pure Rotational Transitions

$So(0) = 6Bo - 36Do + 216Ho$

$So(1) = 10Bo - 140Do + 1,720Ho$

$So(2) = 14Bo - 364Do + 7,784\ Ho$

$So(3) = 18Bo - 756\ Do + 25,272Ho$

$So(4) = 22Bo - 1,364Do + 66,088Ho$

$So(5) = 26Bo - 2,232Do + 148,616Ho$

$So(6) = 30Bo - 5,184Do + 299,160Ho$

Fundamental Transitions

$$Q_1(0) = \nu_{0\to1}$$

$$Q_1(1) = \nu_{0\to1} + 2B_1 - 2Bo - 4D_1 + 4Do + 8H_1 - 8Ho$$

$$Q_1(2) = \nu_{0\to1} + 6B_1 - 6Bo - 36D_1 + 36Do + 216H_1 - 216Ho$$

$$Q_1(3) = \nu_{0\to1} + 12B_1 - 12Bo - 144D_1 + 144Do + 1,728H_1 - 1,728Ho$$

$$Q_1(4) = \nu_{0\to1} + 20B_1 - 20Bo - 400D_1 + 400Do + 8,000H_1 - 8,000Ho$$

$$Q_1(5) = \nu_{0\to1} + 30B_1 - 30Bo - 900D_1 + 900Do + 27,000H_1 - 27,000Ho$$

$$Q_1(6) = \nu_{0\to1} + 42B_1 - 42Bo - 1,764D_1 + 1,764Do + 74,088H_1 - 74,088Ho$$

$$S_1(0) = \nu_{0\to1} + 6B_1 - 36D_1 + 216H_1$$

$$S_1(1) = \nu_{0\to1} + 12B_1 - 2Bo - 144D_1 + 4Do + 1,728H_1 - 8Ho$$

$$S_1(2) = \nu_{0\to1} + 20B_1 - 6Bo - 400D_1 + 36Do + 8,000H_1 - 216Ho$$

$$S_1(3) = \nu_{0\to1} + 30B_1 - 12Bo - 900D_1 + 144Do + 27,000H_1 - 1,728Ho$$

$$S_1(4) = \nu_{0\to1} + 42B_1 - 20Bo - 1,764D_1 + 400Do + 74,088H_1 - 8,000Ho$$

$$S_1(5) = \nu_{0\to1} + 56B_1 - 30Bo - 3,136D_1 + 900Do + 175,616H_1 - 27,000Ho$$

$$S_1(6) = \nu_{0\to1} + 72B_1 - 42Bo - 5,184D_1 + 1,764Do + 373,248H_1 - 74,088Ho$$

TABLE I (continued)

$$O_1(2) = \nu_{0\to1} - 6Bo + 36Do - 216Ho$$
$$O_1(3) = \nu_{0\to1} + 2B_1 - 12Bo - 4D_1 + 144Do + 8H_1 - 1{,}728Ho$$
$$O_1(4) = \nu_{0\to1} + 6B_1 - 20Bo - 36D_1 + 400Do + 216H_1 - 8{,}000Ho$$
$$O_1(5) = \nu_{0\to1} + 12B_1 - 30Bo - 144D_1 + 900Do + 1{,}728H_1 - 27{,}000Ho$$
$$O_1(6) = \nu_{0\to1} + 20B_1 - 42Bo - 400D_1 + 1{,}764Do + 8{,}000H_1 - 74{,}088Ho$$

represents a transition to the second vibrational state, the subscript 2 giving the final vibrational state. Since in the transitions considered here the molecules are all initially in the ground state, the initial v state is understood to be 0 and is not specified in the transition symbol. The 3 in parenthesis represents the initial J state and the S implies a selection rule of $\Delta J = +2$. Therefore a rotational transition from J = 3 in the initial vibrational state 0 to J = 5 in the final vibrational state 2 is specified.

2.2 Strength Factors of a Diatomic Molecule in an Electric Field

The transition probability between two rotational states is proportional to the square of the dipole moment integral linking the two states. Since the intensity of an absorption line is directly proportional to the transition probability the squared dipole moment integral is referred to as the strength factor and is defined by Herzberg (3) as:

$$S_i(J,m;J'm') \equiv |D_i(J,m;J',m')|^2 , \qquad (27)$$

where D_i is the dipole moment integral given by

$$D_i(J,m;J',m') = \int \psi_{RR}\, \mu_i\, \psi_{RR}\, d\tau;\ i=x,y,z \quad . \qquad (28)$$

ψ_{RR} is the wave function of the rigid rotor and μ_i are the components of the dipole moment in the x, y or z direction. Since the diatomic molecule is not strictly a rigid rotor equation (28) is an approximation

to the true equation. Before calculating the strength factors, it is necessary to calculate the dipole moment components in equation (28) for a diatomic molecule in an external electric field.

According to Herzberg (3), when a molecule is subjected to an external electric field, a dipole moment is induced which is proportional to the field intensity. In laboratory coordinates where measurements are made the dipole moment is

$$\mu_i = \alpha_{ij} E_j \ ,$$

where i,j = x,y,z and α_{ij} is the polarizability tensor. x,y,z are laboratory or space fixed coordinates assigned as shown in the following figure.

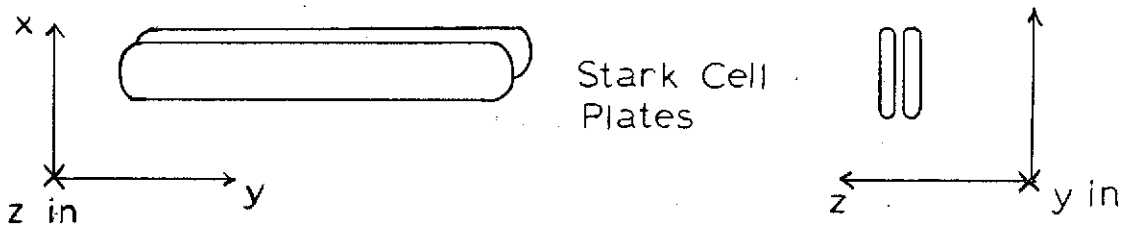

If we expand the expression above we obtain

$$\begin{pmatrix} \mu_x \\ \mu_y \\ \mu_z \end{pmatrix} = \begin{pmatrix} \alpha_{xx} & \alpha_{xy} & \alpha_{xz} \\ \alpha_{yx} & \alpha_{yy} & \alpha_{yz} \\ \alpha_{zx} & \alpha_{zy} & \alpha_{zz} \end{pmatrix} \begin{pmatrix} E_x \\ E_y \\ E_z \end{pmatrix} \ ,$$

where E_x and E_y are zero in our assignment of coordinates. We find then that

$$\mu_x = \alpha_{xz} E_z \ ,$$

$$\mu_y = \alpha_{yz} E_z \text{ and} \qquad (29)$$

$$\mu_z = \alpha_{zz} E_z \ .$$

The polarizability of a molecule is expressed in molecule fixed coordinates so we must transform the space components of the polarizability matrix to molecular coordinates. Let x',y',z' be assigned to the diatomic molecule as shown below,

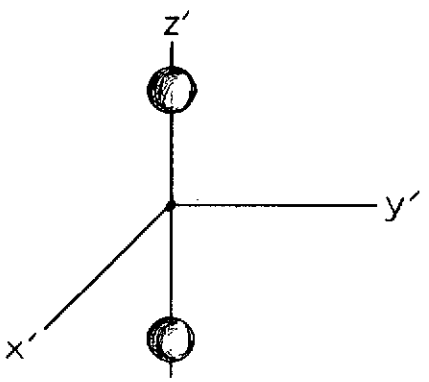

with z' being the symmetry axis. Obviously the x' and y' axes are interchangeable. The transformation of the polarizability tensor is given by

$$\alpha_{ij} = \sum_{s't'} A_{is'} A_{jt'} \alpha_{s't'} \ . \qquad (30)$$

The A's are the direction cosines describing the two rotations which are necessary for the transformation. According to Goldstein (4), A is given by

$$A = \begin{array}{c} \\ x \\ y \\ z \end{array} \begin{array}{c} \begin{array}{cccc} x' & & y' & & z' \end{array} \\ \begin{pmatrix} \cos\phi & -\cos\theta\sin\phi & \sin\theta\sin\phi \\ \sin\phi & \cos\theta\cos\phi & -\sin\theta\cos\phi \\ 0 & \sin\theta & \cos\theta \end{pmatrix} \end{array} . \qquad (31)$$

If we expand equation (30) and let the off diagonal terms go to zero, since the molecular axis is a principle axis system, then we find for the space fixed component α_{xz}

$$\alpha_{xz} = A_{xx'}A_{zx'}\alpha_{x'x'} + A_{xy'}A_{zy'}\alpha_{y'y'} + A_{xz'}A_{zz'}\alpha_{z'z'} .$$

Using equation (31) ,

$$\alpha_{xz} = (\alpha_{z'z'} - \alpha_{y'y'}) \sin\theta \cos\theta \sin\phi .$$

Since x' and y' are interchangable by symmetry let us refer to these axes as $\perp'$ to designate they are perpendicular to the molecular axis. Likewise we let z' be referred to as $\|'$. Therefore

$$\alpha_{xz} = (\alpha_{\|'\|'} - \alpha_{\perp'\perp'}) \sin\theta \cos\theta \sin\phi .$$

Similar expressions for the other two components of interest are obtained and our dipole moment components in equation (29) become

$$\mu_x = (\alpha_{\|'\|'} - \alpha_{\perp'\perp'}) \sin\theta \cos\theta \sin\phi \, E ,$$

$$\mu_y = -(\alpha_{\|'\|'} - \alpha_{\perp'\perp'}) \sin\theta \cos\theta \cos\phi \, E \text{ and}$$

$$\mu_z = (\alpha_{\perp'}\alpha_{\perp'}\sin^2\theta + \alpha_{\|'\|'}\cos^2\theta) \, E .$$

If we introduce the definitions given by Brannon (5) for the anisotropy of polarization, γ, and the average polarization, α, which are

$$\gamma \equiv (\alpha_{\parallel'\parallel'} - \alpha_{\perp'\perp'}) \text{ and}$$

$$\alpha \equiv \frac{1}{3} (2\alpha_{\perp'\perp'} + \alpha_{\parallel'\parallel'}) ,$$

then we find

$$\begin{aligned} \mu_x &= \gamma \sin\theta \cos\theta \sin\phi \, E, \\ \mu_y &= -\gamma \sin\theta \cos\theta \cos\phi \, E \text{ and} \\ \mu_z &= \left[\frac{1}{3} \gamma (3 \cos^2\theta - 1) + \alpha\right] E . \end{aligned} \tag{32}$$

These are the final expressions for the dipole moment components which are needed to calculate the strength factors as outlined in the following treatment.

Manneback (6 and 7) has evaluated the strength factors for Raman spectra which also applies to electric field induced spectra. His treatment however is more general than is needed for the specific case at hand and some details are lacking. Therefore the strength factors were reevaluated for electric field induced spectra specifically and with a more straightforward treatment. We begin by evaluating the dipole moment integrals given by

$$D_i(J,M;J',M') = \int \psi^*_{RR} \, \mu_i \, \psi_{RR} \, d\tau,$$

where the rigid rotor functions are given by

$$\psi_{RR} = \Theta^M_J (\cos\theta) \, \Phi(\phi) .$$

Here Θ are the normalized associated Legendre polynomials and Φ is the usual azimuthal wave function. Since the space fixed coordinates are cylindrically symmetric, the x and y directions are indistinguishable. We can therefore let $\mu_i = \mu_{//}$ or $\mu_\perp$ where $\perp$ refers to a direction perpendicular to the electric field and the $//$ direction is parallel to the electric field. Hence

$$\mu_\perp^{(\pm)} = \frac{1}{\sqrt{2}} (\mu_x \pm i\mu_y) \text{ and}$$

$$\mu_{//} = \mu_z \ .$$

The dipole moment integrals for the parallel and perpendicular directions are, using equations (32),

$$\begin{aligned}
D\ (J,M;J',M') &= \frac{1}{\sqrt{2}} \gamma E I_\perp(\theta) I_\perp(\phi) \ ; \\
I_\perp(\theta) &= \int \Theta_J^{m*}(\theta)\ \sin\theta\ \cos\theta\ \Theta_{J'}^{m'}(\theta) d\tau(\theta) \ ; \\
I_\perp^{(\pm)}(\phi) &= \int \Phi_m^*\ (\phi)[\sin\phi \mp i\cos\phi]\Phi_{m'}(\phi) d\tau(\phi) \ ; \qquad (33) \\
D_{//}(J,M;J',M') &= [\gamma E I_{//}^{(1)}(\theta) + (\alpha - \tfrac{1}{3}\gamma) E I_{//}^{(2)}(\theta)] I_{//}(\phi) \ ; \\
I_{//}^{(1)}(\theta) &= \int \Theta_J^{m*}(\theta)\ \cos^2\theta\ \Theta_{J'}^{m'}(\theta) d\tau(\theta) \ ; \\
I_{//}^{(2)}(\theta) &= \int \Theta_J^{m*}(\theta)\ \Theta_{J'}^{m'}(\theta) d\tau(\theta) \ ; \\
I_{//}(\phi) &= \int \Phi_m^*(\phi)\Phi_{m'}(\phi) d\tau(\phi) \ . \qquad (34)
\end{aligned}$$

Using

$$\Phi_m(\phi) = \frac{1}{(2\pi)^{1/2}} e^{im\phi} \text{ and } d\tau(\phi) = d\phi ,$$

equations (33) and (34) can be evaluated.

$$I_{\perp}^{(\pm)}(\phi) = \mp i\delta_{m\mp1,m'}$$

$$I_{\parallel}(\phi) = \delta_{m,m'} .$$

These expressions give the selection rules for the azimuthal quantum number m, which are

$$\Delta m = 0,\pm1 .$$

Our dipole moment integrals reduce to the following after substituting in the allowed m selection rules:

$$D^{(\pm)}(J,m;J,m \mp 1) = \frac{\mp i}{\sqrt{2}} \gamma E\, I_{\perp}(\theta) ; \tag{35}$$

$$I_{\perp}(\theta) = \int \Theta_J^{m*}(\theta)\sin\theta\cos\theta\, \Theta_{J'}^{m\mp1}(\theta)d\tau(\theta); \tag{36}$$

$$D(J,m;J',m) = \gamma E I_{\parallel}^{(1)}(\theta) + \left(\alpha - \frac{1}{3}\gamma\right) E I_{\parallel}^{(2)}(\theta); \tag{37}$$

$$I_{\parallel}^{(1)}(\theta) = \int \Theta_J^{m*}(\theta)\cos^2\theta\, \Theta_{J'}^{m}(\theta)d\tau(\theta); \tag{38}$$

$$I_{\parallel}^{(2)}(\theta) = \int \Theta_J^{m*}(\theta)\, \Theta_{J'}^{m}(\theta)d\tau(\theta) . \tag{39}$$

Using the orthogonality condition for the associated Legendre polynomials

$$\int_0^{\pi} \Theta_J^{m*}(\theta)\Theta_{J'}^{m}(\theta)d\tau(\theta) = \delta_{J,J'} \text{ and } d\tau(\theta) = \sin\theta d\theta , \tag{40}$$

equation (39) can be evaluated and yields

$$I_{\parallel}^{(2)}(\theta) = \delta_{J,J'} .$$

Equations (36) and (38) can be evaluated using recursion relations for the associated Legendre polynomials. These are given by Condon and Shortley (8) as

$$\cos\theta\ \Theta_J^m = A(J,m)\ \Theta_{J+1}^m + B(J,m)\ \Theta_{J-1}^m \text{ and}$$

$$\sin\theta\ \Theta_J^m = \mp\ C(J,m)\ \Theta_{J+1}^{m\pm1} \pm D(J,m)\ \Theta_{J-1}^{m\pm1} ,$$

where the coefficients are given by

$$A(J,m) = \left[\frac{(J-m+1)(J+m+1)}{(2J+1)(2J+3)}\right]^{1/2};\quad B(J,m) = \left[\frac{(J-m)(J+m)}{(2J-1)(2J+1)}\right]^{1/2};$$

$$C(J,M) = \left[\frac{(J\pm m+1)(J\pm m+2)}{(2J+1)(2J+3)}\right]^{1/2};\quad D(J,m) = \left[\frac{(J\mp m)(J\mp m-1)}{(2J-1)(2J+1)}\right]^{1/2} .$$

Using these recursion relations equation (36) becomes

$$I_{\perp}(\theta) = \mp C(J',m\mp1)I(1) \pm D(J',m\mp1)I(2) ;$$

$$I(1) = \int \Theta_J^{m*} \cos\theta\ \Theta_{J'+1}^m\ d\tau(\theta) ;$$

$$I(2) = \int \Theta_J^{m*} \cos\theta\ \Theta_{J'-1}^m\ d\tau(\theta) .$$

By reapplication of the appropriate recursion relation the two latter integrals break up into two integrals each

$$I(1) = A(J'+1,m)I(3) + B(J'+1,m)I(4);$$

$$I(3) = \int \Theta_J^{m*}\, \Theta_{J'+2}^{m}\, d\tau(\theta) \ ;$$

$$I(4) = \int \Theta_J^{m*}\, \Theta_{J'}^{m}\, d\tau(\theta) \ ;$$

$$I(2) = A(J'-1,m)I(5) + B(J-1,m) \ ;$$

$$I(5) = \int \Theta_J^{m*}\, \Theta_{J'}^{m}\, d\tau(\theta) \ ;$$

$$I(6) = \int \Theta_J^{m*}\, \Theta_{J'-2}^{m}\, d\tau(\theta) \ .$$

The resulting integrals can be evaluated using the orthogonality relation (40) so that

$$I_{\perp}(\theta) = \mp\, C(J',m\mp1)[A(J'+1,m)\delta_{J,J'+2} + B(J'+1,m)\ \delta_{J,J'}]$$

$$\pm\, D(J',m\mp1)[A(J'-1,m)\delta_{J,J'} + B(J'-1,m)\delta_{J,J'-2}].$$

Using the same technique equation (38) can be evaluated with the result

$$I_{\parallel}^{(1)}(\theta) = A(J',m)[A(J'+1,m)\delta_{J,J'+2} + B(J'+1,m)\delta_{J,J'}]$$

$$+\, B(J',m)[A(J'-1,m)\delta_{J,J'} + B(J'-1,m)\delta_{J,J'-2}] \ .$$

Putting all the evaluated integrals back into the expressions (35) and (37), the dipole moment integrals become

$$D_{\perp}^{(\pm)}(J,m;J',m\pm1) = \frac{\mp i}{\sqrt{2}}\,\gamma E\,\Big\{\mp C(J',m\mp1)[A(J'+1,m)\delta_{J,J'+2}$$

$$+B(J'+1,m)\delta_{J,J'}] \pm D(J',m\mp1)[A(J'-1,m)\delta_{J,J'} \qquad (41)$$

$$+\, B(J'-1,m)\delta_{J,J'-2}]\Big\} \ ;$$

$$D_{\parallel}(J,m;J',m) = \gamma E\Big\{A(J',m)\,[A(J'+1,m)\,\delta_{J,J'+2} + B(J'+1,m)\,\delta_{J,J'}] + B(J',m)\,[A(J'-1,m)\,\delta_{JJ'} + B(J'-1,m)\,\delta_{J,J'-2}]\Big\} + \left(\alpha - \frac{1}{3}\gamma\right) E\delta_{J,J'} \quad (42)$$

By inspection of (41) and (42) the selection rules for the rotational quantum number J are easily seen to be

$$\Delta J = 0,\pm 2 \ .$$

If we substitute in the selection rules for all possible cases then

$$D_{\parallel}(J,m;J,m) = \gamma E[A(J,m)B(J+1,m) + B(J,m)A(J-1,m)] + \left(\alpha - \frac{1}{3}\gamma\right)E;$$

$$D_{\perp}(J,m;J,m\mp 1) = \frac{i}{\sqrt{2}}\gamma E[C(J,m+1)B(J+1,m) - D(J,m\mp 1)A(J-1,m)];$$

$$D_{\parallel}(J,m;J+2,m) = \gamma E\ B(J+2,m)B(J+1,m);$$

$$D_{\perp}(J,m;J+2,m\mp 1) = \frac{-i}{\sqrt{2}}\gamma E\ D(J+2,m\mp 1)B(J+1,m)\ ; \quad (43)$$

$$D_{\parallel}(J,m;J-2,m) = \gamma E\ A(J-2,m)A(J-1,m)\ ;$$

$$D_{\perp}(J,m;J-2,m\mp 1) = \frac{i}{\sqrt{2}}\gamma EC(J-2,m\mp 1)A(J-1,m)\ .$$

The strength factor, Si, is the square of these dipole moment integrals and is

$$Si\left[J,m;J'(J),m'(m)\right] = \left[Di[J,m;J'(J),m'(m)]\right]^2 \ .$$

Since the m splitting is too small to be observed, we may average over them by summing over the m states and dividing by the degeneracy of the

particular J state. Therefore

$$Si[J,J'(J)] = \frac{1}{(2J+1)} \sum_{m=-J}^{+J} \left| Di[J,m;J(J'),m(m')] \right|^2 .$$

The summing of the expressions in equations (43) is quite tedious but straight forward. The final expressions are given in Table II. The sums involved in the evaluation of these expressions are given in Table III. The J dependent coefficients of the strength factors are listed in Table IV.

2.3 Stark Splitting of m-Levels

The energy of the split m-levels is, according to Herzberg (3),

$$\omega = \omega_o - \bar{\mu}_E E , \qquad (44)$$

where ω_o is the unsplit energy and $\bar{\mu}_E$ is the average component of the dipole in the direction of the electric field E. The electric field splitting is different from magnetic splitting in that equal values of m with different signs do not lead to different energies. Therefore a J=3 level would be split into 4 levels with 3 of them being doubly degenerate. From equation (44) the energy difference between the split m-levels is

$$\Delta\omega = \bar{\mu}_z E ,$$

where z is the direction of the electric field. From equation (32) of the previous section,

TABLE II

STRENGTH FACTORS

$$S_{\parallel}(J,J) = \alpha^2E^2 + \frac{4}{45}\frac{J(J+1)\gamma^2E^2}{(2J-1)(2J+3)}$$

$$S_{\perp}(J,J) = \frac{1}{15}\gamma^2E^2\frac{J(J+1)}{(2J-1)(2J+3)}$$

$$S_{\parallel}(J,J+2) = \frac{2}{15}\gamma^2E^2\frac{(J+1)(J+2)}{(2J+3)(2J+1)}$$

$$S_{\perp}(J,J+2) = \frac{1}{10}\gamma^2E^2\frac{(J+1)(J+2)}{(2J+3)(2J+1)}$$

$$S_{\parallel}(J,J-2) = \frac{2}{15}\gamma^2E^2\frac{J(J-1)}{(2J-1)(2J+1)}$$

$$S_{\perp}(J,J-2) = \frac{1}{10}\gamma^2E^2\frac{J(J-1)}{(2J-1)(2J+1)}$$

TABLE III

m-SUMS OF SQUARED DIPOLE INTEGRALS

$$\sum_{m=-J}^{+J} \left\{ \gamma E \left[\frac{(J-m+1)(J+m+1)}{(2J+1)(2J+3)} + \frac{(J-m)(J+m)}{(2J-1)(2J+1)} - \frac{1}{3} \right] + \alpha E \right\}^2$$

$$= (2J+1) \left[\frac{4}{45} \frac{J(J+1)\gamma^2 E^2}{(2J-1)(2J+3)} + \alpha^2 E^2 \right]$$

$$\sum_{m=-J}^{+J} \left\{ \left[(J \pm m)(J \pm m+1)(J-m+1)(J+m+1) \right]^{1/2} (2J-1) \right.$$

$$\left. - \left[(J \pm m+1)(J \pm m)(J-m)(J+m) \right]^{1/2} (2J+3) \right\}^2$$

$$= \frac{2}{15} J(J+1)(2J+3)(2J-1)(2J+1)^3$$

$$\sum_{m=-J}^{+J} (J-m+2)(J+m+2)(J-m+1)(J+m+1)$$

$$= \frac{2}{15} (2J+1)(J+1)(J+2)(2J+3)(2J+5)$$

$$\sum_{m=-J}^{+J} (J \overline{+} m+3)(J \overline{+} m+2)(J-m+1)(J+m+1) =$$

$$\frac{2}{10} (2J+1)(J+1)(J+2)(2J+3)(2J+5)$$

$$\sum_{m=-J}^{+J} (J-m-1)(J+m-1)(J-m)(J+m) = \frac{2}{15} J(J-1)(2J-1)(2J+1)(2J-3)$$

$$\sum_{m=-J}^{+J} (J-m)(J+m)(J \pm m-2)(J \pm m-1) = \frac{2}{10} J(J-1)(2J-3)(2J+1)(2J-1)$$

TABLE IV

COEFFICIENTS OF THE STRENGTH FACTORS

J	J´=J Parallel	J´=J+2 Parallel	J´=J-2 Parallel
0	.000000	.088889	.000000
1	.035556	.053333	.000000
2	.025397	.045714	.017778
3	.023704	.042328	.022857
4	.023088	.040404	.025397
5	.022792	.039161	.026936
6	.022626	.038291	.027972
7	.022524	.037647	.028718
8	.022456	.037152	.029281
9	.022409	.036759	.029721
10	.022375	.036439	.030075

J	J´=J Perpendicular	J´=J+2 Perpendicular	J´=J-2 Perpendicular
0	.000000	.066667	.000000
1	.026667	.040000	.000000
2	.019048	.034286	.013333
3	.017778	.031746	.017143
4	.017316	.030303	.019048
5	.017094	.029371	.020202
6	.016970	.028718	.020980
7	.016893	.028235	.021539
8	.016842	.028235	.021961
9	.016807	.027864	.022291
10	.016781	.027569	.022556

$$\mu_z = \left[\frac{1}{3}\gamma(3\cos^2\theta - 1) + \alpha\right]E \ .$$

The average of μ_z is

$$\overline{\mu}_z = \frac{\int_0^\pi \mu_z d\theta}{\int_0^\pi d\theta} = \left[\frac{1}{6}\gamma + \alpha\right] E \ ,$$

so that

$$\Delta\omega = \left[\frac{1}{6}\gamma + \alpha\right]E^2 \ .$$

Using the polarizability of H_2 and a field of 250,000 volts/cm, this equation yields a splitting of about 0.0003 cm^{-1}. This is of course too small to be detected, and does not even contribute to the width of the line (within experimental error). It is therefore necessary to consider the m-levels as degenerate energy levels as was done in the previous section.

2.4 Boltzmann Factors of a Diatomic Molecule

The intensity of an absorption line depends on the number of molecules in the initial state, that is the number of molecules available for transitions to some upper state level. If we first consider vibrational population, the number of molecules in each vibrational state relative to the number in the ground state is

$$\frac{N_v}{N_o} = e^{-G_o(v)hc/KT} \ , \qquad (45)$$

where N_v and N_o are the number of molecules in the vth level and the zero or ground state respectively. $G_o(v)$ are energy differences between the ground state and upper vibrational levels v. The total number of molecules is N and can be expressed simply as

$$N = N_o + N_1 + N_2 + \text{---} ,$$

or using (45)

$$N = N_o(1 + e^{-G_o(1)hc/KT} + e^{-G_o(2)hc/KT} + \text{---}) .$$

If we let

$$Q = 1 + e^{-G_o(1)hc/KT} + e^{-G_o(2)hc/KT} + \text{---} ,$$

then

$$N = N_o Q . \tag{46}$$

Using (45) and (46) the total number of molecules in the vth state is

$$N_v = \frac{N}{Q} e^{-G_o(v)hc/KT} .$$

For the lighter diatomic molecules such as H_2 and D_2 the exponential quantity is of order $1x10^{-9}$ so that for all practical purposes we can consider all molecules to be initially in the ground vibrational state, so that

$$N_o = N .$$

The rotational population levels can be obtained by similar arguments if the degeneracy of the rotational levels is considered. Each rotational level has a degeneracy of 2J+1 which accounts for the m states which are not resolved (see Section 2.3). Therefore

$$N_J = \frac{N}{R} (2J+1) e^{-F(J)hc/KT} \text{ and} \tag{47}$$

$$R = \sum_J (2J+1) e^{-F(J)hc/KT} , \tag{48}$$

where

$$F(J) = BoJ(J+1) - DoJ^2(J+1)^2 + HoJ^3(J+1)^3 .$$

The ground state rotational constants are used since our molecule has been shown to always start in the ground vibrational state. An additional degeneracy exists in homonuclear diatomic molecules due to the identical nuclei. If I is the spin vector of the nuclei then T, the total nuclear spin, takes the possible values

$$T = 2I, 2I-1, 2I-2 \text{ --- } 0 ,$$

For each possible total angular momentum there is a degeneracy of 2T+1. This degeneracy describes the number of wave functions necessary to describe the states. It is found that odd values of T and their associated degeneracy are associated with the odd J value wave functions and the even values of T with the even J value wave functions. This is due to the symmetry requirements of the total wave function. Therefore each odd and each even J state is subject to a further degeneracy

which we will call g(odd) and g(even). For example in D_2 the spin of each Deuterium nucleus is 1. Therefore the total spin can be

$$T = 2 \text{ or } 1 \text{ or } 0.$$

The odd T value 1 is associated with the odd J values and the degeneracy is 2T+1 = 3. The even T values 2 and 0 are associated with even J values and the degeneracy is 5+1 = 6. We therefore have a ratio of 1 to 2 in the degeneracy of the odd to the even levels. Therefore for D_2

$$g(\text{odd}) = 1 \text{ and}$$

$$g(\text{even}) = 2 .$$

Likewise for H_2 where $I = \frac{1}{2}$

$$g(\text{odd}) = 3 \text{ and}$$

$$g(\text{even}) = 1 .$$

Since for N_2, I = 1, the degeneracies are the same as for D_2.

Taking account of this degeneracy in equation (47) and (48) we have

$$N_J = \frac{N}{R} g(2J+1)e^{-F(J)hc/KT} \text{ and} \tag{49}$$

$$R = \sum_J g(2J+1)e^{-F(J)hc/KT} ,$$

where

g = g(odd) when J is odd, and

g = g(even) when J is even.

Equation (49) can be written more conveniently as

$$N_J = Nf_J \ , \tag{50}$$

where f_J the Boltzmann factor is

$$f_J = \frac{g(2J+1)}{R} e^{-F(J)hc/KT} \ .$$

Relative populations calcualted from equation (50) at T = 300°K for H_2, D_2 and N_2 are listed in Table V. From this table it can be seen that the population decreases very rapidly for increasing J values for H_2 and D_2. For this reason relatively few lines in each rotational branch are seen.

2.5 Integrated Absorption

The exponential law of absorption for radiation passing through an absorbing medium of thickness ℓ and with an absorption coefficient K is according to Herzberg (3)

$$I = I_o e^{-K\ell} \ ,$$

where I_o is the incident intensity and I is the intensity after absorption.

In differential form

$$dI = -IN_{V,J} B_{V,J}^{V',J'} h\nu d\ell, \tag{52}$$

where $N_{V,J}$ is the number of molecules in the initial state and $B_{V,J}^{V',J'}$ is the Einstein probability of absorption. From (51) and (52) we see that

TABLE V

RELATIVE POPULATIONS

J	H_2	D_2	N_2
0	.128695	.181242	.012623
1	.656396	.204145	.018578
2	.117728	.384205	.059616
3	.091875	.114468	.039419
4	.004275	.094801	.093943
5	.001014	.014190	.052206
6	.000016	.006285	.110099
7	.000001	.000523	.055608
8	---	.000133	.108272
9	---	.000007	.050996
10	---	.000001	.093227

$$K = N_{v,J} B_{v,J}^{v',J'} h\nu.$$

This expression is valid for a single frequency spectral line centered at the frequency ν. In actuality however we must replace K with an integrated absorption coefficient which is a function of frequency. We have therefore that

$$\int \alpha(\nu)d\nu = N_{v,J} B_{v,J}^{v',J'} h\nu \ . \tag{53}$$

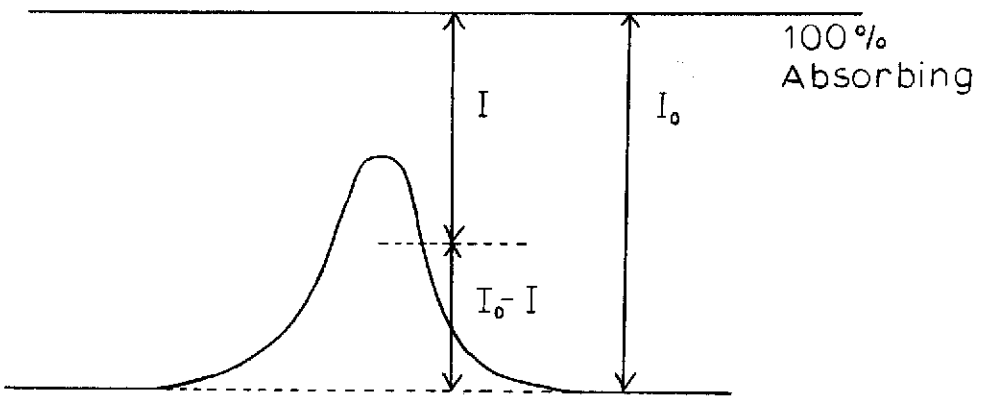

The exponential law of absorption can be reapplied to the finite width lines with which we must deal and becomes

$$I(\nu) = I_o e^{-\alpha(\nu)\ell} \text{ or}$$

$$\frac{I(\nu)}{I_o} = e^{-\alpha(\nu)\ell} \ , \tag{54}$$

where we have assumed that I_o is independent of ν. If the product

$\alpha(\nu)\ell$ is small the right side of (54) can be expanded keeping the first two terms so that

$$\frac{I(\nu)}{Io} = 1-\alpha(\nu)\ell \ .$$

Solving for $\alpha(\nu)$ and integrating over the spectral line then

$$\int \alpha(\nu)d\nu = \ell^{-1} \int \frac{Io-I(\nu)}{Io} \, d\nu \ . \tag{55}$$

If the above approximation holds then it is said that the observed absorption is linear. Inspection of (55) shows that the observed spectral profile is directly proportional to the absorption coefficient curve if we disregard any instrumental distortion. If the product $\alpha(\nu)\ell$ is not small however then using (54)

$$\ln \left(\frac{I(\nu)}{Io}\right) = -\alpha(\nu)\ell \ .$$

Again solving for $\alpha(\nu)$ and integrating over ν

$$\int\alpha(\nu)d\nu = -\ell^{-1} \int \ln \left(\frac{I(\nu)}{Io}\right) \, d\nu \ . \tag{56}$$

The observed curve is no longer the absorption coefficient curve but is related through the logarithm of the fractional absorption. If we let

$$A = \ell \int \alpha(\nu)d\nu \ ,$$

where A is called the integrated absorption, then using (53) and (56)

$$A = \ell N_{v,J} B_{v,J}^{v',J'} h\nu = - \int \ln \left(\frac{I(\nu)}{Io} \right) d\nu \ .$$

The integral on the right is measured from the observed curve; let us now expand the terms in the middle expression into physically observable parameters. N_{vJ} is the number of molecules per unit volume in the initial state and was shown in Section 2.4 to be

$$N_{v,J} = N_J = N f_J \ ,$$

where N is the total number of molecules per unit volume and f_J is the Boltzmann factor also defined in Section 2.4. $B_{v,J}^{v',J'}$ is the Einstein probability of absorption and is given by

$$B_{v,J}^{v',J'} = \frac{8\pi^3}{h\ c} S_{v,J}^{v',J'} \Big|_{\parallel \text{or} \perp} \ .$$

Here $S_{v,J}^{v',J'} \Big|_{\parallel \text{or} \perp}$ are the strength factors calculated in Section 2.2 which contain the squared dipole moment integrals and the electric field squared. If we let

$$S_{v,J}^{v',J'} \Big|_{\parallel \text{or} \perp} = \mathcal{S}_{v,J}^{v',J'} \Big|_{\parallel \text{or} \perp} E^2 \ ,$$

then

$$B_{J,\nu}^{J',\nu'} = \frac{8\pi^3}{h^2 c} \mathcal{S}_{v,J}^{v',J'} \Big|_{\parallel \text{or} \perp} E^2 \ .$$

A factor of three in the denominator is usually included in this expression in other experiments. This factor of 3 results from averaging over the polarization direction of the incident radiation. Since only one direction of polarization is used in this experiment for intensity measurements then

$$A_{v,J}^{v',J'}\Big|_{\parallel \text{or} \perp} = \frac{8\pi^3}{hc} NE^2 \ell f_J \oint_{v,J}^{v',J'}\Big|_{\parallel \text{or} \perp} \nu \ .$$

The number of molecules per unit volume in the initial state is given by

$$N = \frac{n}{V} \ ,$$

where n is the total number of molecules. The ideal gas law holds approximately for H_2 and other light molecules even for pressures as high as 450 p.s.i. so that

$$N = \frac{p}{KT} \ .$$

The final form of the integrated absorption is

$$A_{v,J}^{v',J'}\Big|_{\parallel \text{or} \perp} = \frac{8\pi^3}{hc} \frac{PE^2\ell}{KT} f_J \oint_{v,J}^{v',J'}\Big|_{\parallel \text{or} \perp} \nu = -\int \ln \left[\frac{I(\nu)}{Io}\right] d\nu \ . \quad (57)$$

A is in units of cm^{-1}.

P is in units of dynes/cm^2.

E is in units of statvolts/cm.

ℓ is in units of cm.

$\mathscr{g}$ is in units of cm^6.

ν is in units of cm^{-1}.

T is in units of °K.

2.6 Dicke-Doppler Width

The Doppler contribution to the width of the spectral lines run in this experiment is according to a classical calculation

$$\Delta\nu_c = \frac{2\nu}{c}\left[\frac{2KT\ln 2}{m}\right]^{1/2} .$$

where $\Delta\nu_c$ is the full Doppler width in cm^{-1} at half maximum intensity, ν is the frequency of the spectral line also in cm^{-1}, m is the mass of the molecule and T is the absolute temperature. K and c are constants and are Boltzmann's constant and the speed of light respectively. Classically therefore the Doppler width is independent of the gas pressure. A quantum mechanical derivation of the Doppler contribution to the width of a spectral line is quite different. For instance the derivations of Dicke (9) and Gersten and Foley (10) show that in the limit that the mean free path of the molecule is much less than the wave length of light, the Doppler width of a spectral line is

$$\Delta\omega_o = \frac{2}{3}\tau_o^{-1}(\bar{\ell}/\lambda\!\!\!^{-})^2 . \qquad (58)$$

In this equation $\Delta\omega_o$ is the full width at half maximum intensity expressed as an angular frequency. τ_o is the mean time between collisions, $\bar{\ell}$ is the mean free path of the molecule between collisions and $\lambda\!\!\!^{-} = \lambda/2\pi$

where λ is the wave length of the spectral line. The condition that the mean free path is much less than the wave length is certainly met since for H_2 where $\lambda = 2.4\times10^{-4}$cm($Q_1(1)$ spectral line), the mean free path is about 3.8×10^{-6}cm at 20 atmospheres. If we express (58) in terms of wavenumber units and let $\tau_o^{-1} = f_c$, the collisional frequency, then

$$\Delta\nu_D = \frac{4\pi f c \ell^2 \nu^2}{3c} ,$$

where $\Delta\nu_D$ is the full width at half maximum intensity and is called the Dicke-Doppler width. The collisional frequency is approximately

$$fc \approx N\bar{v}\sigma ,$$

where N is the number density, $\bar{v}$ is the average velocity of the molecules and σ is the collisional cross section. The average velocity $\bar{v}$ is

$$\bar{v} = \left(\frac{3KT}{m}\right)^{1/2} .$$

The mean free path can be expressed as the distance a molecule travels in time t divided by the number of collisions which occur in that time,

$$\bar{\ell} = \frac{\bar{v}t}{f_c t} = \frac{1}{N\sigma} .$$

Therefore

$$\Delta\nu_D = \frac{4\pi\nu^2}{3cN\sigma}\left(\frac{3KT}{m}\right)^{1/2} .$$

In this calculation we see that the width of the line is inversely proportional to the pressure at constant temperature, since the number

density is proportional to the pressure. Hence the greater the pressure, the smaller the Doppler contribution to the line width will be. The Dicke-Doppler width calculated for the conditions and spectral lines used in this experiment are shown in Table VI. The Doppler contribution is seen to be small compared to the width of the lines encountered which were on the order of .050cm^{-1} wide, and is therefore neglected in line width considerations.

The calculated values are rough calculations using a cross sectional area derived from the hard sphere diameter which for H_2 is 2.61×10^{-8}cm. The hard sphere diameter of D_2 was assumed to be about the same as for H_2. Since the Dicke-Doppler width is inversely proportional to the collisional cross section a larger cross section obtained by the inclusion of interacting fields would only decrease the width calculated here. The values calculated therefore comprise an upper limit to the expected Dicke-Doppler contribution.

TABLE VI

DICKE-DOPPLER LINE WIDTHS AT 300°K

Pressure (Amagats)	Width of $Q_1(1)$[1] of H_2 (cm^{-1})	Width of $Q_1(1)$[2] of D_2 (cm^{-1})
7.07	.0052	.0019
10.12	.0035	.0013
13.17	.0026	.0010
16.20	.0021	.0008
19.22	.0017	.0006
22.23	.0015	.0006
25.23	.0013	.0005
28.21	.0012	.0004
31.19	.0010	.0004

[1]Classical Doppler Width = .0363 cm^{-1}

[2]Classical Doppler Width = .0185 cm^{-1}

CHAPTER III

EXPERIMENTAL APPARATUS AND TECHNIQUES

3.1 Stark Cell

The Stark cell shown in Figures 2 and 3 contains the sample gas at high pressure between two parallel and highly reflective condenser plates. A large d.c. potential is maintained across the plates to provide a strong electric field in the sample gas. The condenser plates are ground steel held in a parallel plate arrangement by plexiglas holders. The plates are two inches wide and one-half inch thick with all edges rounded to minimize high local fields and the resulting corona and electrical breakdown. The plates are coated with a reflective nickel plating to transmit light as efficiently as possible by multiple reflections the length of the plates. The plates used in this experiment were 22-7/8" long and were held .067" apart by the plexiglas holder with no spacers between the plates. Many previous cells of this type used spacers between the plates. According to Boyd (11 and 12) these spacers limit the field which can be applied across the gas. The plates used in this experiment are the same that were used in previous work. The plates were badly pitted due to frequent breakdown and were re-ground and gold plated.

The optical quality of the gold plating was far superior to the original nickel plating which was ground off but the strength of the plating was not equal to the task of withstanding the breakdown which

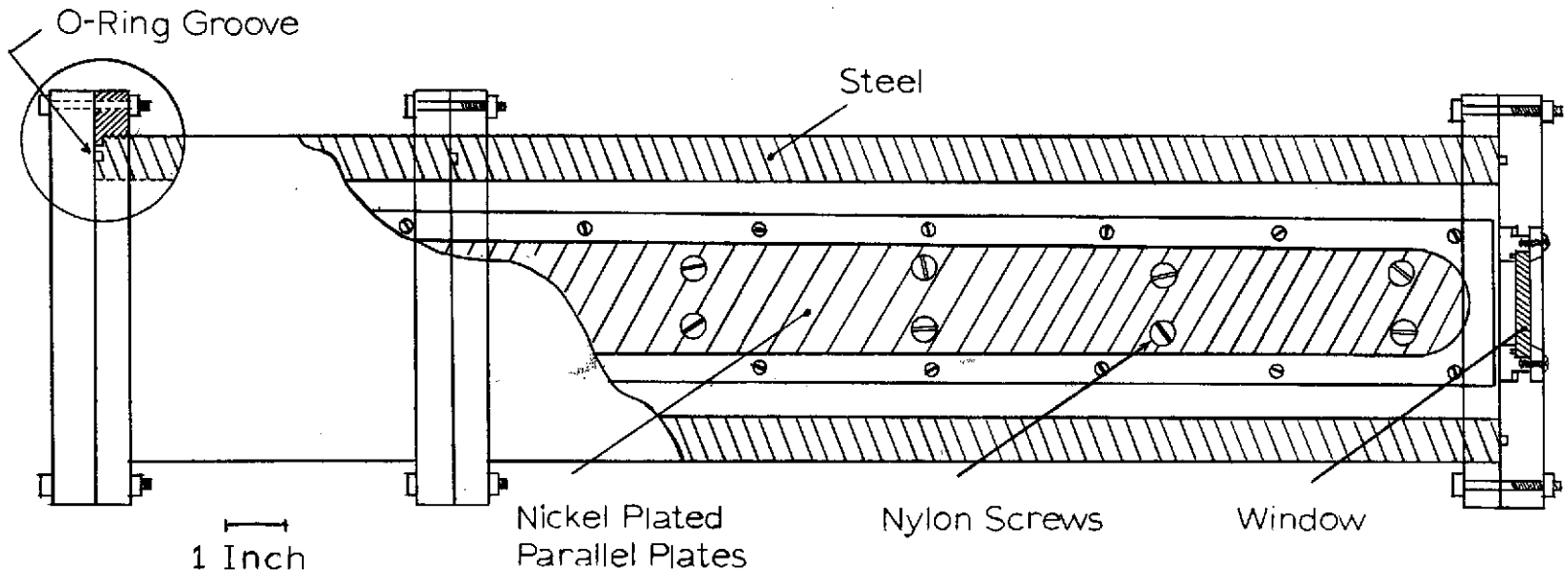

Figure 2. High Pressure Stark Cell

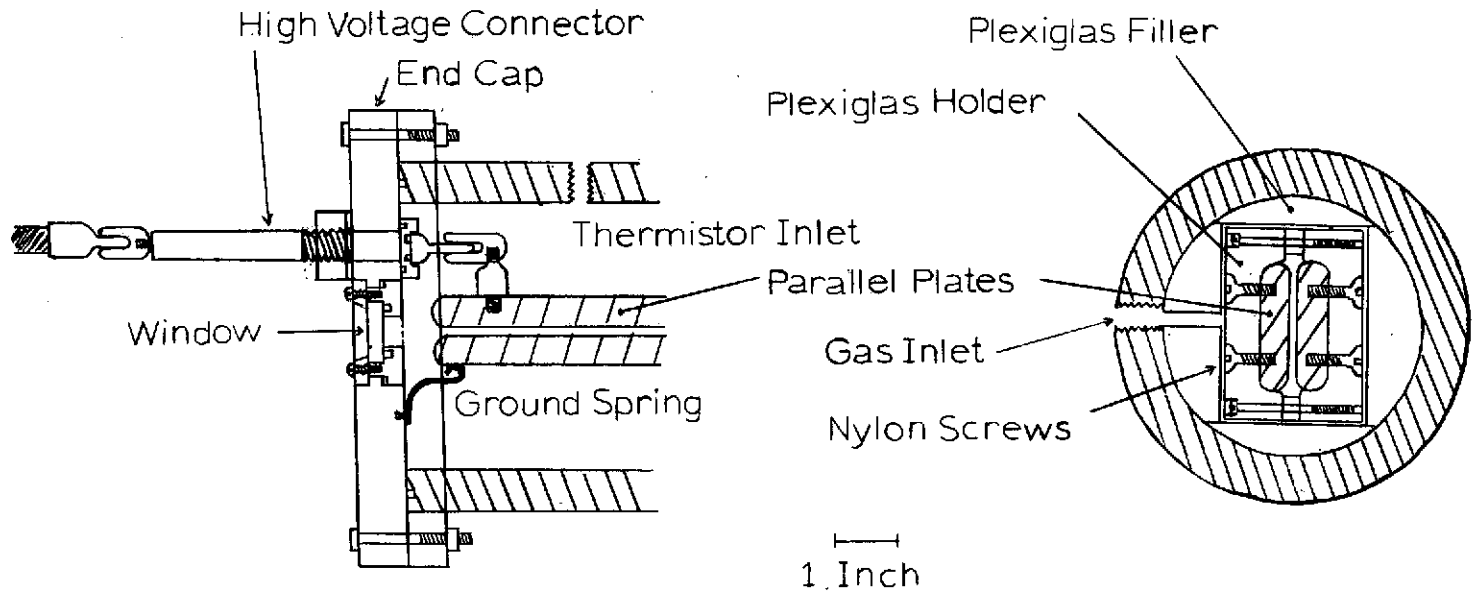

Figure 3. End Cap Detail and Cross Sectional View

either accidentally or purposely occurs. The gold plating was observed to be penetrated completely in several places by the breakdowns and left sharp edges which limited the field. The gold plating was removed and a new nickel plating was deposited which was of much better optical quality than the original nickel plating. As before "aging" the plates by breaking them down purposely appreciably increases the field which can be maintained between the plates. This process apparently burns off dust and high spots on the plates. The plates are held parallel by a plexiglas holder, and nylon screws thru the holders into the plates hold them in place. The plate spacing was at one time increased to .075" to improve the transmission of the cell. This was decreased again due to the problems encountered in the higher potential required to maintain the same electric field across the wider spacing. The plate spacing was measured by placing a small bit of wax between pieces of aluminum foil at several places on the plates which are then clamped together. The flattened pieces can then be measured with a micrometer to obtain the plate separation and its variation. The plate separation measured in this way was .067" ± .001". The entire plate assembly slides into the high pressure cell in a rectangular space created by cementing plexiglas fillers in the cell. These spacers also serve to reduce the unneeded volume of the cell. The cell is evacuated and filled through an inlet in the cell body. A valve is also fitted to the cell body to allow flushing.

The cell body is made from thick wall steel pipe 3/4" thick. This is thicker than necessary to withstand the maximum 450 p.s.i. pressure

used but is used to provide adequate room for O-ring grooves which seal the different lengths of the cell together. The cell is made in sections which can be interchanged to give different cell lengths. The thick wall pipe also provides adequate rigidity to the cell since it is bolted to the spectrometer at one end and must support its own weight.

The end caps are 3/4" thick brass and contain the windows and high voltage connections to the plates. The windows were a continuing problem until the present solution was found. Originally very thick (5/8") windows were seated in a bed of silicone rubber in recesses in the end caps. It was found, however, that the windows bent under the high pressure and pulled away from the gasket material creating a leak. The end caps were changed to accept a much smaller and therefore thinner window sealed with an O-ring. These windows, however, broke when the cell was pressurized. It was discovered with the aid of a dial indicator that the center of the 5/8" thick, original end caps bowed .020" in the center under 400 p.s.i. pressure. This, of course, would bend the rigidly held windows until they broke. New end caps of 3/4" thick brass were made with window holders which "float" with the applied pressure. The window holder holds the window rigidly sealed against an O-ring and the holder itself is sealed against a second O-ring. However as pressure is applied the window holder simply compresses this second O-ring more instead of bending with the end cap. No windows have been broken with the new holders shown in Figure 4. NaCl and CaF_2 windows were used and are 1/4" x 3/4" x 2".

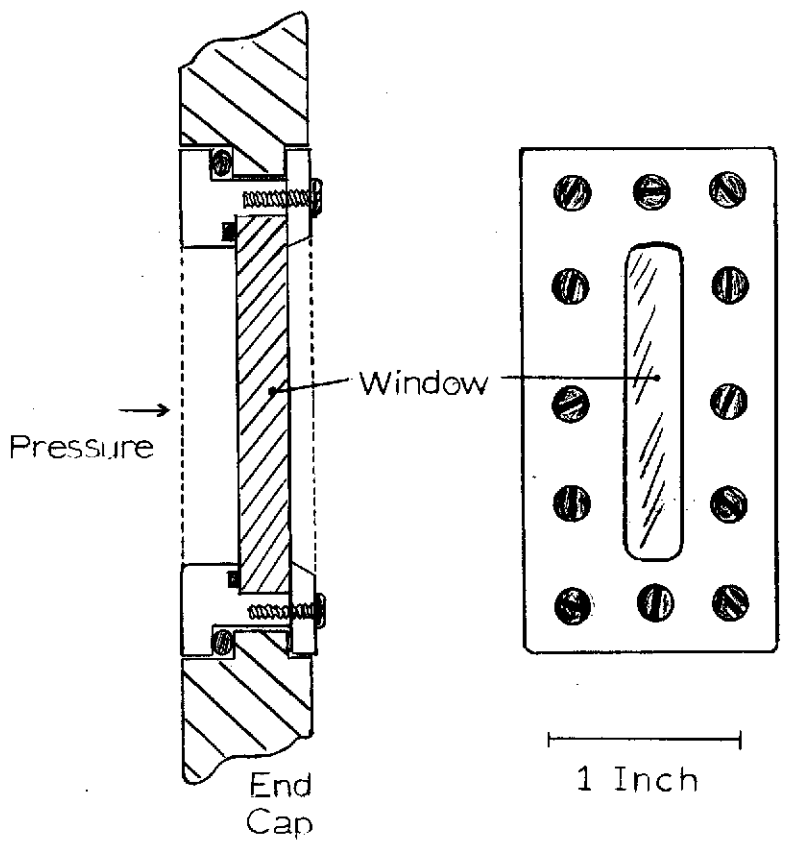

Figure 4. Window Detail

The high voltage connector shown in Figure 5 passes through one end cap and is composed of a machines nylon body sealed with an O-ring. A brass feed-through also sealed with an O-ring carries the voltage into the cell. The connector inside the cell is rounded, as are all metal surfaces inside the cell, and plugs into a socket connected to one of the plates. The other plate is grounded to the cell body by a spring attached to the end cap.

A thermistor was used to monitor the temperature inside the cell. This thermistor was soldered to the end of a feed-through shown in Figure 6. This feed-through was machined from a standard brass fitting and bakelite, and was sealed with epoxy. A bridge circuit with the thermistor as an active element was made and the current in this bridge network was calibrated against a mercury thermometer. The temperature in the cell was on the average 299.8°K and did not vary more than 2°K. In calculations made in this work which involved the temperature, a rounded off value of 300°K was used.

The entire cell is bolted to an access port on the spectrometer using a machined adaptor made for that purpose, and the other end containing the high voltage connection is attached to a flushing cover containing the source optics.

3.2 High Voltage Power Supply

The high voltage supply shown in Figure 7 is used to apply a large static potential across the condenser plates in the Stark cell. The field which can be applied is limited by the dielectric strength of the

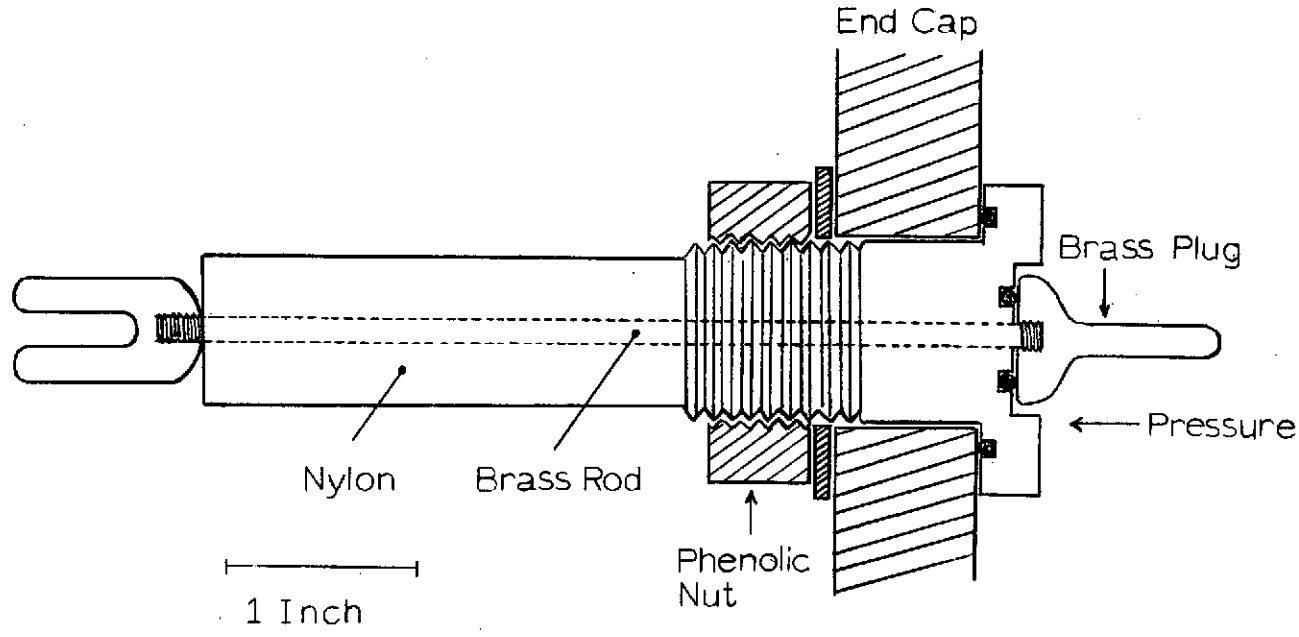

Figure 5. High Voltage Connector

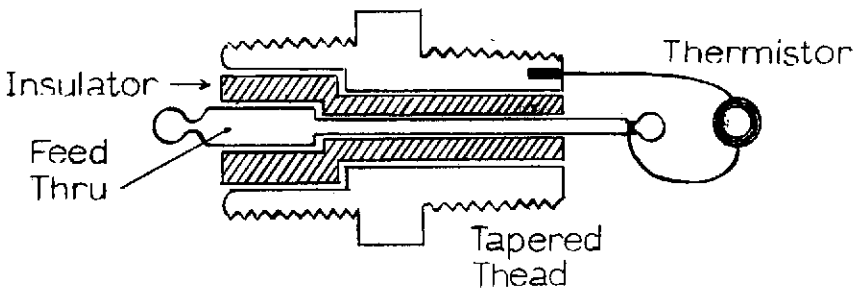

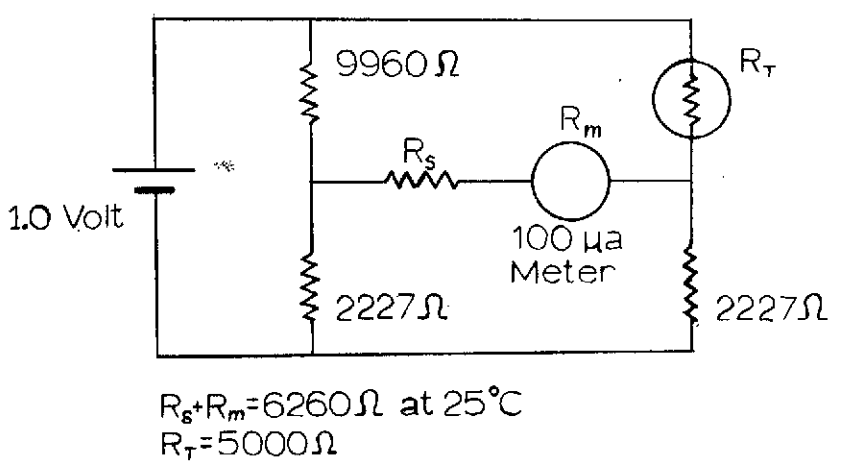

Figure 6. Thermistor Feed-Thru and Circuit

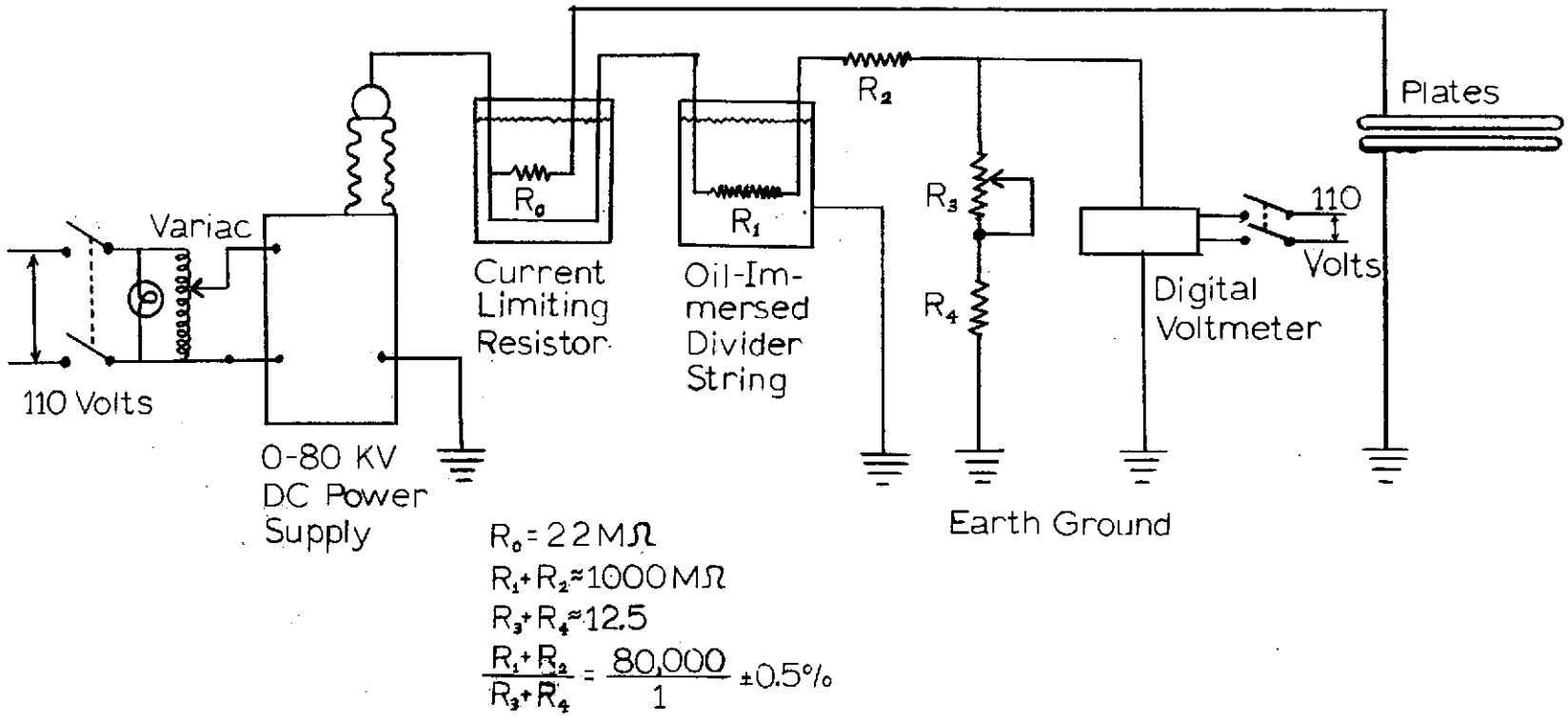

Figure 7. High Voltage Power Supply

compressed gas between the plates. The high voltage is supplied by a large d.c. transformer power supply from Plastic Capacitor. The voltage going to the cell is adjusted by means of a variac on the transformer primary, and is measured through a divider string with a ratio of 80,000 to 1 ± 0.5% and read on a digital voltmeter. The majority of the resistors in the divider string are immersed in oil to prevent corona problems. About 300, 3.3 megohm, 1 watt carbon resistors were soldered together in series and strung between ceramic standoffs in a box filled with transformer oil as seen in Figure 8. The large number of resistors were used to prevent voltage drops across individual resistors which might lead to breakdown across the short physical length of the resistors. The small voltage drop also insures that the wattage rating of the resistors is never approached in the event of cell breakdown since this could change the calibration of the divider string. The voltage is read on a zero to one volt Simpson digital voltmeter. A 22 megohm, one watt resistor is placed in series with the high voltage line leading to the cell to limit the current to less than the five milliampere rating of the power supply in the case of electrical breakdown across the plates. This resistor and the connections leading to the cell and divider string are also immersed in transformer oil to prevent corona problems. Occasionally during breakdowns the wattage rating of the current limiting resistor was greatly exceeded causing the resistor to explode. In this way the resistor also acted as a fuse to protect the power supply. The connection to the cell is made with a brass plug rounded to prevent corona. The dry atmosphere inside the flushing cover

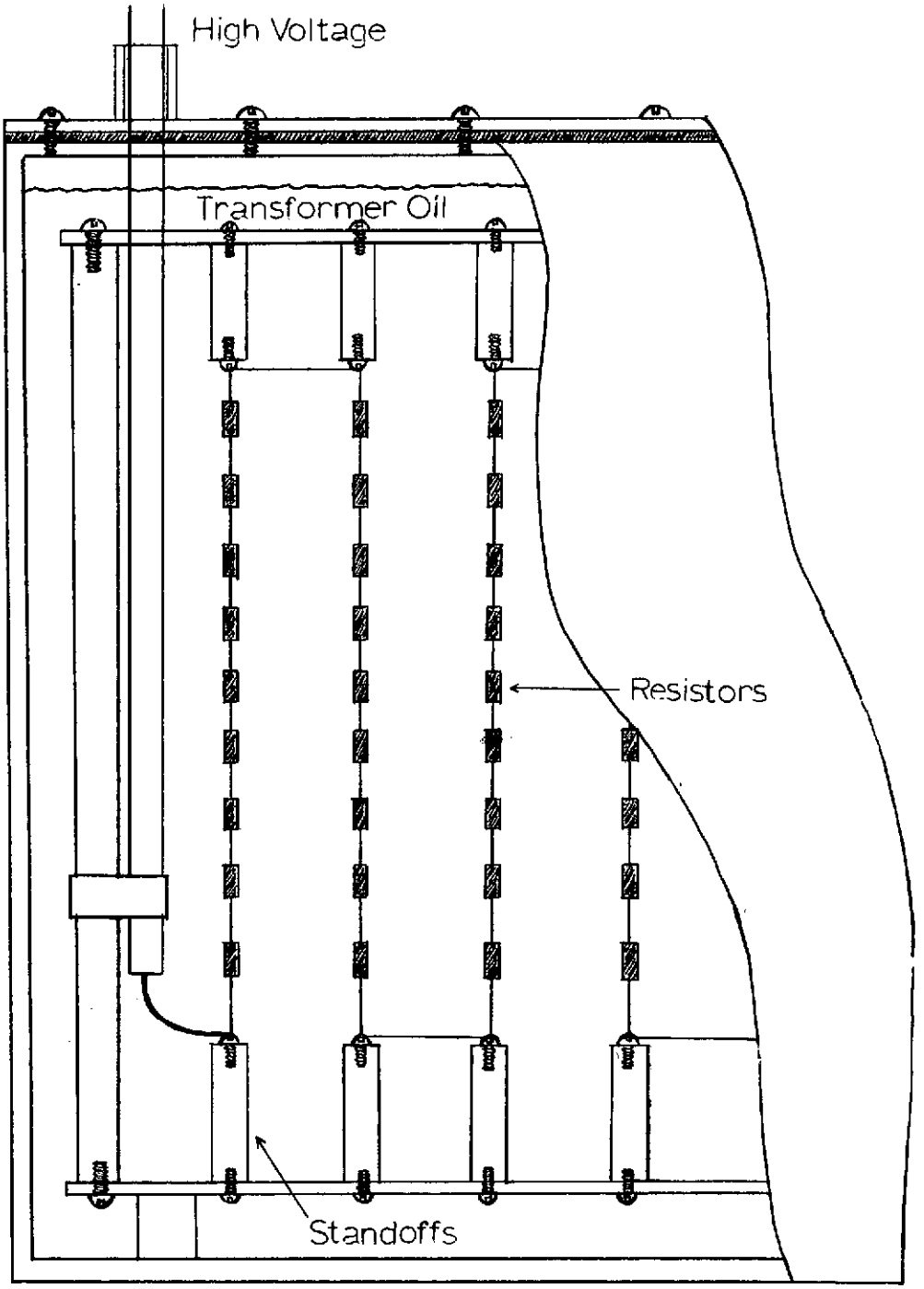

Figure 8. Divider String

also helps with this problem. With the .067" plate spacing the operating potential was about 30,000 volts, corresponding to a field of about 180,000 volts/cm.

3.3 Gas Filling System

The gas filling system shown in Figure 9, is designed to handle the high pressures used in this experiment and is also evacuable. The main manifold is brass, drilled and fitted with adaptors designed to accept large valves, good for pressure or vacuum. A Hastings Gauge thermocouple and mechanical pump are isolated by valves from the manifold when high pressure is being used. A high pressure bourdon type gauge calibrated in two-pound subdivisions can be isolated from the rest of the system if the manifold is being evacuated. Gas lines from the manifold to the cell are 1/4" or 3/16" O.D. to withstand the high pressures. A liquid Nitrogen trap is included in the gas line to the cell. It is of course extremely important to get all the oxygen out of the manifold and cell before operating the reaction chamber or turning on the electric field, which might lead to an explosion. This is accomplished by evacuation and flushing. After the cell is filled, any condensable gases can be removed by the cold trap in the gas line to the cell if H_2 or D_2 is being used. It was found that N_2 liquefies at 400 p.s.i. in a liquid Nitrogen trap which prevents its use in this case.

The N_2, H_2 and D_2 used in this experiment were from Matheson Gas Co., and the stated purity was 99.99% for N_2 and 99.9% for H_2 and D_2.

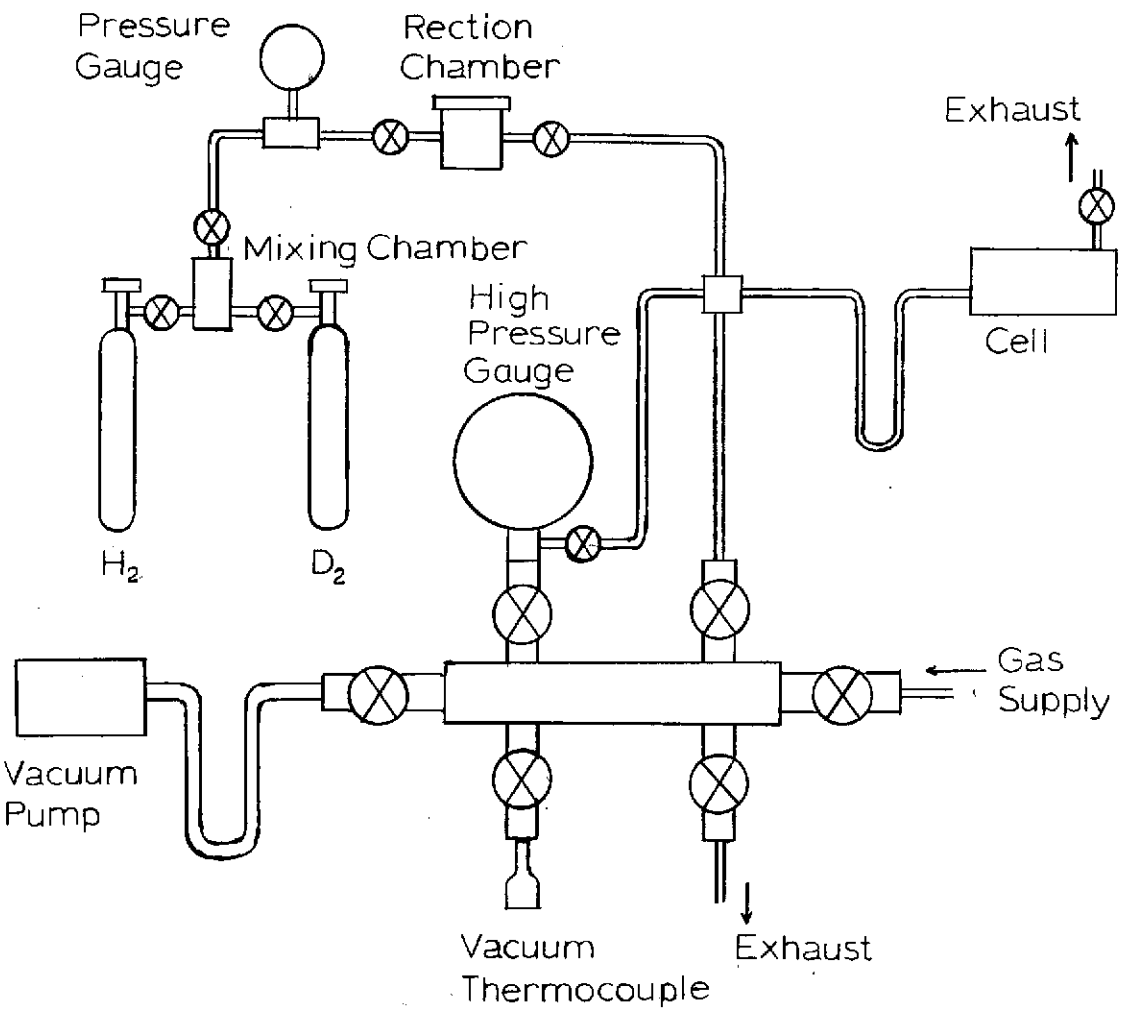

Figure 9. High Pressure Gas Filling System

A small secondary manifold was constructed to mix H_2 and D_2 and to contain a heated platinum wire to attempt to convert the mixture partially to HD. The mixing chamber consists simply of a common chamber into which H_2 and D_2 are admitted simultaneously from lecture bottles of equal volume and pressure. This is released at 400 p.s.i. into a reaction chamber shown in Figure 10. The reaction takes place via a heated platinum wire. The reaction chamber is stainless steel and is sealed with a teflon gasket. Teflon is used instead of an O-ring since silicone grease used on an O-ring will "poison" a platinum wire and render it almost inactive. Four feet of platinum wire .005" in diameter is wrapped around ceramic insulators and is connected to a variac through small glass feed-throughs. 15 volts at 1.1 amps are used to heat the wire. The gas is valved off in the reaction chamber and kept there for 25 minutes while the platinum wire is heated, before being passed to the cell. This procedure is repeated until the cell is pressurized. The platinum wire was obtained from the Poly Research Corporation.

The equilibrium constants for the reaction is according to Hill (13) given by the equation

$$H_2 + D_2 \rightleftarrows 2HD$$

is according to Hill (13) about 3.5, so that if the reaction goes to equilibrium the final mixture of gases should contain almost 50 percent HD. At 445 p.s.i. total pressure this would correspond to a 215 p.s.i. partial pressure of HD which should be observable. Observation of the partial pressures of H_2 and D_2 in the gas mixture indicated approximately equal parts of each but far more than would be expected if the reaction

Page intentionally left blank

had gone to equilibrium. No HD absorption lines were observed. It is felt that the high pressures reduced the mean free path to the point that only relatively few molecules came in the vicinity of the platinum wire.

3.4 Carbon Rod Furnaces

Two carbon rod furnaces have been built for use as infrared radiation sources and are shown in Figures 11, 12 and 13. The furnaces consist mainly of a carbon rod held in large copper electrodes through which a very high current is conducted. The resistive heating of the rod causes it to reach a temperature of about 2500°K as measured with an optical pyrometer. This provides usable energy throughout the infrared and since the emmisivity of carbon is close to unity its radiation curve should closely resemble a black body curve. The rod is slotted in the center to increase the resistance of this portion of the rod and therefore increase the temperature. This slotted portion is the part of the rod which is used as a source.

The carbon rods used in the source are spectroscopically pure carbon purchased from Ultra Carbon Inc. and are 5/16" in diameter and 3-3/4" long in the first furnace built and 5/16 by 4-7/8" in the new automatic furnace. The rods are slotted in the center at a length of 1-1/2" in the furnace used in this experiment and 2-1/2" in the other furnace which was made to bolt to the spectrometer. The cross section of the slot is V-shaped and is made with a 60° end mill cutter to a depth of .110". The V-cross section was found to have a longer life than a rectangular cross section slot also tried. Another advantage

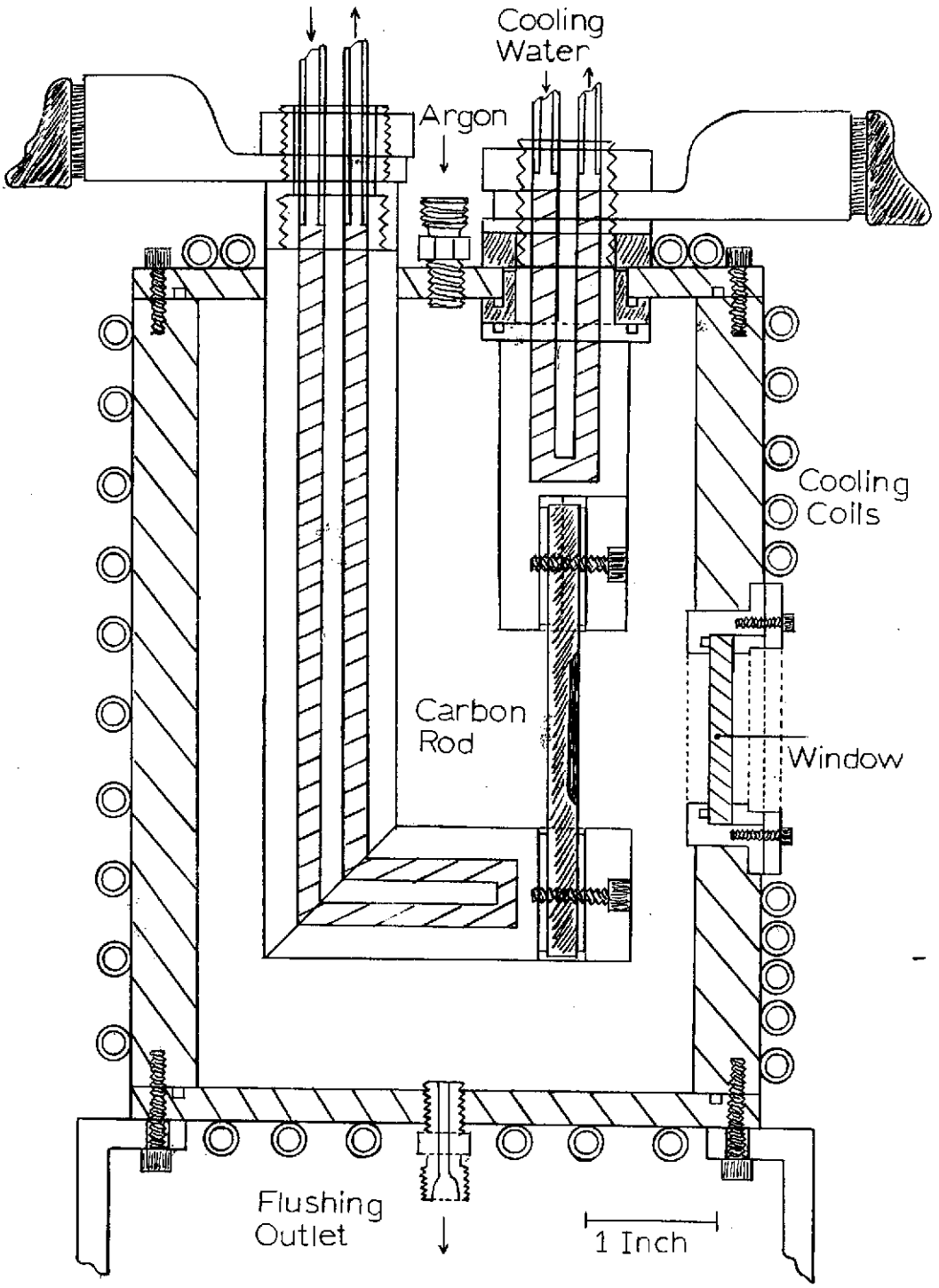

Figure 11. Carbon Rod Furnace

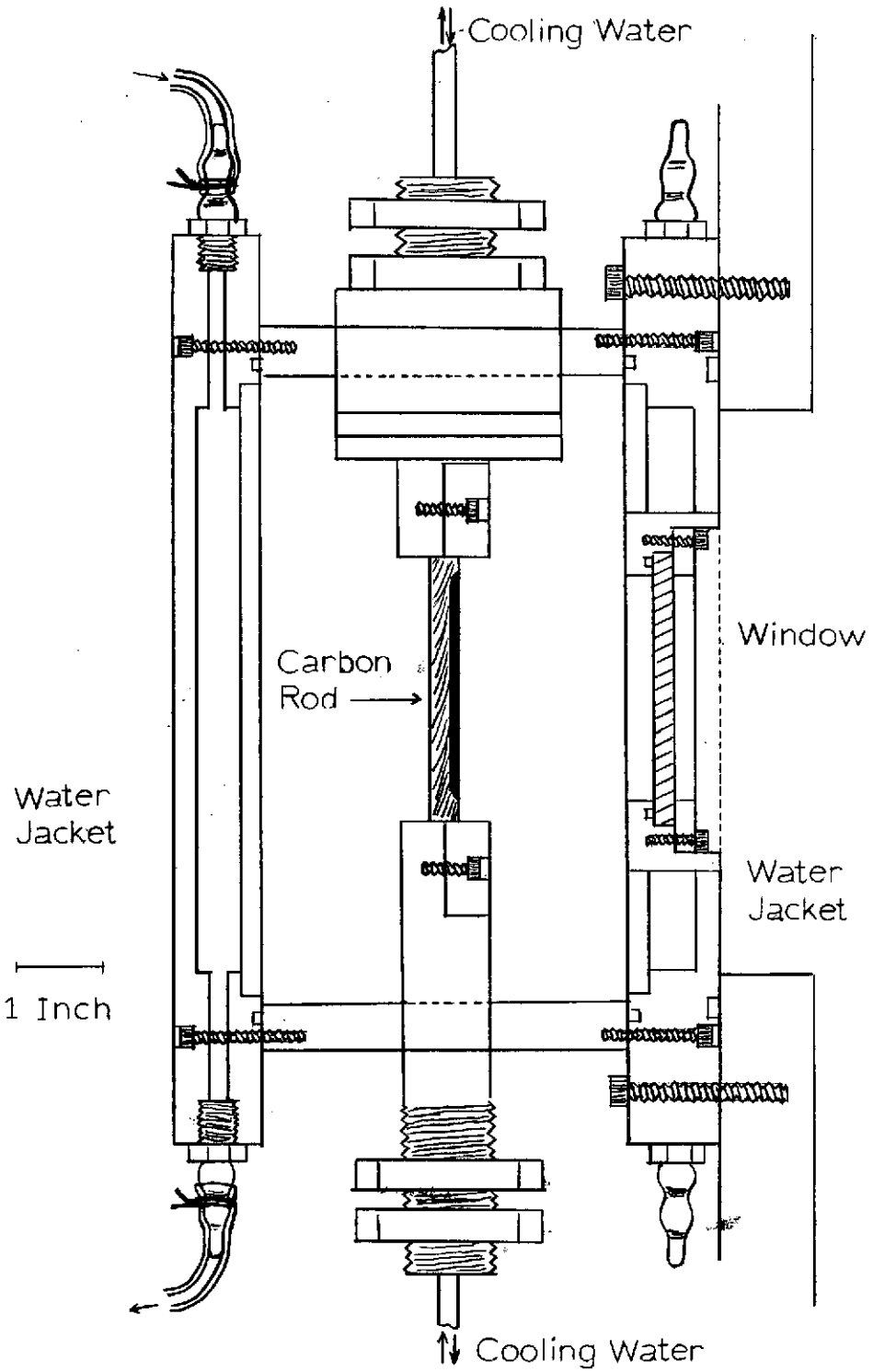

Figure 12. Automated Carbon Rod Furnace Side View

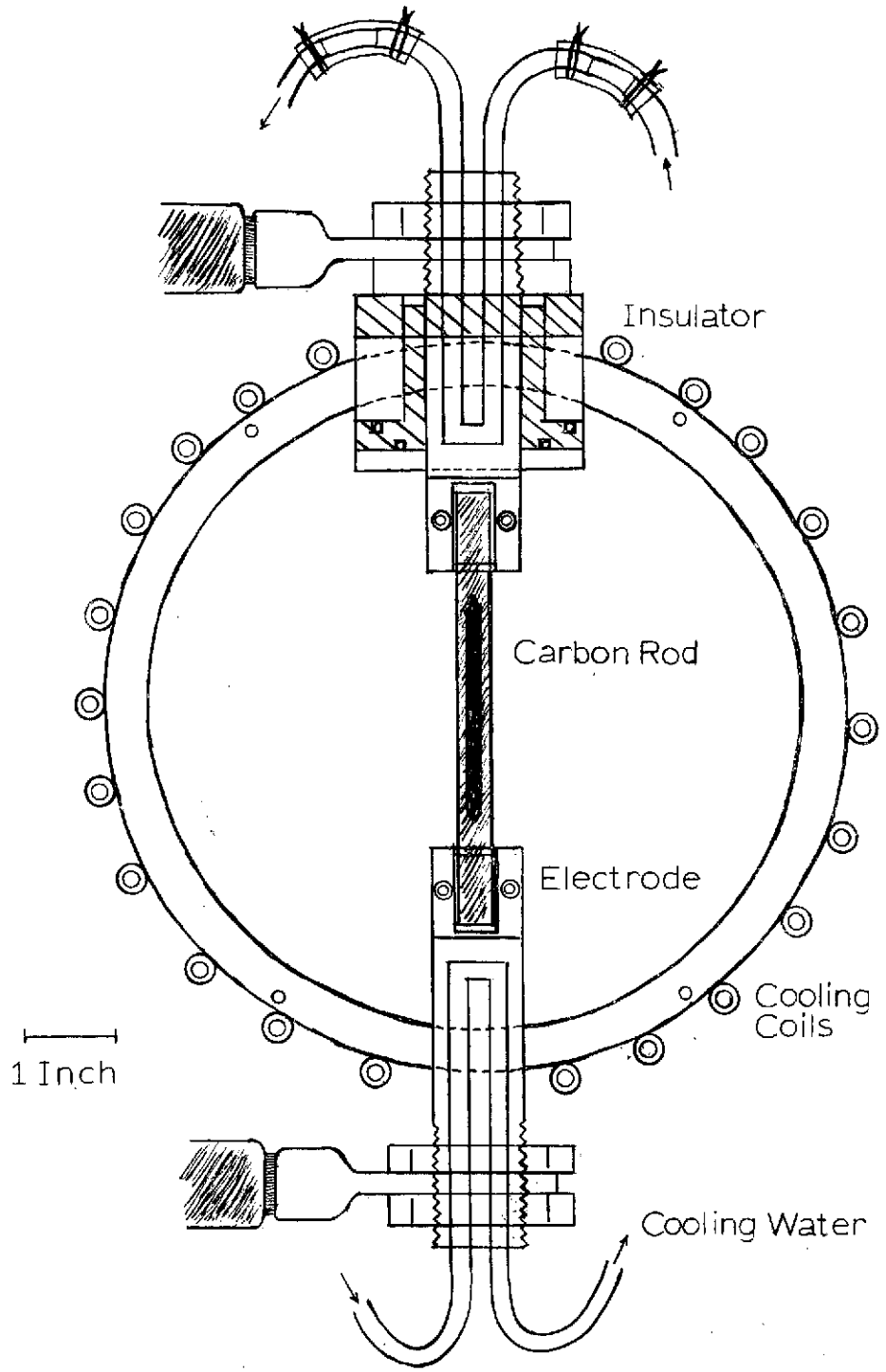

Figure 13. Automated Carbon Rod Furnace Front View

of the V-slot is that a slight misalignment in the rotational placement of the rod in its holder should make no difference.

The rod is held in place by two, one-inch diameter copper electrodes which carry power to the rod. Because of the high temperature of the rod the electrodes are water cooled by means of holes drilled in the electrodes. The entire body of the furnace is also water cooled. In the older furnace this is accomplished with copper tubing soft soldered to the outside of the case and to the top and bottom. In the newer furnace this is also done on the main body of the furnace but the front and back plates have been made hollow to allow water circulation for cooling.

The case is flushed with argon before turning on the furnace and kept at about 5 to 10 p.s.i. positive pressure (gauge) while the rod is operating. The gas line to the argon supply is left open to maintain the pressure against any leaks. Some form of drying agent is used in the gas supply line. Water inside the case drastically shortens rod life as was evidenced by small accidental cooling water leaks. The drying agent also protects the hydroscopic windows used in the furnaces. NaCl and KBr windows have been used and withstand the high temperature very well, as long as no large sudden temperature changes take place.

3.5 Carbon Rod Furnace Power Supplies

Because of the large power requirements 220 volt transformers are used in the carbon rod furnace power supplies shown in Figures 14 and 15. The secondary of the transformer will deliver up to 500 amps at 12 volts. The primary voltage is adjusted by a large variac rated at

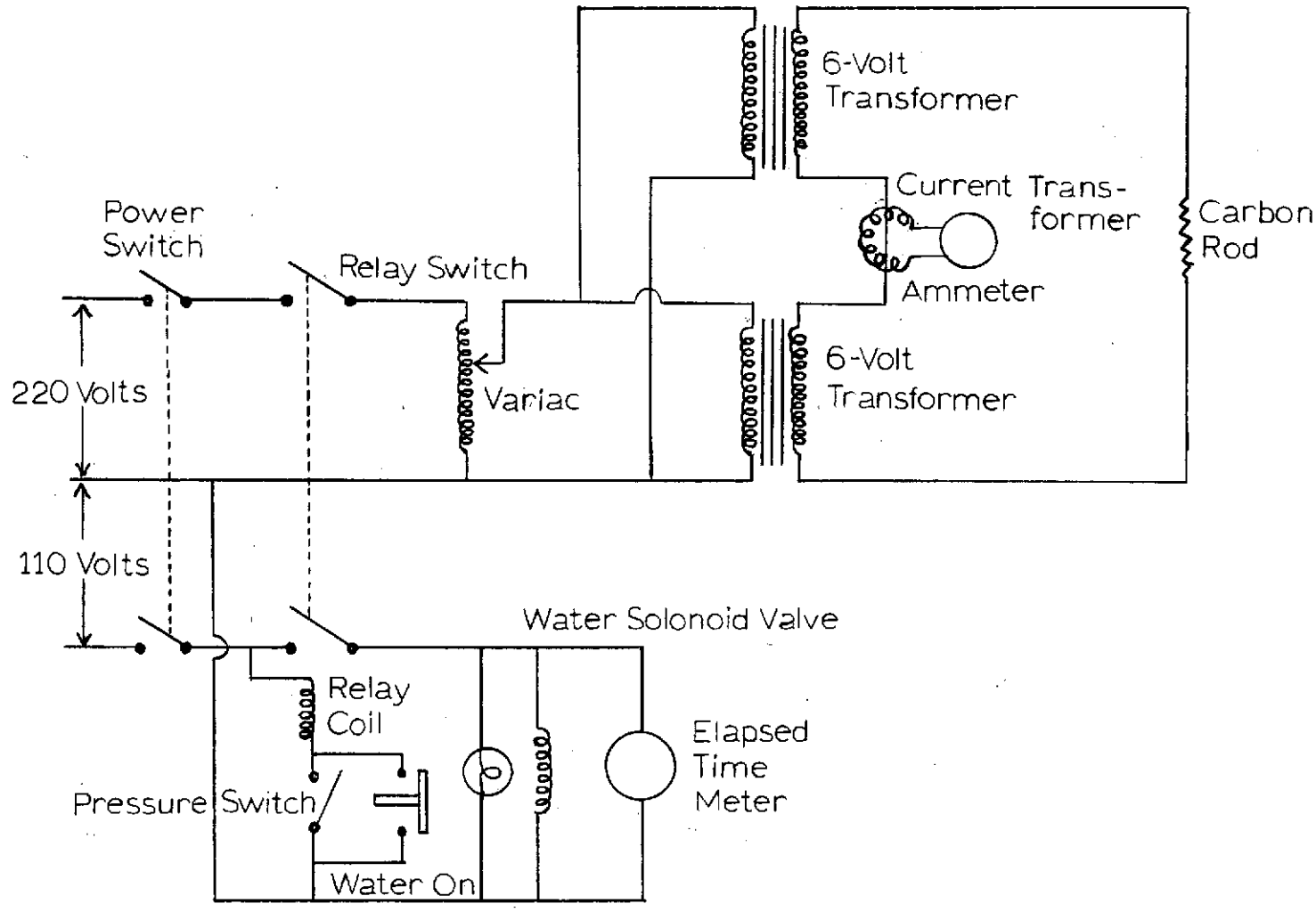

Figure 14. Carbon Rod Furnace Power Supply

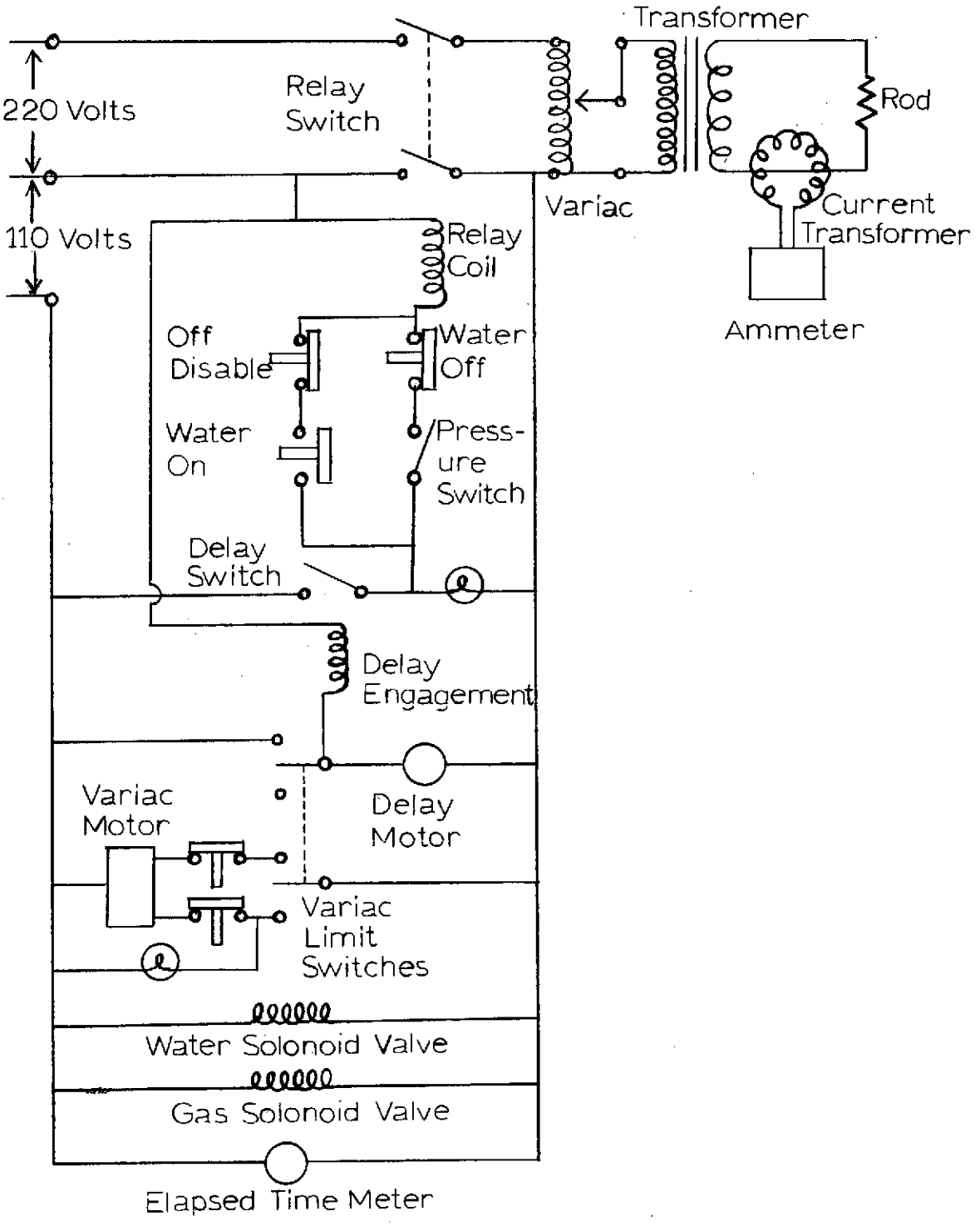

Figure 15. Automated Carbon Rod Furnace Power Supply

25 amps. The current in the secondary is measured by a loop type current transformer and Simpson meter calibrated to read 500 amps full scale. The furnace is normally operated at 400 amps.

A safety feature included in both power supplies automatically turns off the power to the rod in case the cooling water is turned off or drops significantly in pressure while the furnace is in operation. Also the rod cannot be heated without turning on the water. This is accomplished by passing the primary current through a large normally open relay before going to the transformer. The relay coil closing this relay switch can be energized only if a diaphragm type pressure switch is held closed by the cooling water pressure. The pressure switch is placed in the exhaust water to insure that a broken or leaking line anywhere in the series of cooling lines will open the relay and shut off power to the rod before any damage can occur to the furnace. To prevent excessive water from being spilled in case of a water line leak or breakage the pressure switch also controls a solenoid in the water supply line which shuts off the water supply. A bypass around the pressure switch is necessary to initially set the system.

The current to the rod is increased and decreased slowly by means of the variac to prevent thermal shock to either the carbon rod or the furnace windows. About 15 minutes is sufficient time to turn the furnace up to 400 amps.

The newer power supply has been automated so as to free the operator from the tedious chore of turning the current up and down slowly. This was accomplished by attaching a properly geared down motor with a chain

drive to the variac shaft. Microswitches limit the variac travel to the proper current. So to turn the furnace on, it is necessary only to throw a switch which delivers power to the variac motor after the bypass button is depressed to initially set the pressure switch. To turn the furnace off the switch is reversed which reverses the variac motor. A timer mechanism is then automatically actuated which shuts off power to the relay coil after the variac motor has had sufficient time to turn the current down. Changing a rod in either furnace is a fairly rapid process. After the power is turned off the access flange is removed and four Allen screws are removed to replace the rod which is pressed into a copper collar at each end of the rod to provide good contact between the rod and the electrode. Periodic cleaning of the contact surfaces is necessary to maintain good contact. Poor contact results in a very eratic and lower rod current. The surfaces inside the furnace should also be wiped off periodically. These surfaces become coated with a carbon film and there is some evidence that this film conducts some current away from the insulated electrode to the grounded case. This was observed on one occasion on the newer furnace after it had not been cleaned for some time. The source was noticeably dimmer at the regular operating current. After cleaning off the accumulated carbon film, the original light intensity was recovered. This was confirmed by temperature measurements with an optical pyrometer. Often when a rod breaks arcing across the break will occur. This accelerates the deposit of the carbon film and can quickly cause a decrease in the intensity of the light if it is not removed.

3.6 Flushing Cover

The flushing cover is a sheet metal box enclosing the source optics which is sealed and used to flush atmospheric gas from the source to the cell. The flushing cover is attached with machine screws to a table built to hold the source optics and is sealed with silicone rubber cement and Apeazion-Q. A sealable plexiglas access port allows working inside the flushing cover. An ordinary light bulb, switched on and off from outside the flushing cover, is kept inside near the hydroscopic window of the carbon rod furnace. This light serves to illuminate the interior of the cover for working inside and also keeps the temperature of the window above the ambient temperature of the surroundings and reduces condensation of atmospheric water on the window when the flushing cover is not purged.

Nitrogen is used to flush the atmospheric gas from the flushing cover. The nitrogen is kept at a slight positive pressure to keep unwanted gases from re-entering the cover when it is not purged.

Nitrogen is used to flush the atmospheric gas from the flushing cover. The nitrogen is kept at a slight positive pressure to keep unwanted gases from re-entering the cover since it leaks slowly. The pressures used are up to 10 inches of water (less than 1/2 p.s.i.). Because this low pressure is difficult to regulate from a high pressure gas cylinder and since even a few pounds could exert several hundred pounds total force on the large surface area of the cover, a safety device was installed to limit the pressure to 10 inches of water.

A solenoid operated valve is used in the gas line leading to the flushing cover. The solenoid is normally closed and is therefore "fail safe" in case of a power failure. A variable diaphragm type pressure is actuated by the pressure inside the cover and is set to open at 10" of water cutting off the power to the solenoid and shutting off the gas supply. When the pressure falls below 9" of water the gas line is re-opened. Since the solenoid opening and closing causes noise transients in the electronics, the pressure is kept below 9" of water so that the solenoid remains open, unless the pressure accidentally exceeds 10" of water.

Several other devices are used in addition to flushing for removing water and carbon dioxide from the light path. Two open containers of sodium hydroxide and alumina are kept in the flushing cover. Sodium hydroxide absorbs water and carbon dioxide and alumina absorbs water. In addition to these chemicals, another device for removing condensable gases has been installed. A cold trap of 3/4" copper tubing with a valve at each end is attached to the flushing cover with one end opening through one valve to the interior of the flushing cover and the other opening through the other valve outside the cover. When the valve to the cover is opened and the trap immersed in liquid nitrogen, condensable gases are collected in the trap. If this valve is closed after a few minutes and the liquid nitrogen removed then the gases can be exhausted through the other valve. The gas removed is replaced with nitrogen.

3.7 Spectrometer and Optics

The spectrometer used in this experiment is a high resolution 5-meter Littrow built at the University of Tennessee shown in schematic

in Figure 16. Details of the construction and operation of the spectrometer are given by Jennings (14). The spectrometer is constructed in four separate optical sections, each evacuated. The sample section is designed to hold source optics and sample cells. The Stark cell used in this experiment is bolted to an access port cover outside the spectrometer by means of an adaptor plate made for that purpose. The cell is operated outside of the evacuated spectrometer since the high voltage, high pressure and normal maintenance make it impractical to operate the cell in a vacuum. The access port cover has been stiffened with steel members to prevent any flexing of the port cover and subsequent movement of the cell bolted to it when the sample section is evacuated. O-rings seal the cell to the access port.

The external cell necessitates an external source and source optics. The source used is a carbon rod furnace described in Section 3.5. The source is bolted and sealed with an O-ring to the flushing cover described in Section 3.6. The flushing cover contains the source optics and makes it possible to flush atmospheric gas from the path from the source to the cell which is also bolted and sealed with O-rings to the flushing cover.

The source optics are shown in Figure 17. A cylindrical lens is placed in front of the source and is used to get more light through the Stark cell than would be possible without the lens. Theoretically 50% more light would be possible, in practice about 30% more was achieved in comparison tests. The cylindrical lens is Calcium Fluoride 1-1/2" x2-1/2" with a focal length of 3" and was obtained from John Unertl Inc.

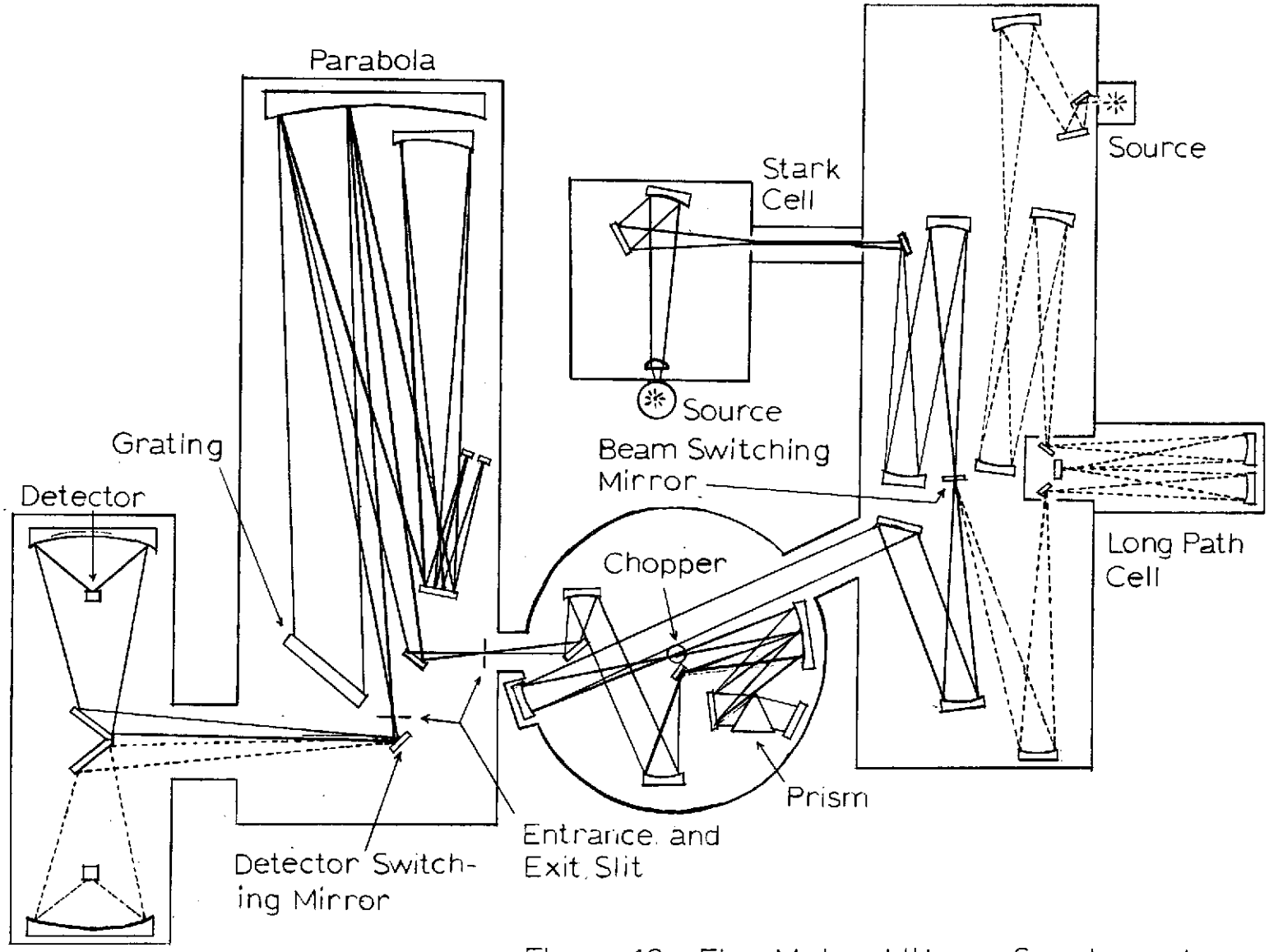

Figure 16. Five Meter Littrow Spectrometer

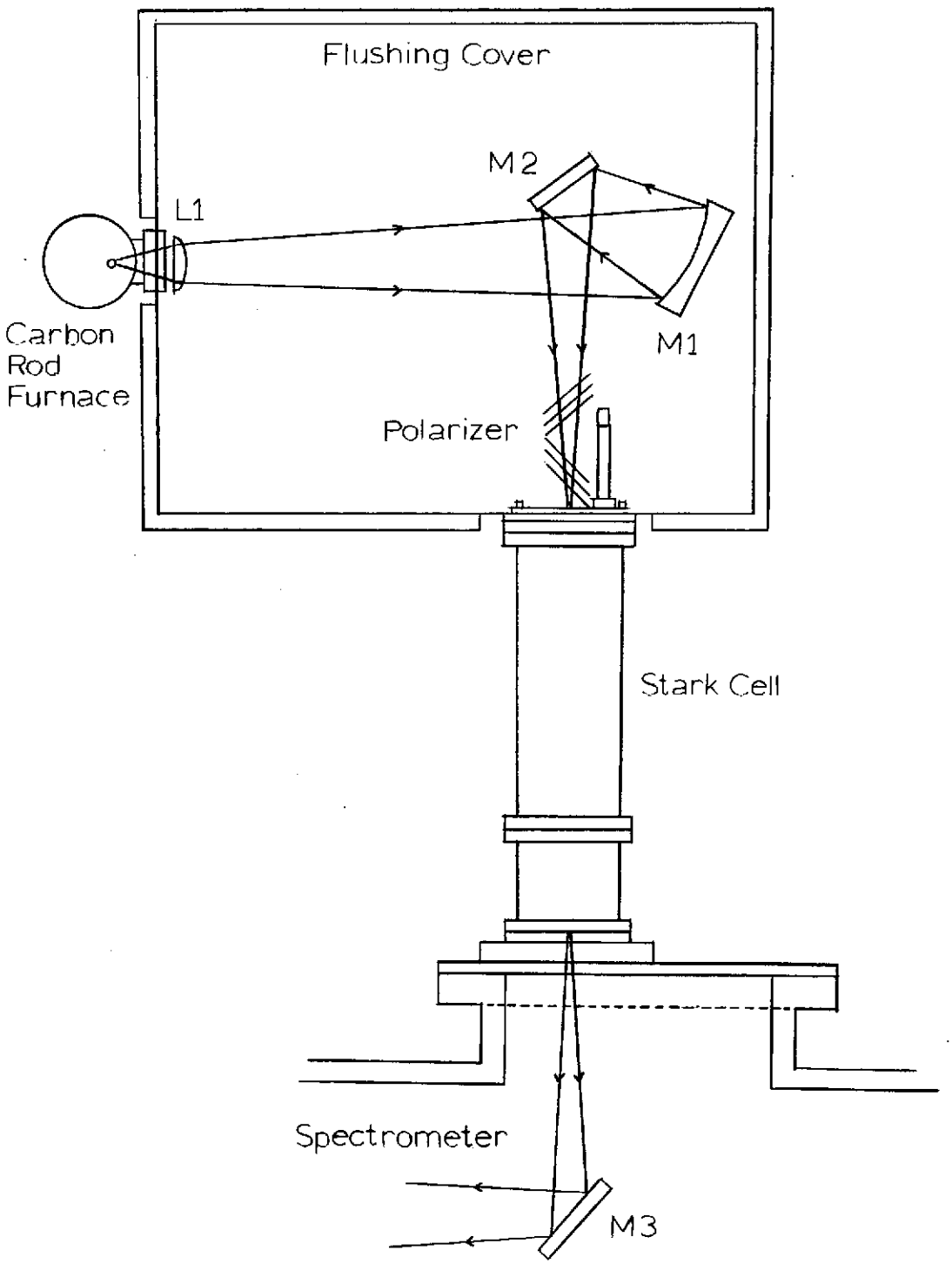

Figure 17. Source Optics and Stark Cell

The lens does not affect the vertical diverging light coming from the source, but reduces the divergence of the horizontal light. The horizontal diverging light striking the focusing mirror (M_1) is focused on the end of the cell, as is necessary in this type cell, but the vertical light is delayed in focusing until the center of the cell. In this way double the solid angle in the vertical direction can be accepted by the cell.

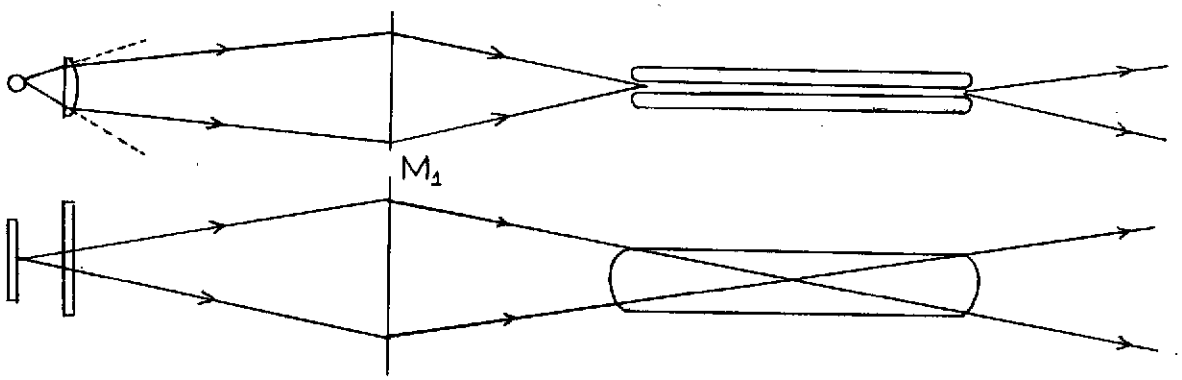

The light from the focusing mirror is directed to the cell via a flat (M_2) which provides the proper distance to the cell for focusing. The light enters the spectrometer and passes through the optics (M_3 to M_5) designed to contain a sample cell. At a focus a mirror (M_6) has been installed on a raising and lowering apparatus. This mirror elevator was adapted from a cell elevator previously used in this laboratory. The mirror is attached to a plate riding in a dovetail track and is driven up and down by a rack and pinion driven by a servo. Microswitches

limit the travel of the mirror. The cycle time was decreased from about a minute to five seconds, and so to slow down and stop the mirror after the driving servo has been turned off by the limit microswitches, springs were installed which stop the mirror very effectively. The slave servo is driven by a master servo outside the spectrometer which is in turn driven by a geared down motor. Thus, only a switch need be activated to move the mirror up or down. The mirror enables either the primary or Stark cell beam to be used. With the mirror up, the light from the primary beam is reflected from the mirror and goes to the prism pre-disperser section. With the mirror down, the light from the Stark cell beam is allowed through and follows the same path through the spectrometer. In this way two experiments can remain set up in the same section. This setup also allows one section to contain an experiment and the other a calibration gas. It is for this purpose that the cycle time was decreased so that only a small amount of information is lost in switching from the experimental beam to the calibration beam. The primary beam contains a long path white cell being used in an experiment but was "borrowed" when calibration lines were needed. Carbon monoxide absorption lines were used for calibration with pressures of only 2 to 5 millimeters needed in the 12 meter path for the overtone band.

The prism predisperser section contains the light chopper described in Section 3.8 and the optics necessary to double pass the prism. Both NaCl and LiF_2 prisms were used. From the prism predisperser the light is passed into the monochrometer and is focused onto the entrance slit.

The monochromator optics are designed to double pass a 10" x 16" grating. Both a 31.6 groove per millimeter and a 79 groove per millimeter grating blazed at 63° and 65° respectively, were used. After passing through the exit slit, the light strikes a mirror which has been mounted on a rotating table made from old spectrometer parts. A slave servo turns a worm gear which turns the table and is linked to an external hand turned servo allowing the table to rotate the mirror so that the light from the exit slit strikes either one of two detectors available in the detector section. Since the angle through which the detector switching mirror turns is very small, the driving servo is turned with a vernier type adjustment to allow fine angular adjustments.

The detector section holds two detector cryostats and detectors. Liquid nitrogen cooled PbS and InSb detectors were used in this experiment. The detectors are from Santa Barbara Research and are contained in vacuum insulated dewars. The dewar pumping system is described in Section 3.9.

3.8 Light Chopper

A barrel type light chopper was designed and constructed and is shown in Figure 18 and 19 and used to chop the radiation reaching the detectors, and to produce a reference signal in synchronization with the radiation chopping frequency for the amplificiation electronics. The chopper barrel has 18 slots and is driven by a 3600 rpm synchronous motor to chop the radiation at 1080 Hertz. The slots are 2-1/2" tall to accommodate the tallest image the spectrometer is designed to accept in this section of the optics. The barrel diameter, the f-number of the

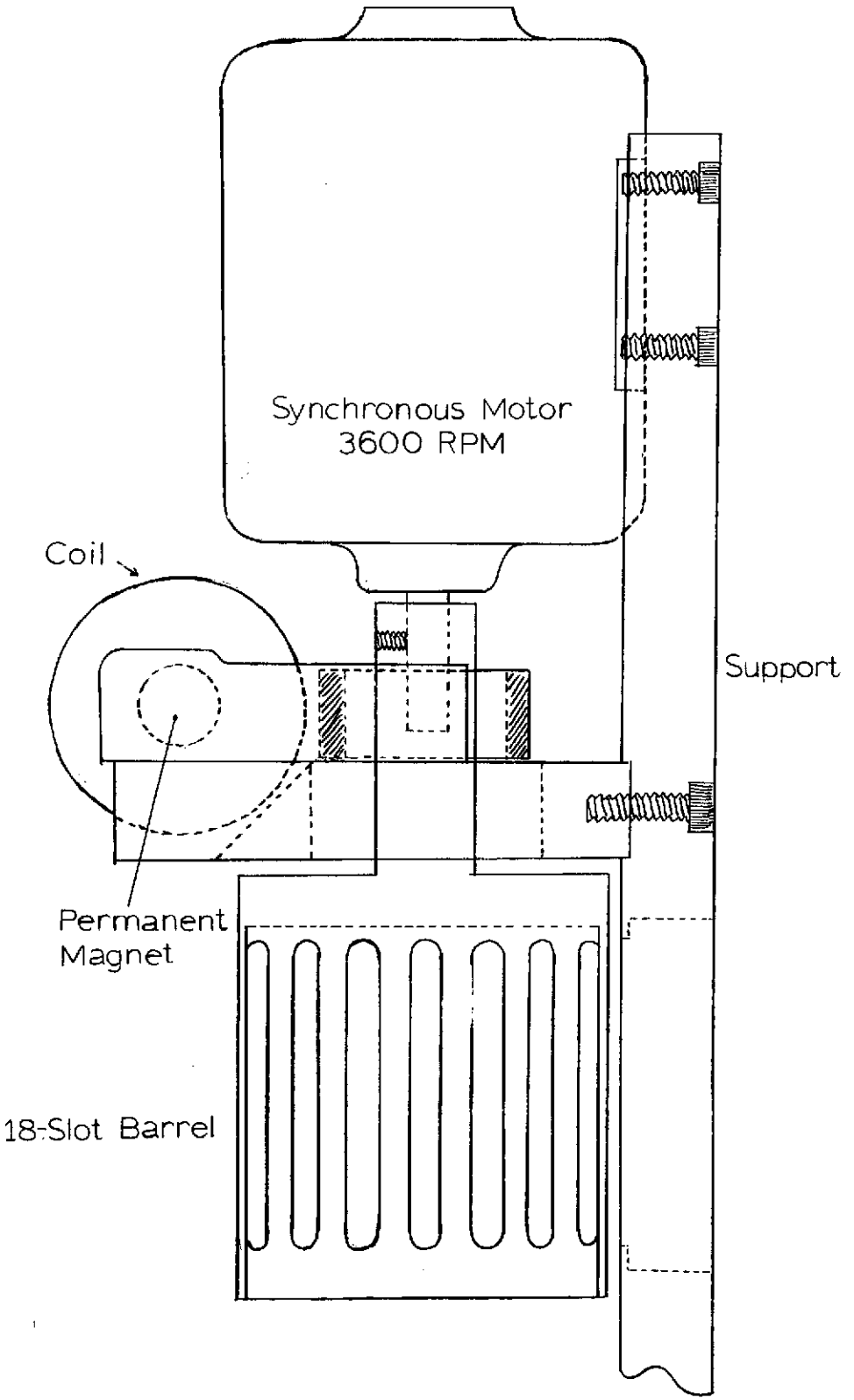

Figure 18. Light Chopper Side View

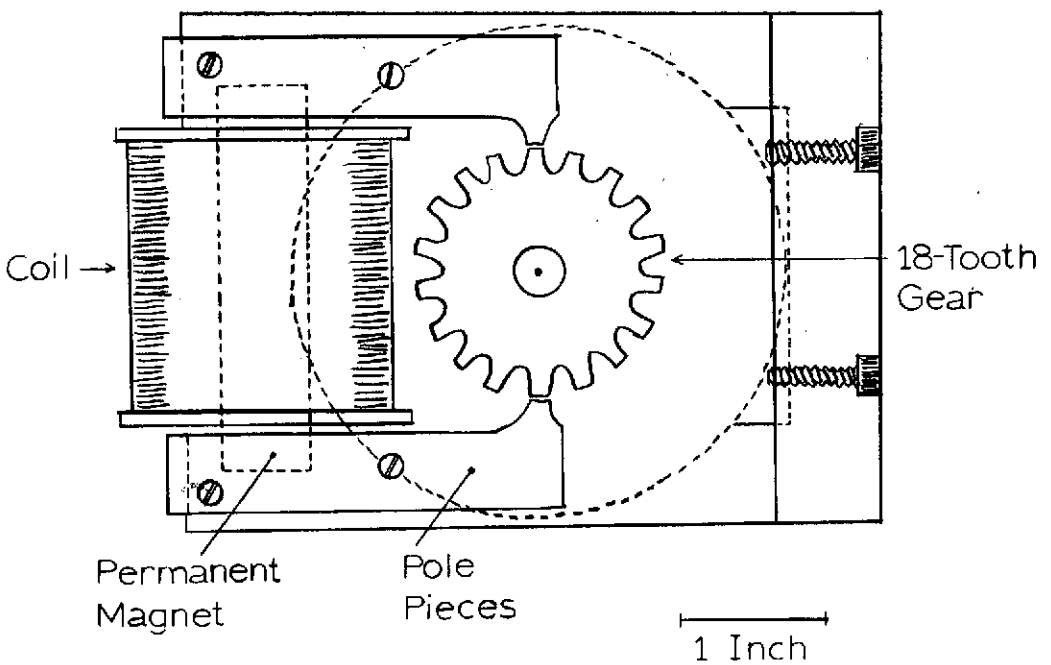

Figure 19. Light Chopper Top View

beam focused at the center of the barrel, and the chopping frequency were all considered as variables in arrving at a barrel size and number of slots. The barrel diameter is 2.865" and the slots are 1/4" wide with 1/4" between the slots to give an approximate sine wave output. The barrel and barrel shaft were made in one piece to assure good alignment of their axes and the barrel was made as thin as practical (.030") to reduce the inertial loading of the motor. A steel 18-tooth gear on the shaft with the chopper barrel turns between two iron pole pieces carrying the field from a permanent bar magnet. As the gear teeth pass between the poles a small emf is picked up and transformed by a coil wound on an insulating form around the permanent magnet. This signal is of course an AC signal in synchronization with the light chopping frequency and is used for the lock in amplifier. The coil is shielded with layers of Netic and Conetic metal to eliminate any electrical noise from being picked up in the reference circuit since it operates in the close vicinity of the chopper motor.

The motor used to drive the chopper has been a problem to operate in the evacuated spectrometer. The 3600 rpm synchronous motors used originally were purchased from Bodine. The bearing grease was replaced with a mixture of molybdenum disulfide and diffusion pump oil which has been used successfully in this laboratory in vacuum conditions. The motors, however, would not hold up for long periods of time. The heat generated by the motors is thought to be the cause of the problem. In a vacuum very little heat is conducted away from the motor, even though a large ground strap is attached to the motor mount for this purpose,

and it is thought that this heat led to the destruction of the motor directly or else vaporized the diffusion oil lubrication leading to the destruction of the bearings. Occasionally the fields would burn out from overheating before the bearings stopped the motors. Operating the motor at a lower voltage did not help the problem nor did other lubricants including the grease shipped in the motor. After several motors were tried lasting from a few days to three months depending on the usage, a surplus motor was obtained which was apparently not synchronous but very constant in rpm. This motor was tried because of its availability and precision bearings. The motor is also totally enclosed so that no lubrication can be lost through vaporization. The mount was adapted slightly to accept the new motor which was fortunately almost the same physical size. Thus far this motor has operated without failure for six months under heavy usage. The original lubrication in the motor was left unchanged. It is thought that the precision bearings and the total enclosure of the motor allow the motor to operate properly even in vacuum conditions.

3.9 Detector Pumping System

The PbS and InSb detectors from Santa Barbara Research Corporation used in this experiment operate at liquid nitrogen temperatures and are contained in vacuum insulated dewars. A pumping system consisting of a mechanical forepump, a diffusion pump and a cold trap was constructed for evacuation of the vacuum jacket. One inch copper line was run from the pumping system to both dewars which are mounted in either end of

the detector section of the spectrometer, and short lengths of rubber hose are used to connect from the copper line to the dewars. This pumping system is capable of vacuums of .2 to .4 microns as measured on a Mercury McLeod Gauge back near the pump. The pressure is the dewars is probably somewhat greater. The dewars pumped with this system and closed off will hold liquid nitrogen for about 30 hours and can be refilled without repumping for 3 to 4 days. After this time, however, the liquid nitrogen hold time is reduced due to leakage and outgassing, to the point that the dewars have to be warmed up and be re-pumped. It is not possible to pump continuously with this system since the liquid nitrogen in the dewars produce a better vacuum than the pumps can achieve and the pumps simply backstream into the dewars. For this reason small one liter per second ion pumps from Ultek Corporation were installed directly on the dewars so they could be pumped continuously even when they contained liquid nitrogen. The original pumping system is used to rough pump the dewars and ion pump manifold down to less than a micron and then is valved off and the ion pump is turned on. By pumping continuously with the ion pumps the liquid nitrogen hold time was increased to 50 hours. Also repumping is not necessary so that the dewars never have to be warmed up. The ion pump and manifold is shown in Figure 20 and is constructed entirely of stainless steel with heliarced joints to hold a high vacuum. A stainless diaphragm is connected to the manifold which expands against a microswitch triggering an alarm if the dewar should warm up and come up to atmospheric pressure.

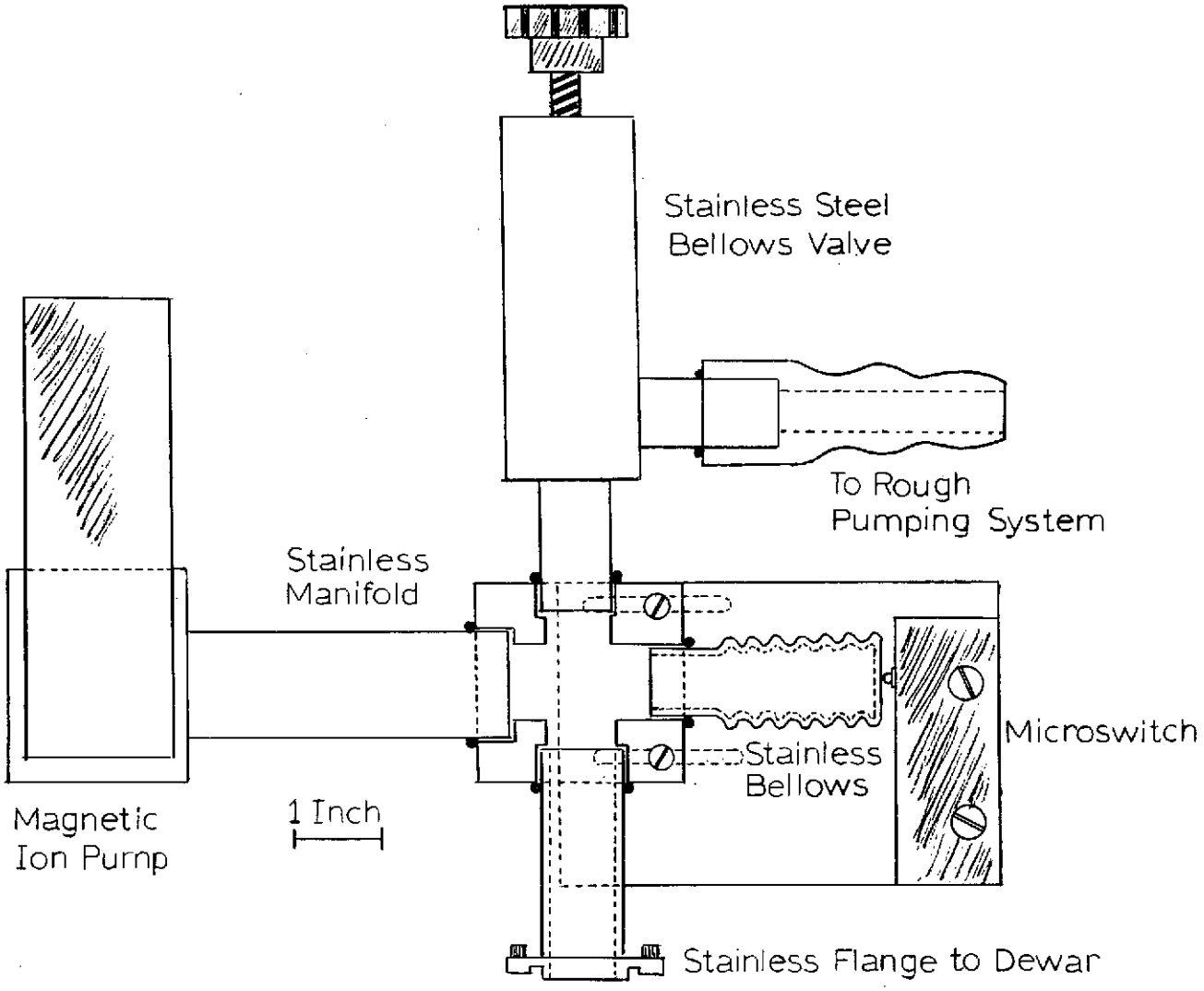

Figure 20. Detector Dewar Pump

3.10 Electronics

Both the PbS and InSb detector signals were amplified using a Princeton Applied Research Type A preamplifier and HR-8 lock in amplifier. The amplified signal was recorded on a Texas Instrument chart recorder. Records were made simultaneously on chart paper and on magnetic tape for computer assisted analysis. In these cases the monitor signal from the amplifier was routed to an analog to digital converter and put on tape in digital form, using a PDP-11 computer. The software and some of the hardware for this data taking system was developed at The University of Tennessee Molecular Spectroscopy Laboratory.

CHAPTER IV

DATA AND ANALYSIS OF DATA

4.1 Analysis Techniques

Practically all of the data taken was digitally recorded on magnetic tape in addition to analog recordings on chart paper. For frequency measurements the data records included calibration lines of known frequency. The serial data point numbers of the known and unknown lines were determined from the magnetic tape record by displaying the data on a Tennecomp display scope using a PDP-11 computer. Software developed at the University of Tennessee Molecular Spectroscopy Laboratory displays and moves the data across the screen face. The frequency coordinate can be expanded at will, and a cursor can be moved to locate the line center. The software keeps track of the serial data point number at the position of the cursor, and the data point number of the line center located by the cursor can be output to a teletype or line printer record, along with an identification of the line measured. The data point number of each line was measured three times, and the results averaged. The reproducability on the CO calibration lines was about one to two data points with the frequency interval between data points about 0.00035 cm^{-1}. For the H_2 and D_2 lines the reproducibility was somewhat poorer, due in part to a weaker signal intensity and also due to noisier and in some cases very weakly absorbing lines. The reproducibility of the H_2 and D_2 measured lines varied from about 2 to 6 data

point numbers. The known frequencies and their serial data point numbers were fitted either to a quadratic or cubic equations of the form,

$$\nu = A + BX + CX^2 + \text{----} \ ,$$

where ν is the frequency of the line and X is the data point number. A, B and C the coefficients were determined by a least squares fit Basic program using the PDP-11 computer. The program carries seven significant figures which was adequate after subtracting a constant from all the frequencies of the lines. These coefficients were used to determine the unknown line frequencies.

For line width measurements the particular line to be measured was recorded several times on magnetic tape. Since the deconvolution program as well as the response function program needs block numbers bracketing the data of interest (each block contains 256 data points), the data from magnetic tape was plotted in a compressed form using the Calcomp plotting system and the UTCC, IBM 360/65 system with the block numbers indicated on the plots. The block number data can then be quickly determined for use in the appropriate program.

The digitally recorded data were invaluable for line width measurements since it eliminates the tedium and inaccuracy of transferring measurements from chart paper to a form which can be read by the computer. The speed of making frequency measurements is also increased using the displayed data. In both cases magnetic tape provides a more compact and more readily accessed data source.

4.2 Effect of the Electric Field on Line Position

Before drawing any conclusion concerning the pressure shifts of H_2 and D_2 spectral lines it was necessary to determine the effect of the electric field on the line position. The lines are usually measured using the maximum electric field possible at a particular pressure in order to obtain the most intense, easily measurable line. So in addition to varing the pressure it is convenient to also vary the field in measuring the pressure shifted frequencies. To observe any electric field shift which might occur, the $Q_1(0)$ and $Q_1(1)$ lines of H_2 were recorded at a constant pressure of 19.22 Amagat at several field intensities from 160,000 to 50,000 volts/cm. The results of these measurements shown in Table VII and Figure 21 indicate that, within experimental error of about .003 cm^{-1} and within the range of fields used, no field dependent frequency shift of the H_2 lines appears.

4.3 Pressure Shifted Frequencies of H_2

The pressure dependent frequencies of the $Q_1(0)$ through $Q_1(3)$ spectral lines of H_2 were measured both as a check on the performance of the 5-meter Littrow spectrometer and because more accurate measurements could be made than in previous work. The pressure range used was from about 7 to 28 Amagats with three measurements made at each pressure for each line. Frequency measurements were made using the first overtone band of CO for calibration lines and the published frequencies of these lines given by Rao (15). With the 31.6 groove per millimeter grating it was possible to choose calibration lines either in the same or adjacent

TABLE VII

FREQUENCY OF H_2 LINES AS A FUNCTION OF THE ELECTRIC FIELD INTENSITY AT CONSTANT PRESSURE[1]

$Q_1(0)$ Field (volts/cm)	$Q_1(0)$ Frequency[2] (cm^{-1})	$Q_1(0)$ Field (volts/cm)	$Q_1(0)$ Frequency[3] (cm^{-1})
159,000	4161.1250	164,000	4155.1961
150,000	4161.1277	150,000	4155.1973
135,000	4161.1267	135,000	4155.1970
121,000	4161.1239	122,000	4155.1971
108,000	4161.1301	109,000	4155.2000
94,000	4161.1301	93,500	4155.1983
80,900	4161.1289	79,900	4155.1977
67,200	4161.1292	67,200	4155.1985
51,200	4161.1248	51,200	4155.1971

[1]Density = 19.22 Amagat

[2]Average Frequency = 4161.1274 ± .0024 cm^{-1}

[3]Average Frequency = 4155.1966 ± .0037 cm^{-1}

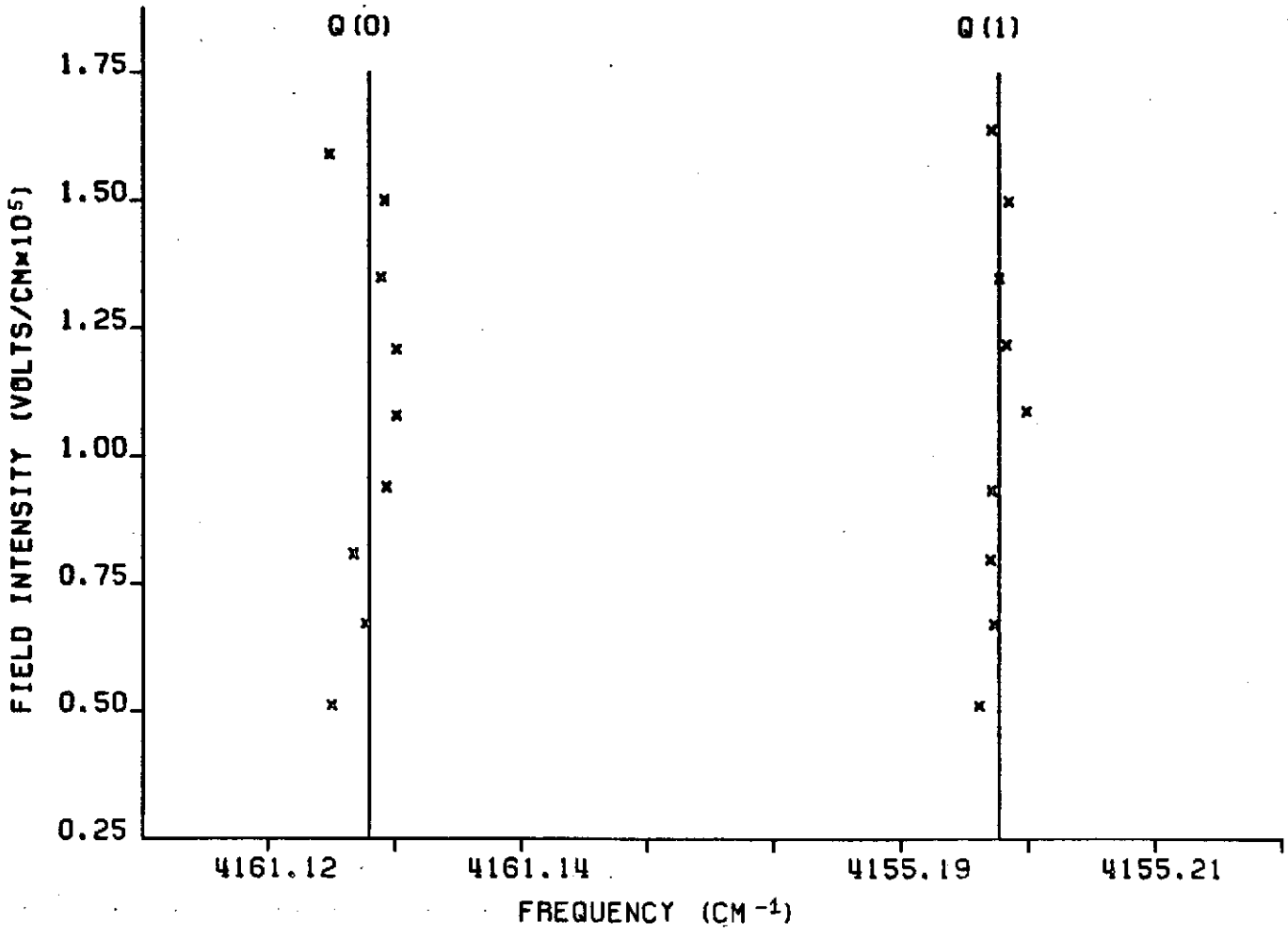

Figure 21. H_2 Line Position versus Electric Field Intensity at Constant Pressure

order as that of the unknown line. The 12-meter path of the long path cell was used to hold 5 millimeters pressure of CO and the beam switching mirror described in Section 3.7 was used to switch from the Stark cell beam to the calibration beam. Both signals were detected using the cooled lead-sulfide detector and recorded on chart paper magnetic tape. The $Q_1(1)$ lines were so close together that they could be measured together in the 24th order of the grating along with three calibration lines also in 24th order. The calibration lines were fitted to a quadratic equation in position using the least squares regression technique discussed in Section 4.1 and the unknown line frequencies calibrated from this quadratic equation. The $Q_1(2)$ and $Q_1(3)$ lines also occuring in 24th order were calibrated by linear extrapolation from two very close CO calibration lines occuring on either side of each line in 23rd order.

Each line was measured three times at each pressure. The three determinations were averaged and a standard deviation calculated to give an indication of the reproducibility of the measurements. The resultant frequencies for each line were fitted to a straight line using a least squares method. The intercept of this line gives the zero pressure frequency of the line of interest and the slope gives the pressure shift. Tables VIII to XI show the observed and calculated frequenices of the lines measured, and Figures 22 to 25 show the best fit straight line through the data points. Table XII gives the zero pressure frequenices and the shifts of the H_2 lines. The slopes of the lines measured can be compared in Figure 25. Table XIII compares the

TABLE VIII

OBSERVED AND CALCULATED FREQUENCY OF THE $Q_1(0)$, H_2 LINE AS A FUNCTION OF DENSITY

Density (Amagats)	Measured Frequency (cm^{-1})	Calculated Frequency (cm^{-1})	Observed-Calculated
28.21	4161.1014 ± .0014	4161.1026	-.0012
25.23	4161.1084 ± .0008	4161.1090	-.0006
22.23	4161.1153 ± .0019	4161.1155	-.0002
19.22	4161.1256 ± .0019	4161.1219	+.0037
16.20	4161.1290 ± .0013	4161.1284	+.0006
13.17	4161.1343 ± .0019	4161.1349	-.0006
10.12	4161.1399 ± .0004	4161.1415	-.0016
7.07	4161.1481 ± .0020	4161.1480	+.0001

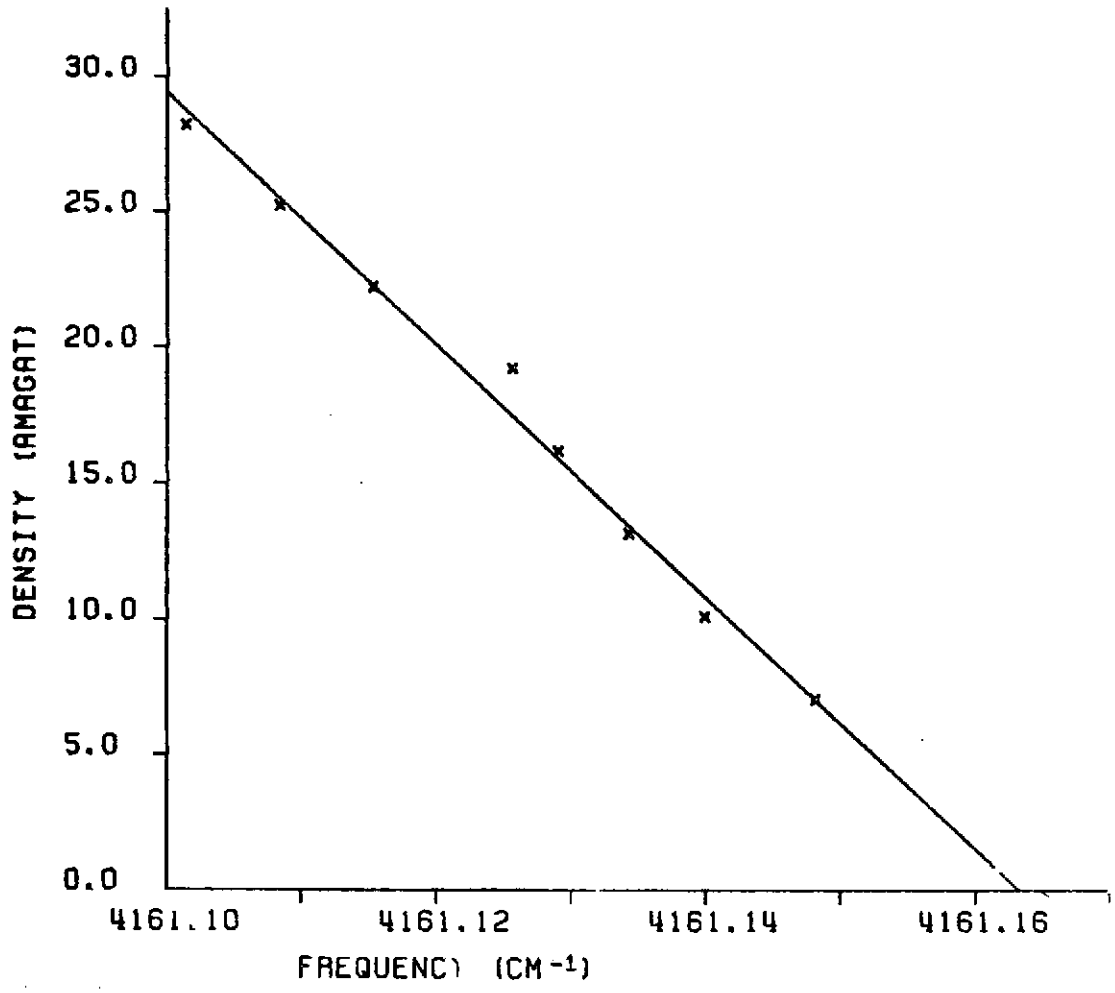

Figure 22. $Q_1(0)$, H_2 Line Position versus Density

TABLE IX

OBSERVED AND CALCULATED FREQUENCY OF THE $Q_1(1)$, H_2 LINE AS A FUNCTION OF DENSITY

Density (Amagats)	Measured Frequency (cm^{-1})	Calculated Frequency (cm^{-1})	Observed-Calculated
28.21	4155.1638 ± .0011	4155.1660	-.0022
25.23	4155.1750 ± .0009	4155.1753	-.0003
22.23	4155.1862 ± .0021	4155.1847	+.0015
19.22	4155.1956 ± .0007	4155.1941	+.0015
16.20	4155.2051 ± .0009	4155.2036	+.0015
13.17	4155.2127 ± .0025	4155.2131	-.0004
10.12	4155.2220 ± .0010	4155.2226	-.0006
7.07	4155.2311 ± .0011	4155.2322	-.0011

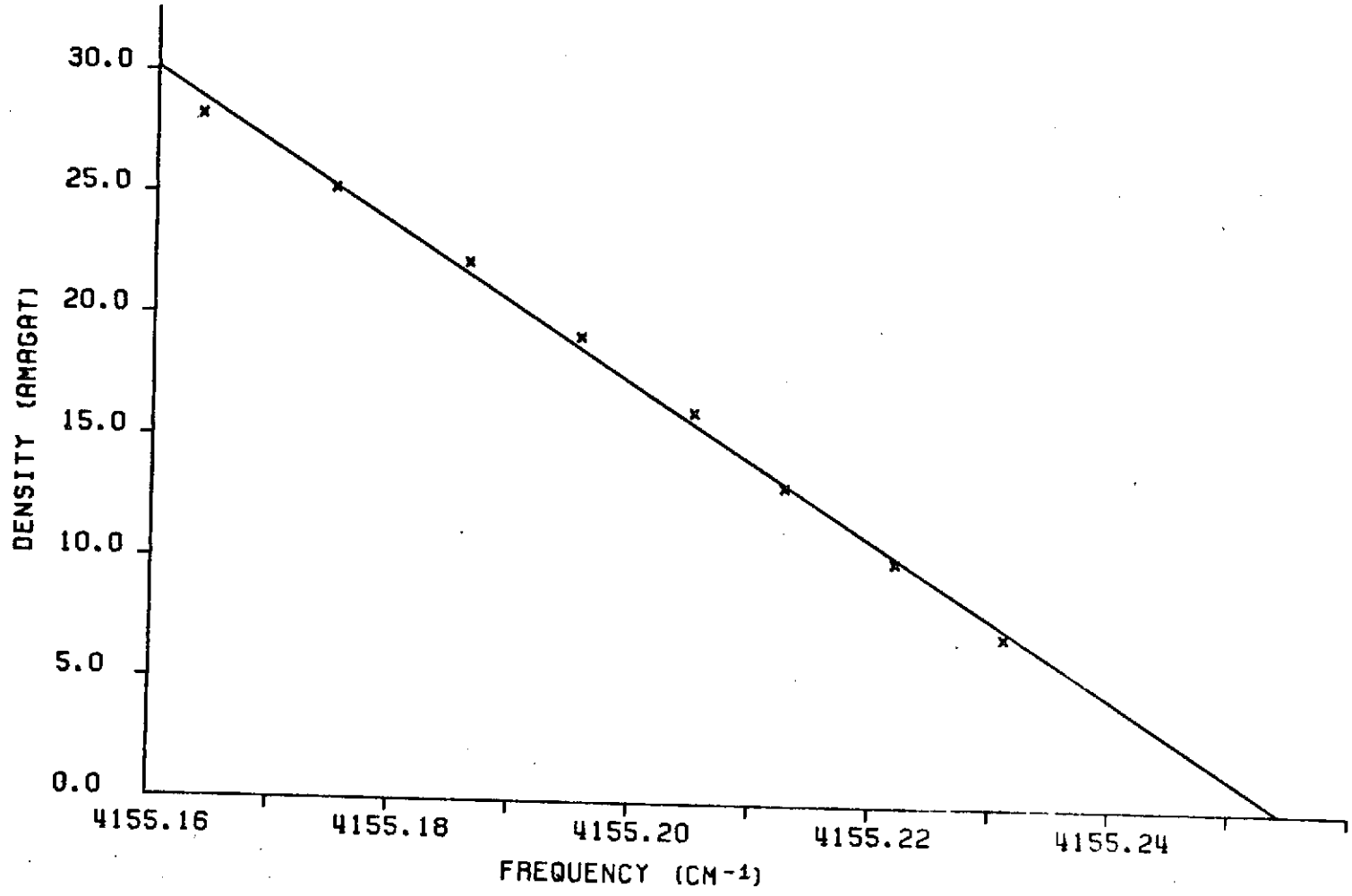

Figure 23. $Q_1(1)$, H_2 Line Position versus Density

TABLE X

OBSERVED AND CALCULATED FREQUENCY OF THE $Q_1(2)$, H_2 LINE AS A FUNCTION OF DENSITY

Density (Amagats)	Measured Frequency (cm^{-1})	Calculated Frequency (cm^{-1})	Observed-Calculated
28.21	4143.4139 ± .0021	4143.4136	-.0007
25.23	4143.4205 ± .0020	4143.4207	-.0002
22.23	4143.4281 ± .0030	4143.4269	+.0012
19.22	4143.4344 ± .0009	4143.4331	+.0013
16.20	4143.4384 ± .0023	4143.4393	-.0009
13.17	4143.4447 ± .0048	4143.4455	-.0008
10.12	4143.4521 ± .0037	4143.4518	-.0003

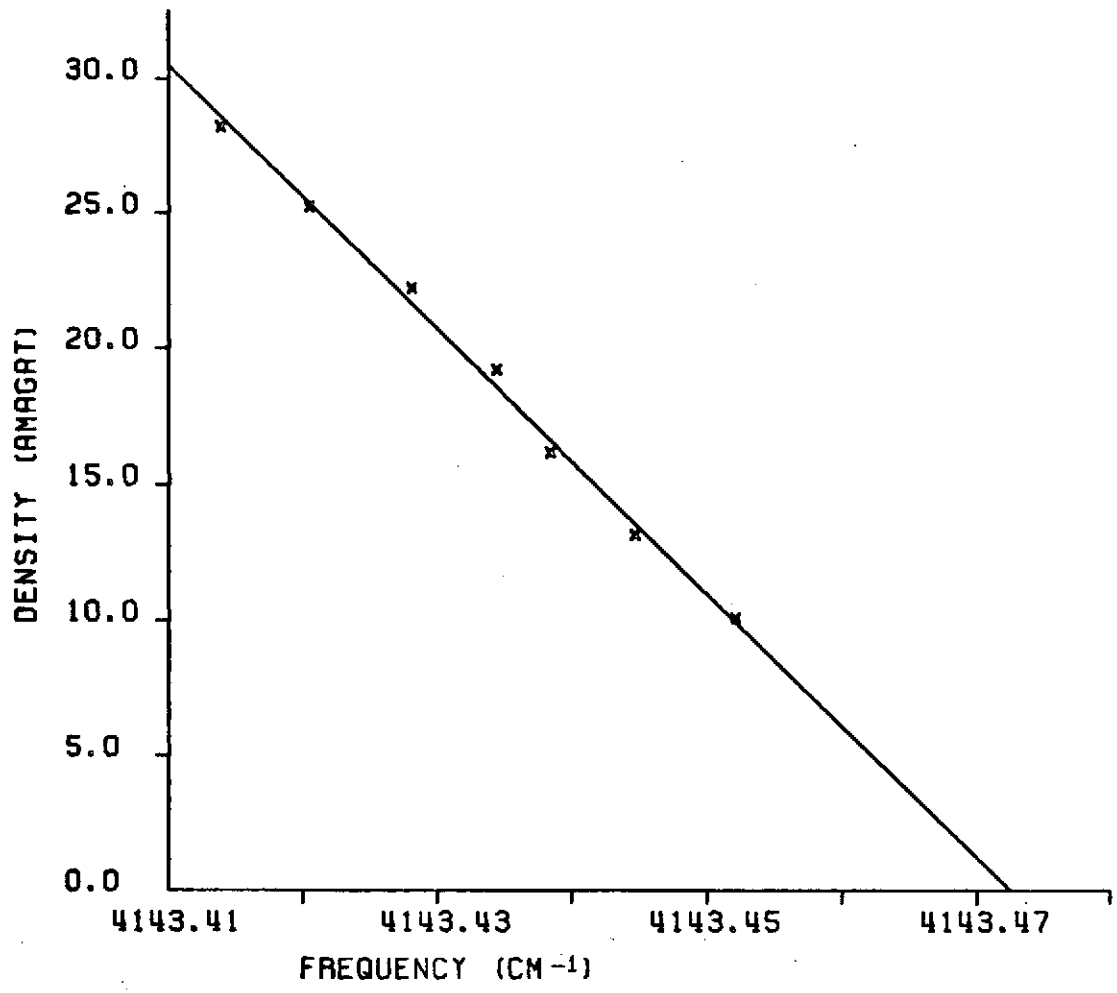

Figure 24. $Q_1(2)$, H_2 Line Position versus Density

TABLE XI

OBSERVED AND CALCULATED FREQUENCY OF THE $Q_1(3)$, H_2 LINE AS A FUNCTION OF DENSITY

Density (Amagats)	Measured Frequency (cm^{-1})	Calculated Frequency (cm^{-1})	Observed-Calculated
28.21	4125.8326 ± .0016	4125.8332	-.0006
25.23	4125.8410 ± .0025	4125.8386	+.0024
22.23	4125.8441 ± .0076	4125.8440	+.0001
19.22	4125.8473 ± .0034	4125.8495	-.0022
16.20	4125.8518 ± .0032	4125.8550	-.0032
13.17	4125.8638 ± .0016	4125.8605	+.0033

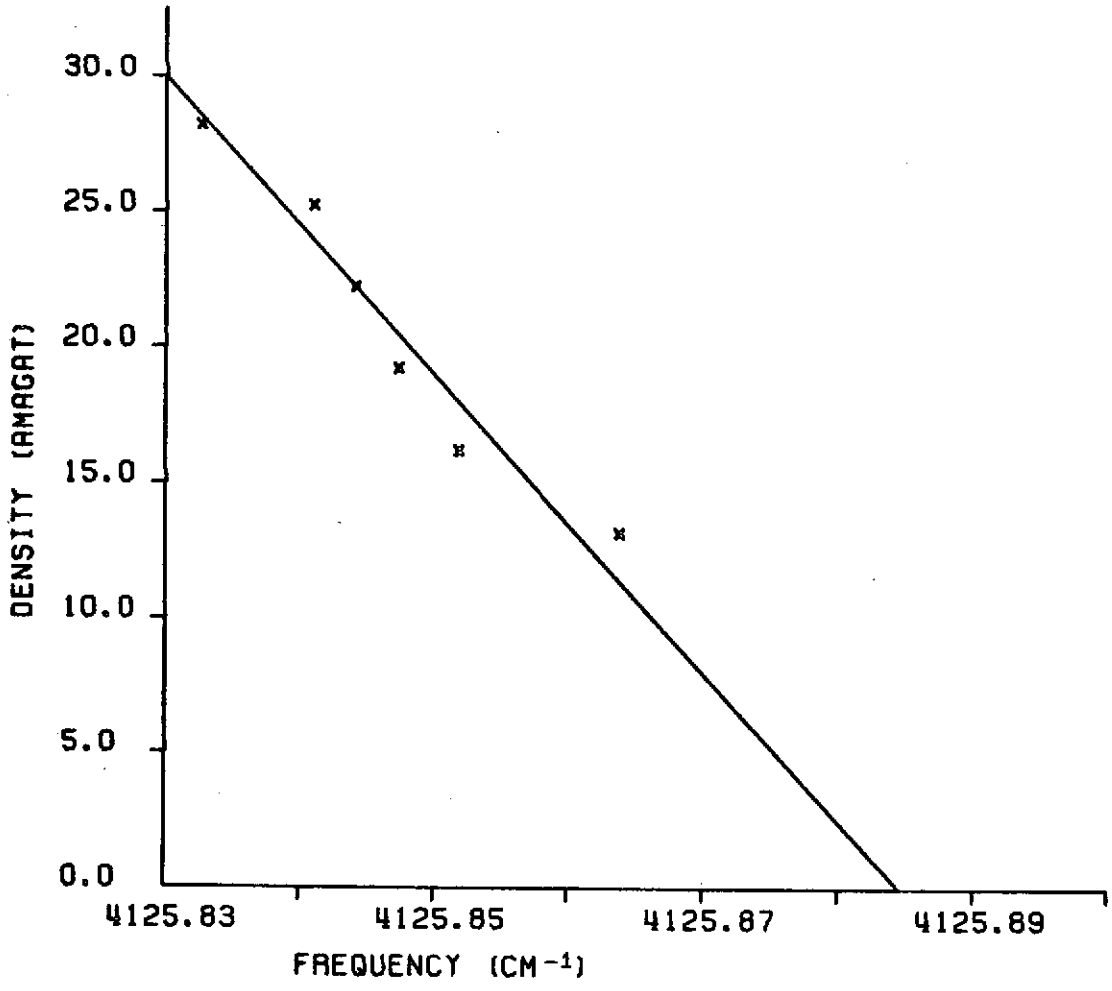

Figure 25. $Q_1(3)$, H_2 Line Position versus Density

TABLE XII

CALCULATED ZERO PRESSURE FREQUENCY AND PRESSURE SHIFT OF H_2 LINES

Line	Frequency (cm^{-1})	Pressure Shift (cm^{-1}/Amagat)
$Q_1(0)$	4161.1632 ± .0017	$-.00215 \pm .89 \times 10^{-4}$
$Q_1(1)$	4155.2543 ± .0014	$-.00313 \pm .75 \times 10^{-4}$
$Q_1(2)$	4143.4725 ± .0013	$-.00205 \pm .64 \times 10^{-4}$
$Q_1(3)$	4125.8845 ± .0048	$-.00182 \pm .23 \times 10^{-3}$

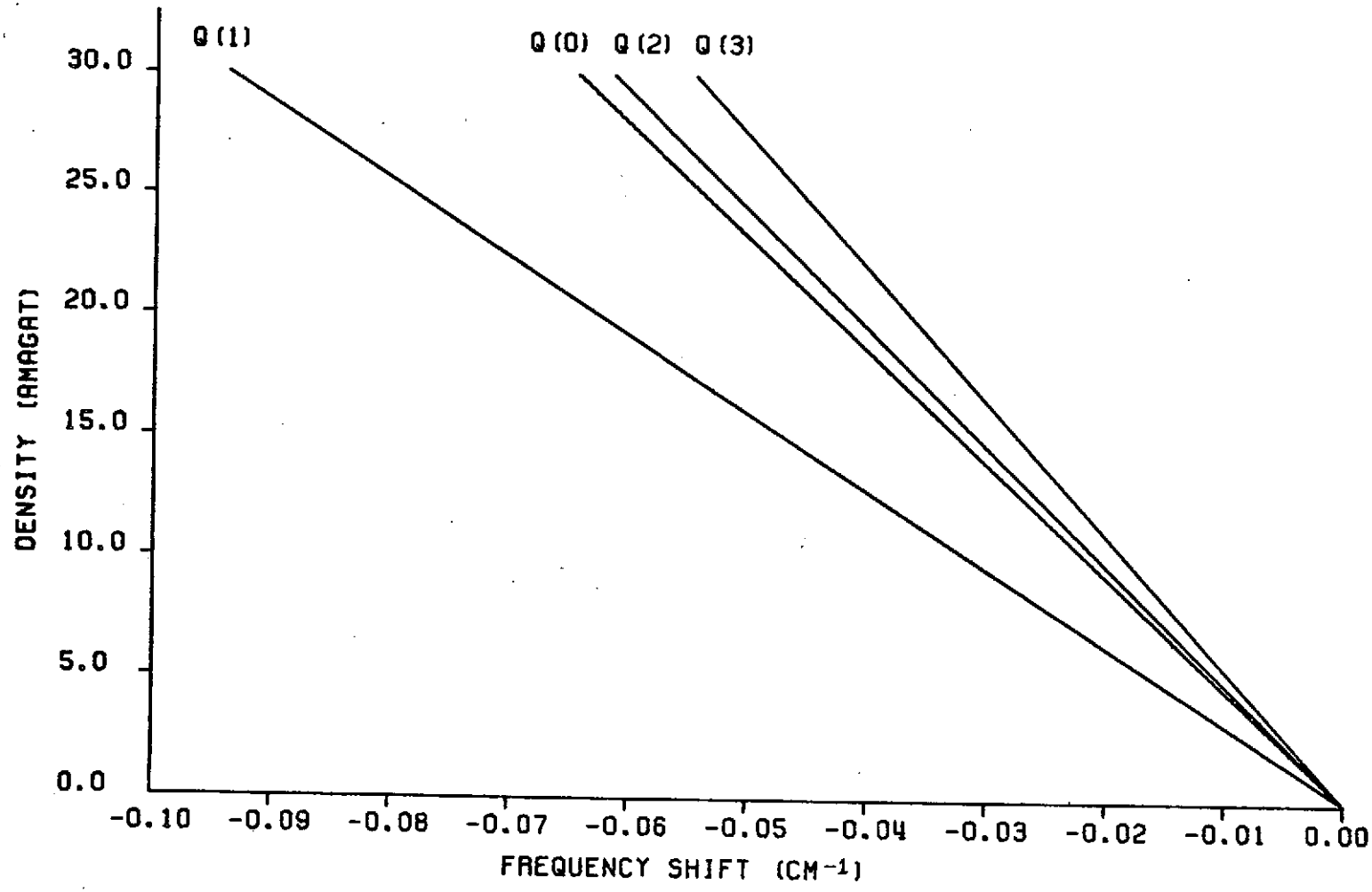

Figure 26. Slopes of the H_2 Pressure Shifted Lines

TABLE XIII

H_2 FREQUENCIES AND PRESSURE SHIFTS MEASURED IN THIS EXPERIMENT COMPARED TO OTHERS

Line	Frequency Measured this Experiment (cm^{-1})	Frequency[1] Measured by Brannon (cm^{-1})	Frequency[2] Measured by Stoicheff (cm^{-1})	Frequency[3] Measured by Fink et al. (cm^{-1})	Frequency[4] Measured by Foltz et al. (cm^{-1})
$Q_1(0)$	4161.1632	4161.158	4161.134		
$Q_1(1)$	4155.2543	4155.240	4155.202	4155.2575	4155.259
$Q_1(2)$	4143.4725	4143.449	4143.387	4143.4688	
$Q_1(3)$	4125.8845	4125.867	4143.832	4125.8718	

Line	Pressure Shift Measured this Experiment (cm^{-1}/Amagat)	Pressure Shift Measured by Brannon (cm^{-1}/Amagat)	Pressure Shift Measured by Fink et al. (cm^{-1}/Amagat)	Pressure Shift Measured by Foltz et al. (cm^{-1}/Amagat)
$Q_1(0)$	-.00215	-.0018		-.00234
$Q_1(1)$	-.00313	-.0029	-.00240	-.00318
$Q_1(2)$	-.00205	-.0015		-.00202
$Q_1(3)$	-.00182	-.0018		-.00185

[1]Electric Field Induced Technique

[2]Raman Technique

[3]Quadrupole Technique

[4]Electric Field Induced and Raman Technique

frequencies and shifts measured in this experiment with those measured by Brannon (5), Stoicheff (16), Fink et al. (17) and Foltz et al. (18).

The frequencies measured in this experiment are shifted with respect to those quoted by Brannon and Stoicheff, but agree very well with the values measured by Fink et al. and Foltz et al. The calibration techniques used and the resolution available in this experiment were better than that available to either Brannon or Stoicheff. Their quoted precisions were .02cm^{-1} and.01cm^{-1} respectively whereas this experiment is able to quote a precision of about .002cm^{-1}. The agreement of the linear shift coefficients measured in this experiment. with those measured by Foltz et al. is very good.

Both the relative and absolute accuracy of the frequency measurements made in this experiment are felt to be very good. The direct calibration techniques used and the resolution available were excellent and make highly accurate measurements possible.

4.4 Pressure Shifted Frequencies of D_2

The pressure shifted frequencies of the $Q_1(0)$ through Q(4), D_2 lines were measured since more precise measurements were possible than in previous work. The methods used were essentially the same as employed for H_2 described in the previous section. All of the lines, occuring in 17th order of the 31.6 groove per millimeter grating, were run together with 8 calibration lines of CO occuring in 24th order, interspersed among the Q-branch lines. A cubic equation was fitted to the calibration lines using a least squares technique and the unknown

lines calibrated from this curve. Again as for H_2 a straight line was fitted to the line positions as a function of density to obtain a zero pressure intercept frequency and pressure shift coefficient. Tables XIV through XIX show the measured pressure shift data and the calculated values from the best fitted straight line. Figures 27 through 31 show the best fit line drawn through the measured data points and Figure 32 compares the slopes of the D_2 Q-branch lines.

A comparison of the frequencies and pressure shifts measured in this experiment as compared to measurements made by Brannon (5) and Stoicheff (16) is shown in Table XX. Again the frequencies measured in this experiment are shifted from those measured by Brannon or Stoicheff but agree more closely with Brannon. It is felt that the frequencies measured here are the more accurate of the two. The accuracy of the frequencies and shifts measured in this experiment was demonstrated by the H_2 data discussed in the previous section. Again superior resolution and the calibration techniques used are felt to contribute to more accurate measurements

4.5 Field Induced Q Branch of N_2

The unresolved Q branch of N_2 shown in Figure 33 was observed but was too weak to make any new quantitative measurements. The peak absorption observed for the Q branch was 3.5% with no zero off set at an electric field intensity of 220,000 volts/cm. This measurement was made with no polarizer in the beam. The closely spaced lines of the Q branch were not expected to be resolved at the 28.21 Amagat pressure

TABLE XIV

OBSERVED AND CALCULATED FREQUENCY OF THE $Q_1(0)$, D_2 LINE AS A FUNCTION OF DENSITY

Density (Amagat)	Measured Frequency (cm^{-1})	Calculated Frequency (cm^{-1})	Observed-Calculated
28.21	2993.5724 ± .0013	2993.5686	+.0038
25.23	2993.5735 ± .0029	2993.5743	-.0008
22.23	2993.5773 ± .0030	2993.5801	-.0028
19.22	2993.5825 ± .0002	2993.5859	-.0034
16.20	2993.5912 ± .0042	2993.5917	-.0005
13.17	2993.6014 ± .0029	2993.5976	+.0038

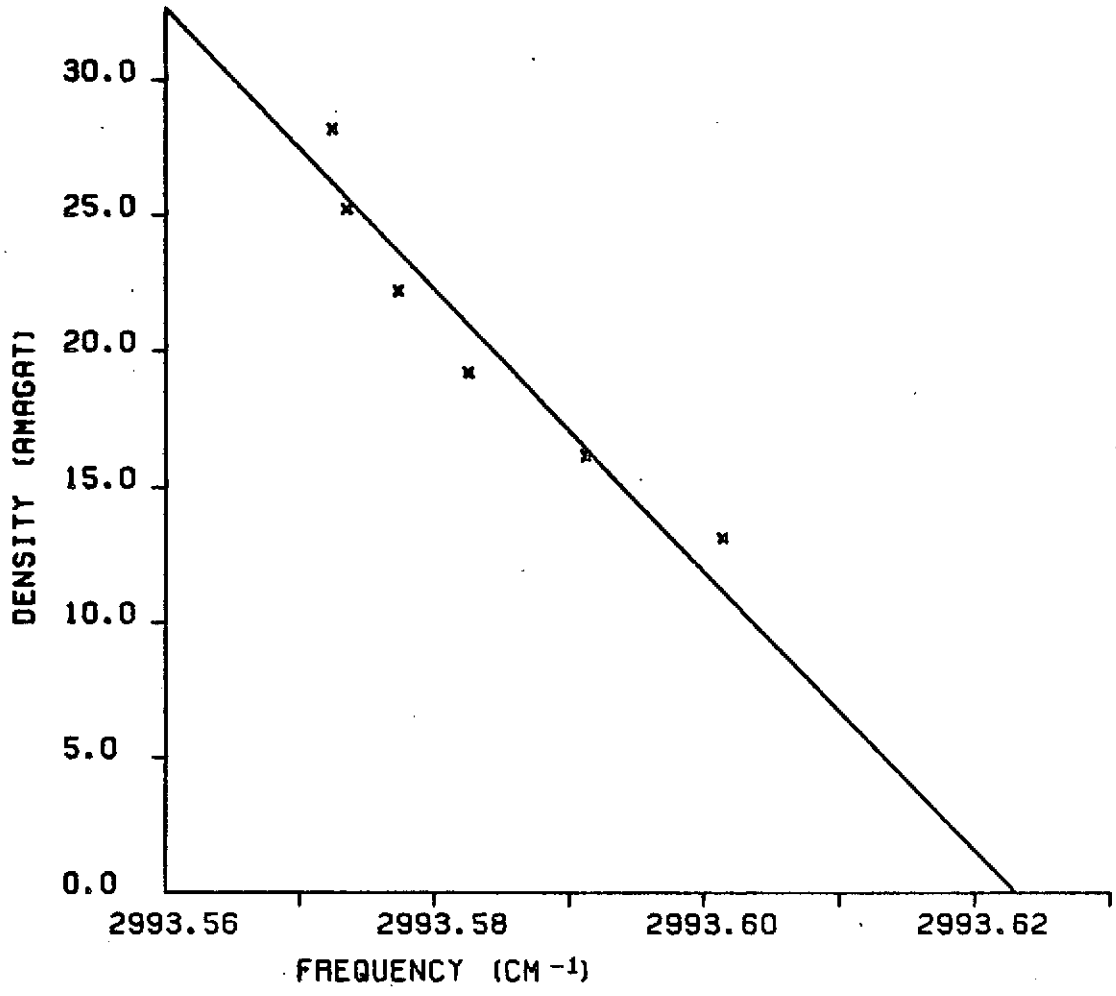

Figure 27. $Q_1(0)$, D_2 Line Position versus Density

TABLE XV

OBSERVED AND CALCULATED FREQUENCY OF THE $Q_1(1)$, D_2 LINE AS A FUNCTION OF DENSITY

Density (Amagat)	Measured Frequency (cm^{-1})	Calculated Frequency (cm^{-1})	Observed-Calculated
28.21	2991.4605 ± .0009	2991.4592	+.0013
25.23	2991.4652 ± .0009	2991.4646	+.0006
22.23	2991.4673 ± .0008	2991.4699	-.0026
19.22	2991.4747 ± .0010	2991.4754	-.0007
16.20	2991.4809 ± .0005	2991.4808	-.0001
13.17	2991.4880 ± .0021	2991.4863	+.0017
10.12	2991.4914 ± .0020	2991.4918	-.0004

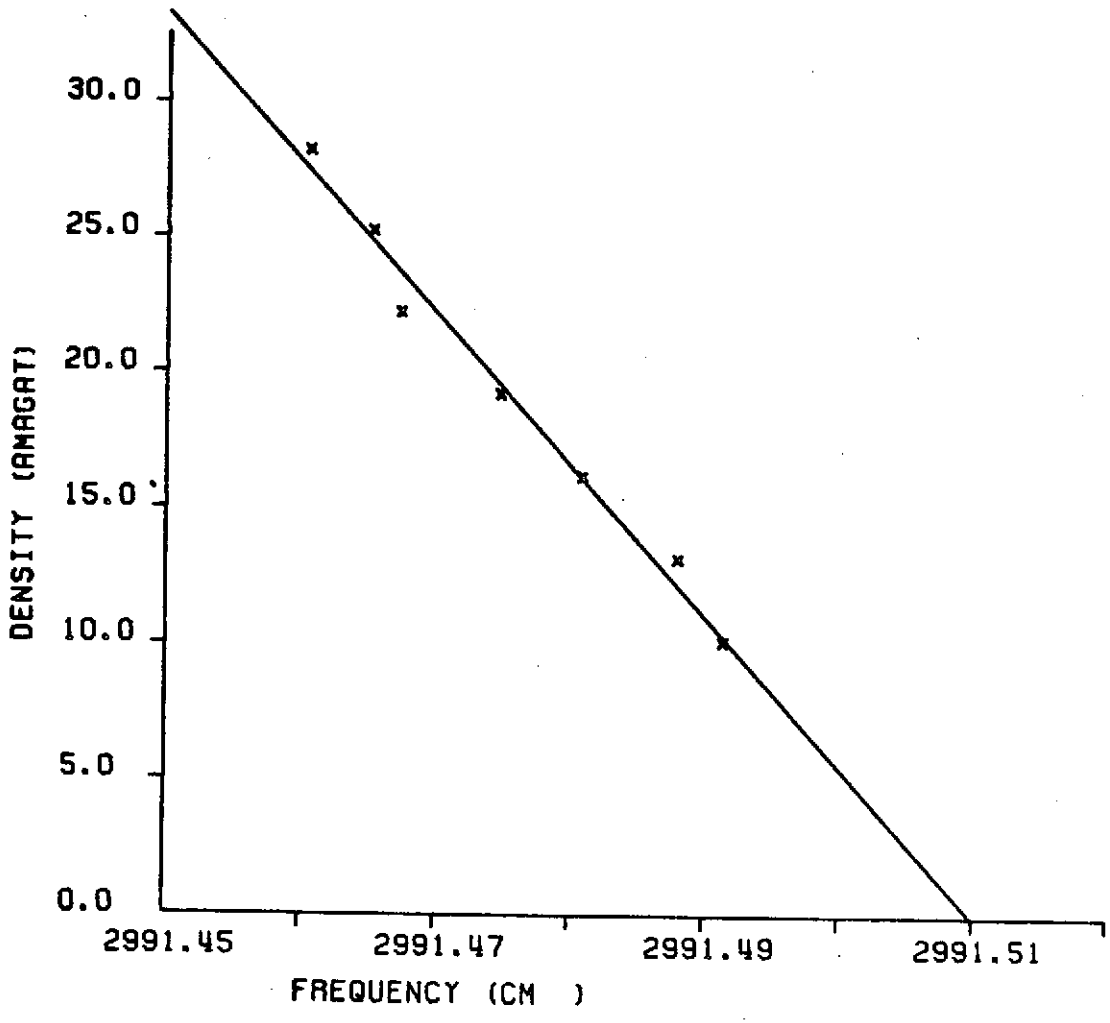

Figure 28. $Q_1(1)$, D_2 Line Position versus Density

TABLE XVI

OBSERVED AND CALCULATED FREQUENCY OF THE $Q_1(2)$, D_2 LINE AS A FUNCTION OF DENSITY

Density (Amagat)	Measured Frequency (cm^{-1})	Calculated Frequency (cm^{-1})	Observed-Calculated
28.21	2987.2406 ± .0035	2987.2395	+.0011
25.23	2987.2454 ± .0018	2987.2458	-.0004
22.23	2987.2503 ± .0016	2987.2521	-.0018
19.22	2987.2584 ± .0005	2987.2585	-.0001
16.20	2987.2642 ± .0018	2987.2648	-.0006
13.17	2987.2737 ± .0023	2987.2712	+.0025
10.12	2987.2786 ± .0019	2987.2776	+.0010
7.07	2987.2825 ± .0017	2987.2841	-.0016

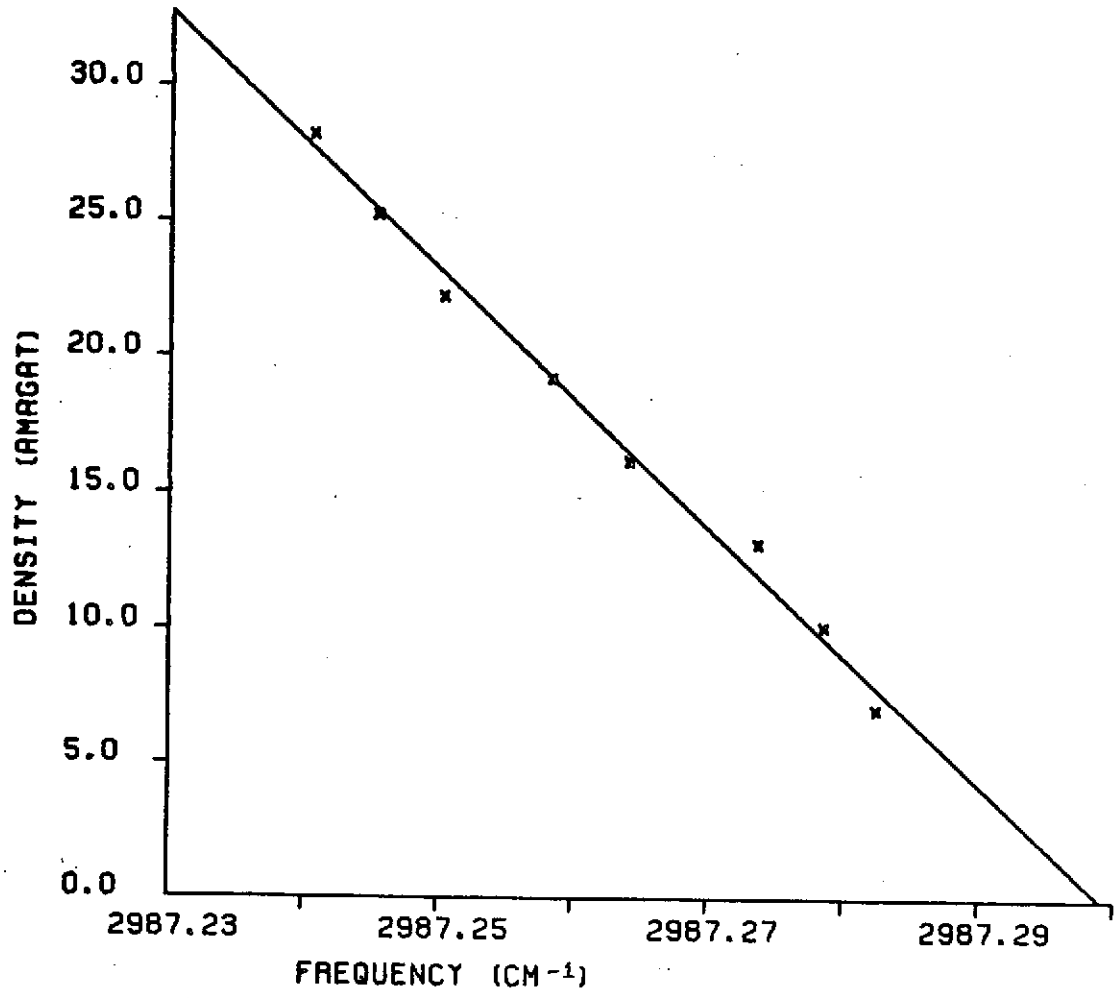

3

Figure 29. $Q_1(2)$, D_2 Line Position versus Density

TABLE XVII

OBSERVED AND CALCULATED FREQUENCY OF THE $Q_1(3)$, D_2 LINE AS A FUNCTION OF DENSITY

Density (Amagat)	Measured Frequency (cm^{-1})	Calculated Frequency (cm^{-1})	Observed-Calculated
28.21	2980.9465 ± .0032	2980.9450	+.0015
25.23	2980.9496 ± .0068	2980.9501	-.0005
22.23	2980.9537 ± .0045	2980.9552	-.0015
19.22	2980.9603 ± .0047	2980.9603	.0000
16.20	2980.9642 ± .0045	2980.9655	-.0013
13.17	2980.9724 ± .0112	2980.9707	+.0017

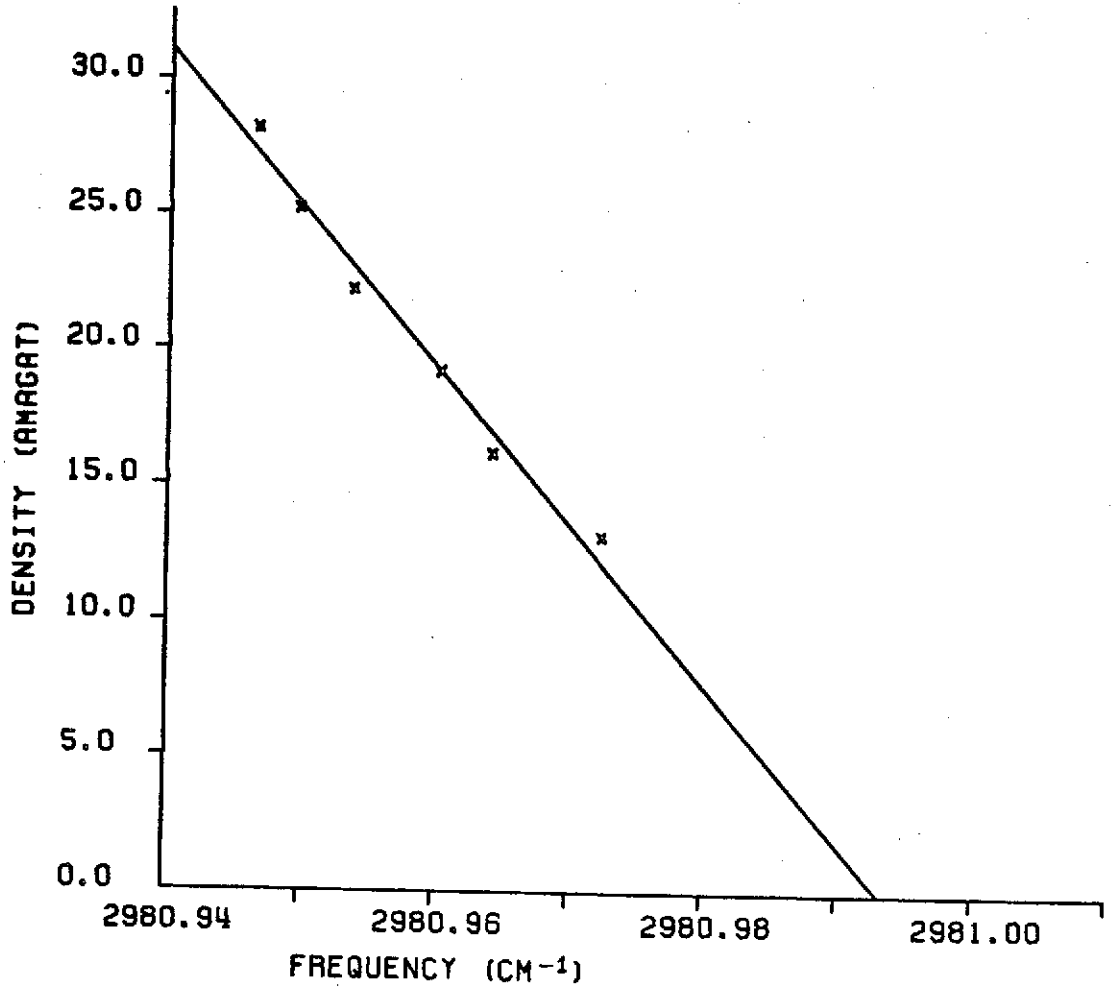

Figure 30. $Q_1(3)$, D_2 Line Position versus Density

TABLE XVIII

OBSERVED AND CALCULATED FREQUENCY OF THE $Q_1(4)$, D_2 LINE AS A FUNCTION OF DENSITY

Density (Amagat)	Measured Frequency (cm^{-1})	Calculated Frequency (cm^{-1})	Observed-Calculated
28.21	2972.5710 ± .0086	2972.5726	-.0016
25.23	2972.5799 ± .0038	2972.5779	+.0020
22.23	2972.5838 ± .0072	2972.5832	+.0006
19.22	2972.5884 ± .0108	2972.5885	-.0001
16.20	2972.5925 ± .0051	2972.5938	-.0013
13.17	2972.5996 ± .0027	2972.5992	+.0004

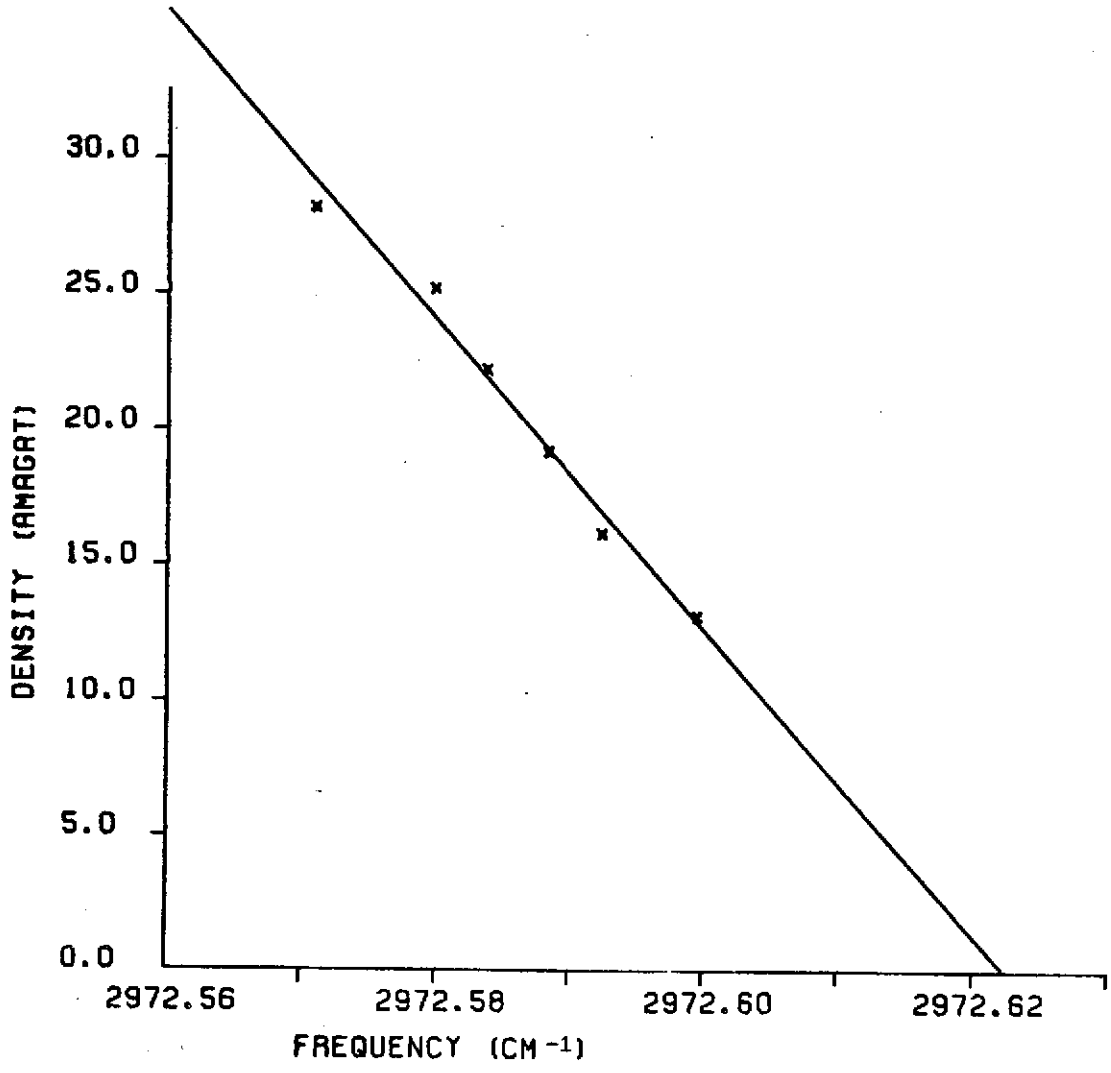

Figure 31. $Q_1(4)$, D_2 Line Position versus Density

TABLE XIX

CALCULATED ZERO PRESSURE FREQUENCY AND PRESSURE SHIFT OF D_2 LINES

Line	Frequency (cm^{-1})	Pressure Shift (cm^{-1}/Amagat)
$Q_1(0)$	2993.6230 ± .0059	$-.00193 \pm .28 \times 10^{-3}$
$Q_1(1)$	2991.5099 ± .0020	$-.00180 \pm .10 \times 10^{-3}$
$Q_1(2)$	2987.2990 ± .0015	$-.00211 \pm .80 \times 10^{-4}$
$Q_1(3)$	2980.9932 ± .0026	$-.00171 \pm .12 \times 10^{-3}$
$Q_1(4)$	2972.6224 ± .0026	$-.00176 \pm .12 \times 10^{-3}$

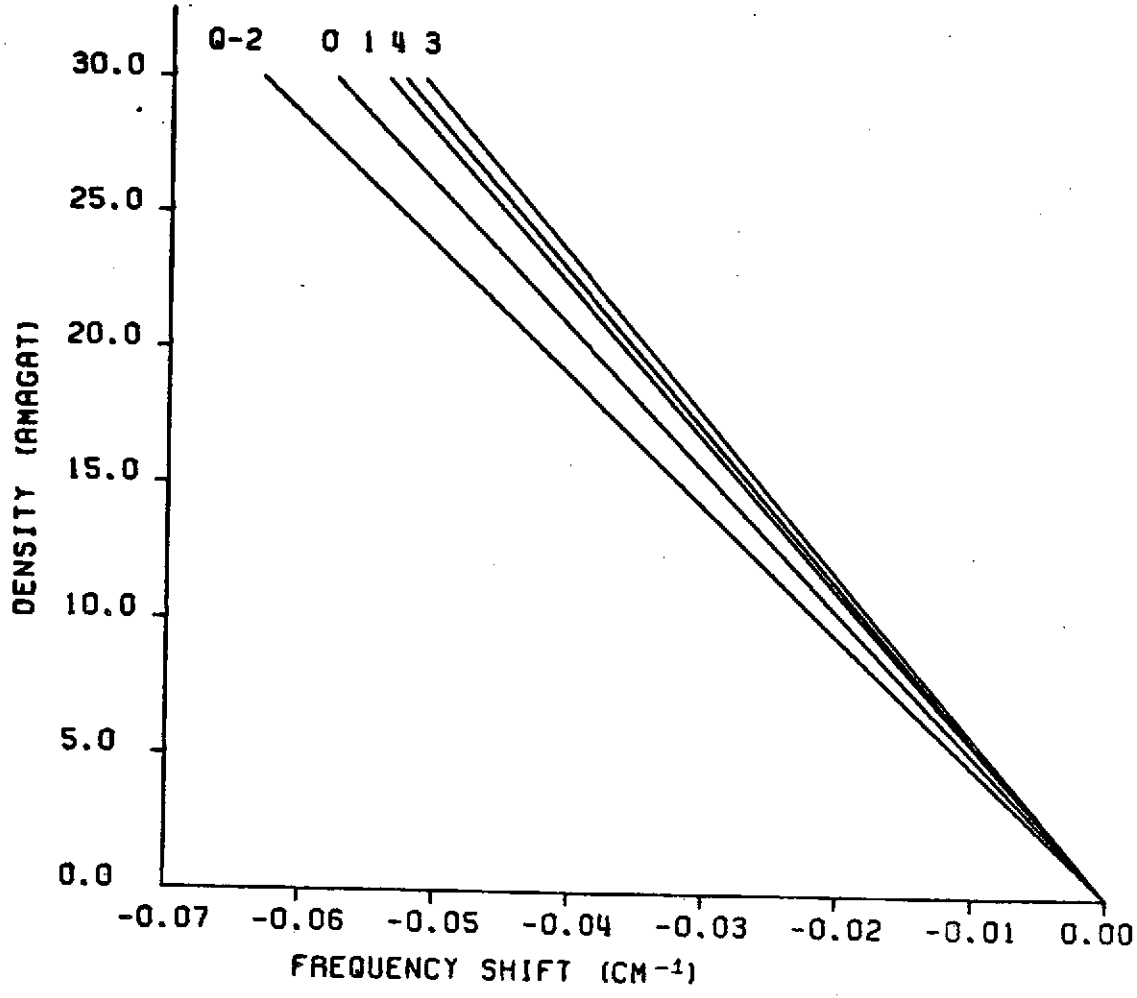

Figure 32. Slopes of the Pressure Shifted D_2 Lines

TABLE XX

D_2 FREQUENICES AND PRESSURE SHIFTS MEASURED IN THIS EXPERIMENT COMPARED TO OTHERS

Line	Frequency Measured this Experiment (cm^{-1})	Frequency Measured by Brannon (cm^{-1})	Frequency Measured by Stoicheff (cm^{-1})
$Q_1(0)$	2993.6230	2993.600	2993.548
$Q_1(0)$	2991.5099	2991.486	2991.446
$Q_1(2)$	2987.2990	2987.268	2987.230
$Q_1(3)$	2980.9932	2980.967	2980.877
$Q_1(4)$	2972.6224	2972.597	2972.557

Line	Pressure Shift Measured this Experiment (cm^{-1}/Amagat)	Pressure Shift Measured by Brannon (cm^{-1}/Amagat)
$Q_1(0)$	-.00193	-.0017
$Q_1(1)$	-.00180	-.0016
$Q_1(2)$	-.00211	-.0017
$Q_1(3)$	-.00171	-.0014
$Q_1(4)$	-.00176	-.0020

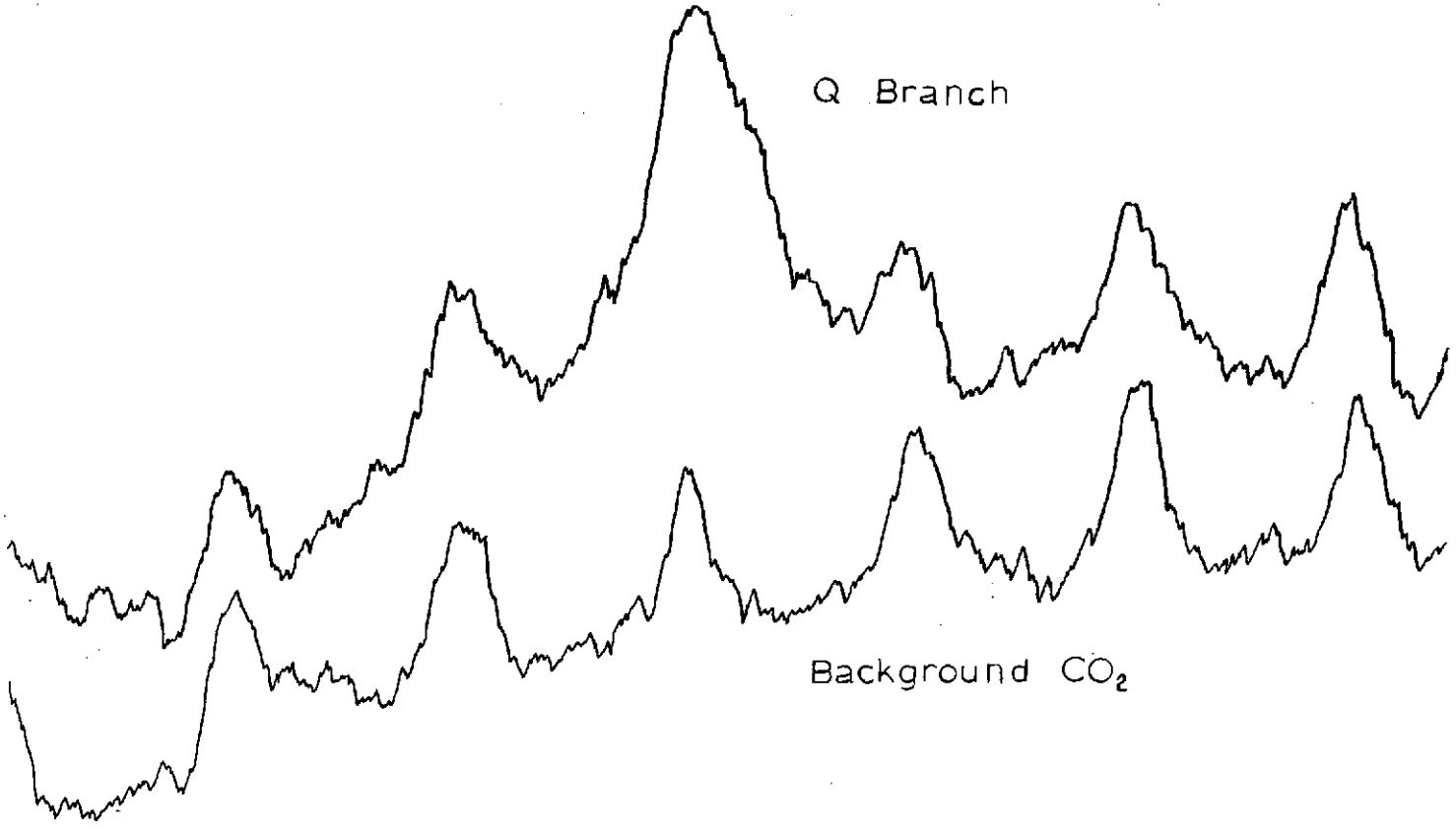

Figure 33. N_2, Q Branch

used to observe the lines; however the wider spaced S and O branch lines could be used for quantitative measurements. These lines are however four to five times less intense than the Q branch lines and could not be detected.

Some problems were encountered in trying to detect the N_2 lines. The N_2 frequencies lie in a region where CO_2 is strongly absorbing. The flushing cover described in Section 3.6 was successful in removing practically all of the CO_2 in the light path from the source to the Stark cell, however as observed in Figure 33 on page 119, some small amount remains. The bottom trace show the CO_2 background in the light path with the electric field off. The zero has been offset to increase the recorded signal. The top trace has been offset slightly less, and shows the N_2, Q branch after the field has been turned on and the same region rescanned. The two traces are aligned only approximately. Most of the CO_2 seen here is in the flushing cover. These lines were used to calibrate the frequency of the N_2, Q branch. A greater problem however was encountered with CO_2 absorption in the Stark cell itself. It was found that CO_2 appeared slowly and grew within the cell over a period of 24 to 36 hours. Repeated evacuation and refilling did not seem to slow down the reappearance of the CO_2. Since the cell is pressurized to 450 p.s.i. the CO_2 appeared as a broad absorption envelope, and until the problem was discovered, masked the small Q branch absorption. The source of the CO_2 is not known but it is possible that it could be generated somehow by the plexiglas or other materials used in the cell.

The center of the absorption of the Q branch was measured to be 2328.8 cm^{-1}. From molecular constants given by Herzberg (3) the frequencies and relative intensities of the N_2 lines were calculated and show the center of the Q branch should occur at a frequency of 2329.67 cm^{-1} corresponding to the $Q_1(7)$ line. This is a total shift of about -0.9 cm^{-1} or about -.03 cm^{-1}/amagat. A measurement of the full width at half maximum of the observed absorption revealed a width of 1.0 cm^{-1} indicating that the $Q_1(3)$ through $Q_1(9)$ lines were contributing significantly to the absorption.

4.6 Polarizability Constants of H_2

The polarizability of H_2 was determined using the linear absorption approximation given in equation (55). The integrated intensity of the $Q_1(0)$ line, which depends only on the polarizability constant α, was measured at several pressures and electric field intensities with a 6-plate glass polarizer in the beam to allow only the parallel polarized component of the incident radiation through the cell. No instrument function correction is needed for this measurement since according to Brannon (5) the integrated area is approximately independent of the instrument function. The area is then normalized to the value of the 100 percent absorbing point which was determined by pressurizing the Stark cell with about 125 p.s.i. of carbon monoxide in order to make the weak overtone line in that region 100 percent absorbing. This value is adjusted using the efficiency of the polarizer determined from the maximum absorption of $Q_1(1)$ line at 31.22 amagat and a field of 193,000 volts/cm. In this particular case the area was measured using a polar

planimeter directly from the recorded data on chart paper. The normalized area is then multiplied by the wave number interval per inch determined from calibration lines to give the resultant integrated absorption in units of cm^{-1}. A total of 20 individually measured areas were used to determine α. The large number of measurements were used because of the inherent large error in measurements of the area. The individual measurements were scattered randomly about an average value. Since γ makes only about a 3 percent or less, contribution to the intensity of the Q branch lines it was not possible to determine this constant from the Q branch lines. The $S_1(1)$ line was used to determine the polarizability γ for H_2. The strength factors for the S-branch lines depend only on the polarizability constant γ, and $S_1(1)$ line is the strongest of the S lines. The line is never the less still very weak and so the line was run 15 times at 28.21 amagat and the maximum field possible, to get a measurable absorption. The area was normalized as before and converted to an integrated absorption in units of cm^{-1}.

Equation (57) and (55) along with the appropriate Boltzmann factor from Table V on page 38 and the appropriate strength factor from Table IV on page 32 were used to calculate the constants α and γ given in Table XXI. A standard deviation of the individual measurements for both determinations is also given in Table XXI. A comparison of the polarizability constants measured by Brannon (5) and Foltz (15) shows good agreement for the constant γ between all experiments. The agreement for α is not as good. To check the value of α calculated in this experiment,

TABLE XXI

POLARIZABILITY CONSTANTS OF H_2

α Measured this Experiment (cm^3)	γ Measured this Experiment (cm^3)
$0.802 \times 10^{-25} \pm .049 \times 10^{-25}$	$0.772 \times 10^{-25} \pm .035 \times 10^{-25}$
0.805×10^{-25}[1]	

α Measured by Brannon (cm^3)	γ Measured by Brannon (cm^3)
$0.97 \times 10^{-25} \pm 3\%$	$0.81 \times 10^{-25} \pm 5\%$

α Measured by Foltz (cm^3)	γ Measured by Foltz (cm^3)
1.04×10^{-25}	0.79×10^{-25}

[1]Measured from the deconvoluted data of this experiment.

the integrated absorption data taken from the absorption coefficient curves of the deconvoluted $Q_1(0)$, H_2 line were used to recalculate α. The use of this data removes the restriction of the linear absorption approximation. As seen in Table XXI the recalculated value of α using the deconvoluted data is virtually the same as the previously calculated value. The reason for the discrepancy is the values calculated for the different experiments is not known.

4.7 Deconvolution of Spectral Lines

In order to determine more accurately the true width of a spectral line it is necessary to subtract out the influence of the spectrometer on the observed line profile. This influence is mainly due to finite width slits but also includes such effects as optical abberations and electronic distortion. If we can determine accurately enough the influence of the spectrometer which we will call the response function, then it can be removed by solving the convolution integral

$$Fo(\nu) = \int_{-\infty}^{\infty} R(\nu-\nu')F_T(\nu')d\nu' ,$$

where Fo is the observed fractional absorption, R is the response function and F_T is the true fractional absorption. Determination of the response function is discussed in detail in Section 4.8. To solve for the response function using computer techniques the convolution integral is usually written as

$$(Fo)i = \sum_{\ell} R_{i\ell} \ (F_T)_{\ell} .$$

The commonly used solution to this equation is the Van Cittert approximation. This is an interative process and the K+1 approximation is according to Jansson et al. (19).

$$(F_T)_i^{(K+1)} = (F_T)_i^{(K)} + \left\{ (Fo)_i - \sum_{\ell=1}^{n} (R)_{i\ell} (F_T)_\ell^{(K)} \right\} .$$

Jansson has modified this solution to assure convergence and good physical results by introducing a variable parameter κ, multiplying the applied correction factor to control the amount of correction used in each interaction. This prevents over correction and rapidly increasing oscillations in the solution which result from over correction. Jansson used a parameter κ_i which also was varied with the value of the fractional absorption at the point being corrected. The parameter was

$$\kappa_i = \kappa_o \left\{ 1-2 \left| (F_T)_i^{(\kappa)} - \frac{1}{2} \right| \right\} ,$$

where κ_o is a constant with a value between zero and one. This factor is in effect a weighting factor which varies the constant correction factor parameter from a maximum at 50 percent absorption to zero at both 0 and 100 percent absorption. This factor was not used in the deconvolution programs used in this work since it seemed possible that the line shape of the final result could be modified by the inclusion of the factor.

Jansson's final expression for the K+1 approximation (substituting the constant κ for the weighting factor κ_o) is

$$(F_T)_i^{(K+1)} = (F_T)_i^{(K)} + \kappa \left\{ (Fo)_i - \sum_{\ell=1}^{i} (R)_{i\ell} (F_T)_\ell^{(K+1)} - \sum_{\ell-i}^{n} (R)_{i\ell} (F_T)_\ell^{(K)} \right\},$$

where it can be noted that the calculated $(F_T)_i$ values are used immediately as they are obtained. The deconvolution program works in four loops. Loop zero uses a polynomial fit to smooth the input data a variable number of times without deconvolution. Loop one deconvolutes and then smoothes the input data a variable number of times with an input smoothing parameter κ. Loop two repeats the same process with a different κ if desired. Loop three deconvolutes without smoothing, a variable number of times again with a different κ if desired. Jannson's program was modified to deconvolute only every seventh point in loop one and every fourth point in loop two with the points in between obtained by interpolating, thus increasing the speed of the program. In the H_2 data used, one initial smooth was used with three, four and five passes used respectively in loop one, two and three. The κ values used were 0.3, 0.5 and 1.0 respectively in each of the three loops. The complete program for the deconvolution process is listed in Appendix B and C, and includes Jansson's modified program in the subroutines. The widths of the lines were observed to vary some what due to noise, which made several determinations of each line width necessary. In order not to have to repeat the time consuming deconvolution process for each individual measurement, the program was written

to be able to take several measurements of the same line at the same conditions and align and average them so that the deconvolution is performed only once on the averaged data. This has the additional advantage of reducing the noise on the lines which improves the performance and results of the deconvolution process. The individual measurements are smoothed once and the base line subtracted out. The 100 percent absorbing value and polarizer efficiency is used to convert the data to a fractional absorption and the center of each line measurement is found at the value of the 50 percent peak absorbing value. The progress of the program is checked at various points by plotting the data using the Calcomp plotter and the UTCC IBM 360/65 system. The deconvoluted data are converted to an absorption coefficient curve and plotted in the final steps. The program measures the half width of the absorption coefficient curve and also integrates the area under the curve. Figures 34 and 35 show the results of the averaging process for the $Q_1(0)$ line of H_2, before and after deconvolution. Figure 36 shows the absorption coefficient curve calculated from the deconvoluted line.

4.8 Determination of the Response Function

In order to determine the response function used in the deconvolution program, a line was chosen in the very close vicinity of the lines of interest. The line chosen was negligibly broadened by pressure effects, so that the line width is due solely to the Doppler broadening, instrumental broadening and to a negligible degree to natural

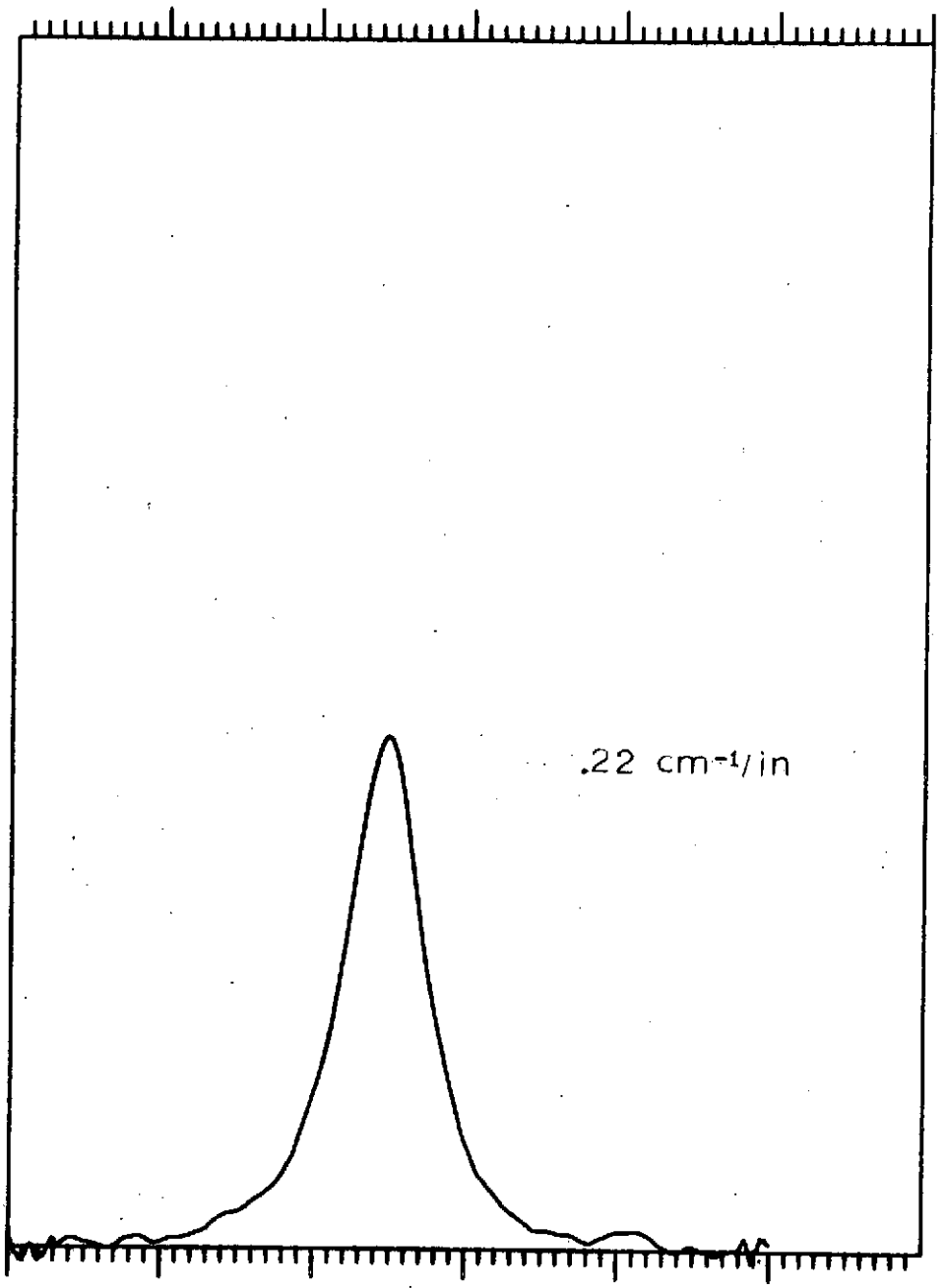

Figure 34. Averaged Profile of the $Q_1(0)$, H_2 Line

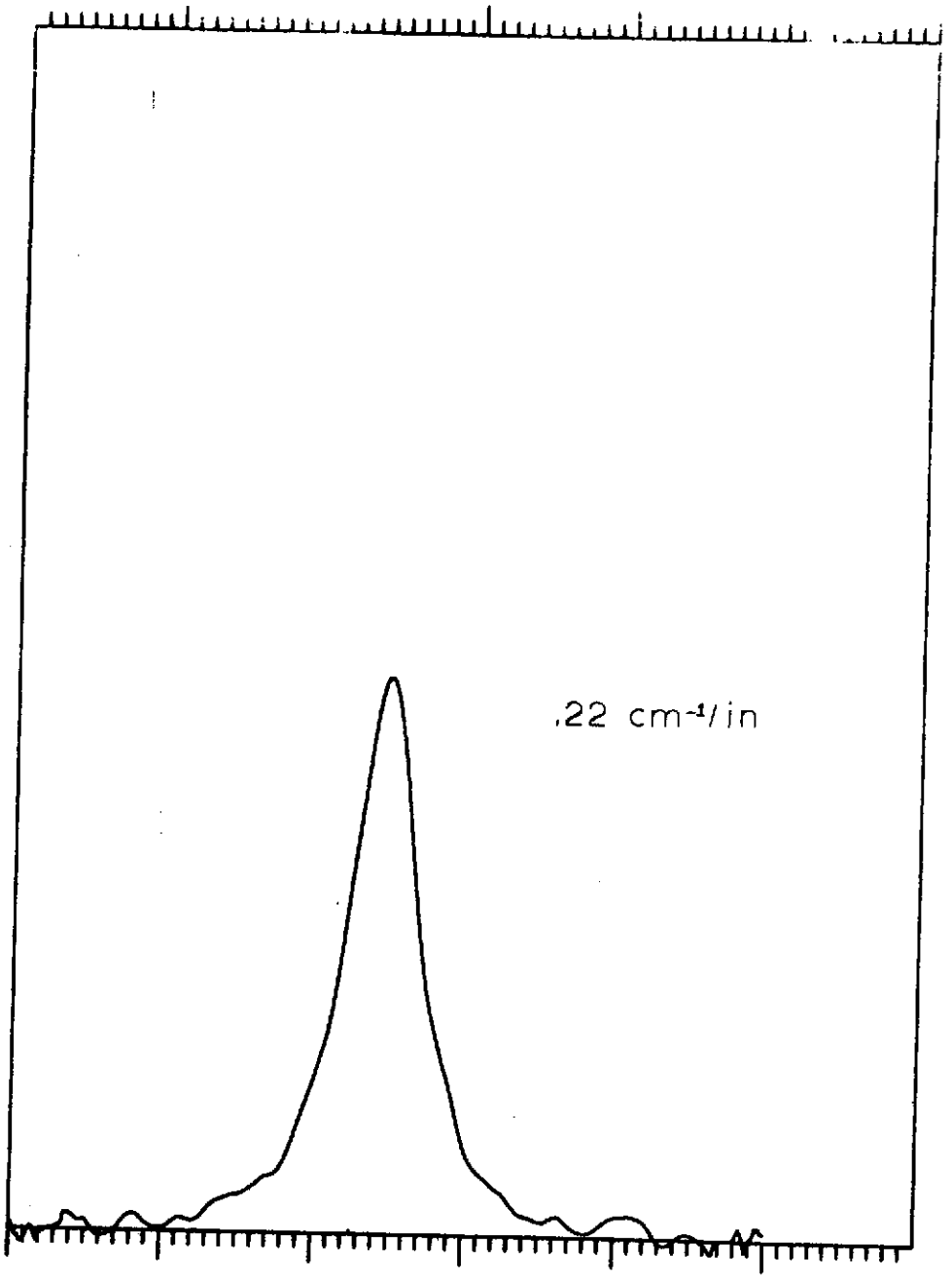

Figure 35. Deconvoluted Profile of the $Q_1(0)$, H_2 Line

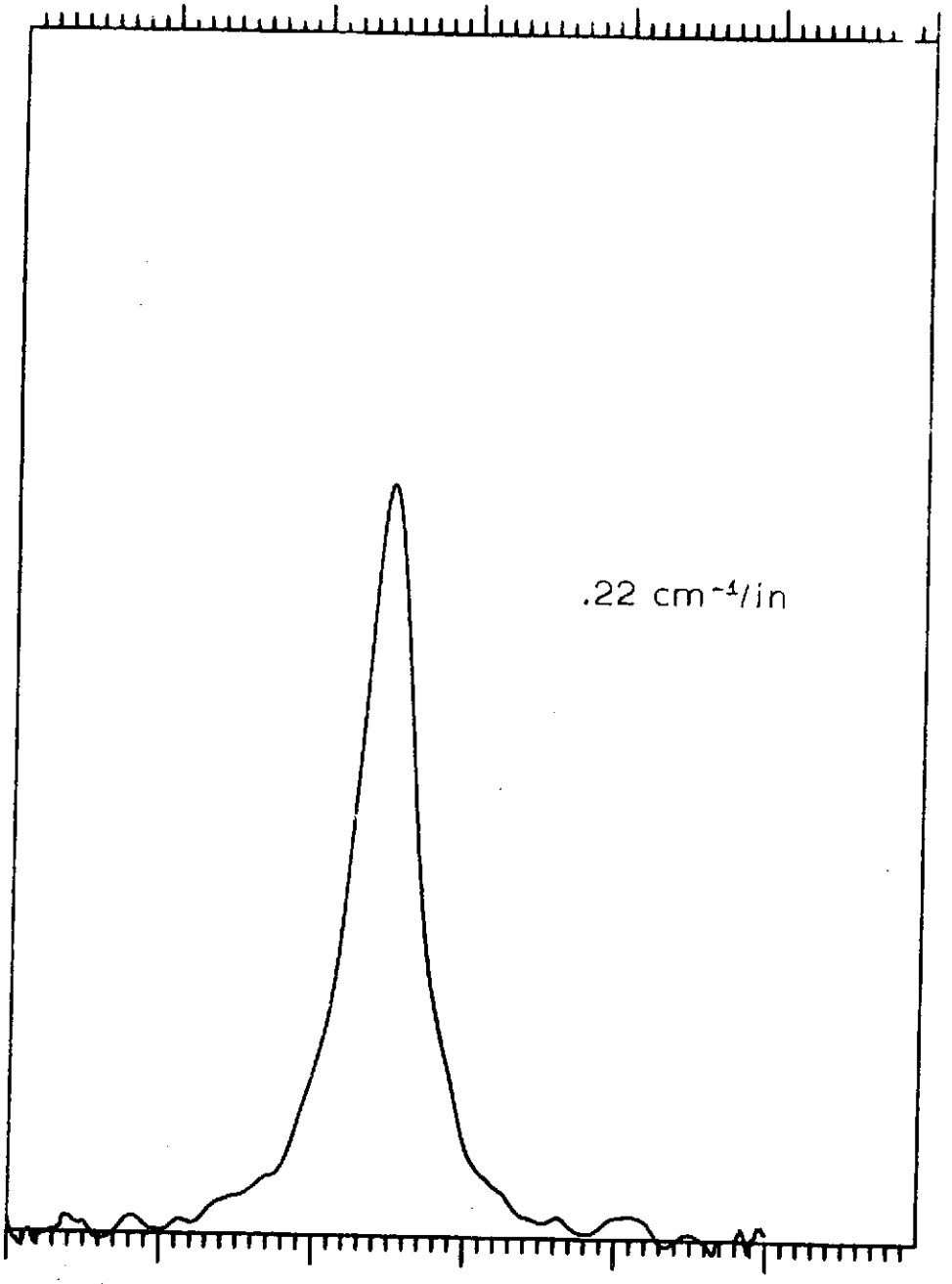

Figure 36. Absorption Coefficient Curve for the $Q_1(0)_J$ H_2 Line

broadening. Pressure broadening was eliminated by admitting CO into the spectrometer tank. With a 72 meter path, 0.6 millimeters of carbon monoxide was sufficient pressure to use the P(21) line in the first overtone with no observable pressure broadening. This line was chosen for the deconvolution of the $Q_1(0)$ and $Q_1(1)$ H_2 lines since its frequency was between the two lines of interest and was in the same order as the H_2 lines. The CO line was observed at a scan rate and slit width corresponding to the data to which it would be applied. The line was observed several times and recorded on magnetic tape as well as on chart paper. The portions of the runs containing the lines were then smoothed and plotted from the magnetic tape record using the IBM Calcomp plotting system. Figures 37 and 38 show the raw data and the smoothed data plotted out by the Calcomp plotter. The same process of averaging several measurements was used for the response function as was used for the data in the deconvolution process. After the base line was subtracted and the data converted to fractional absorptions, the line centers were used to align the several measurements and the average was found. The result of this process is shown in Figures 39 and 40. This averaging process results in a significant reduction of the noise on the response function. The observed line profile is a convolution of the actual response function and the natural Doppler width. The Doppler profile is gaussian and can be calculated from the formula,

$$A(\nu) = \left(\frac{mc^2}{2\pi\nu_o^2 KT}\right)^{1/2} e^{-\frac{mc^2(\nu-\nu o)^2}{2\nu_o^2 KT}} .$$

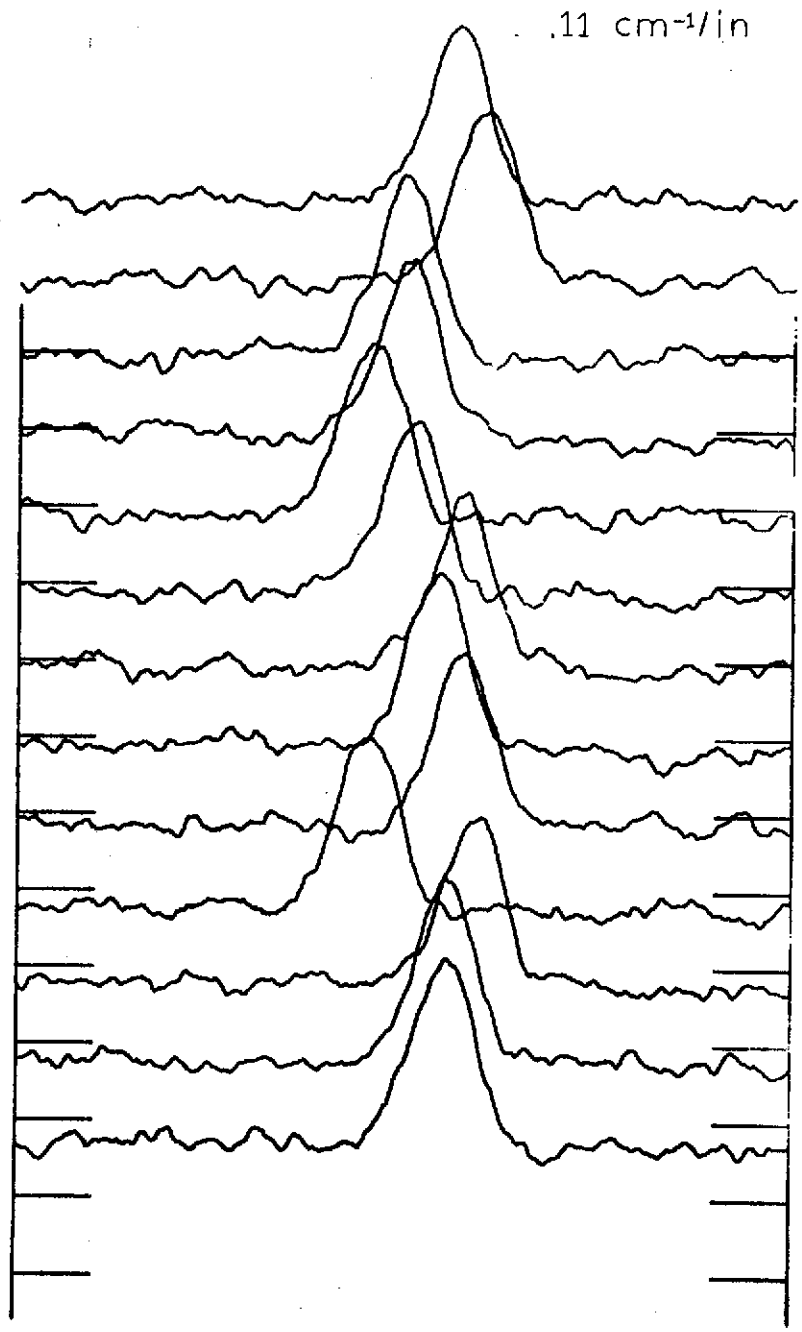

Figure 37. Raw Data

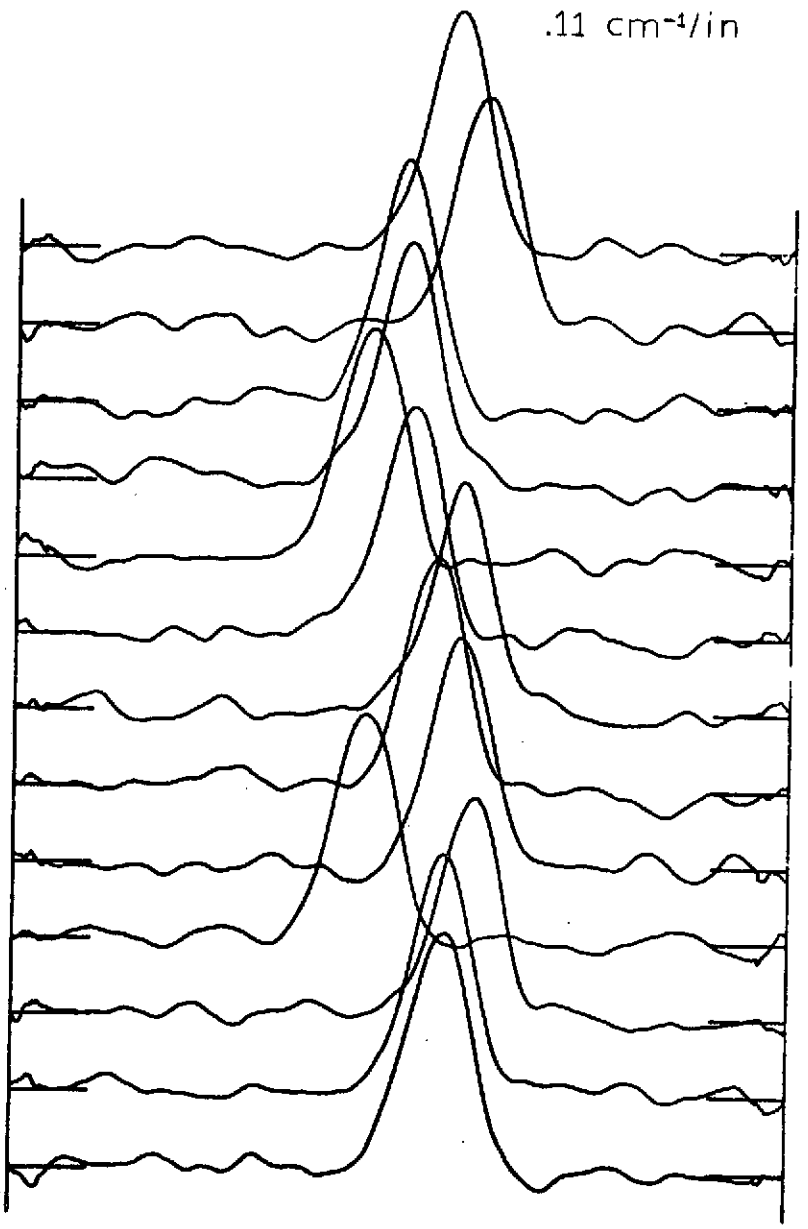

Figure 38. Smoothed Data

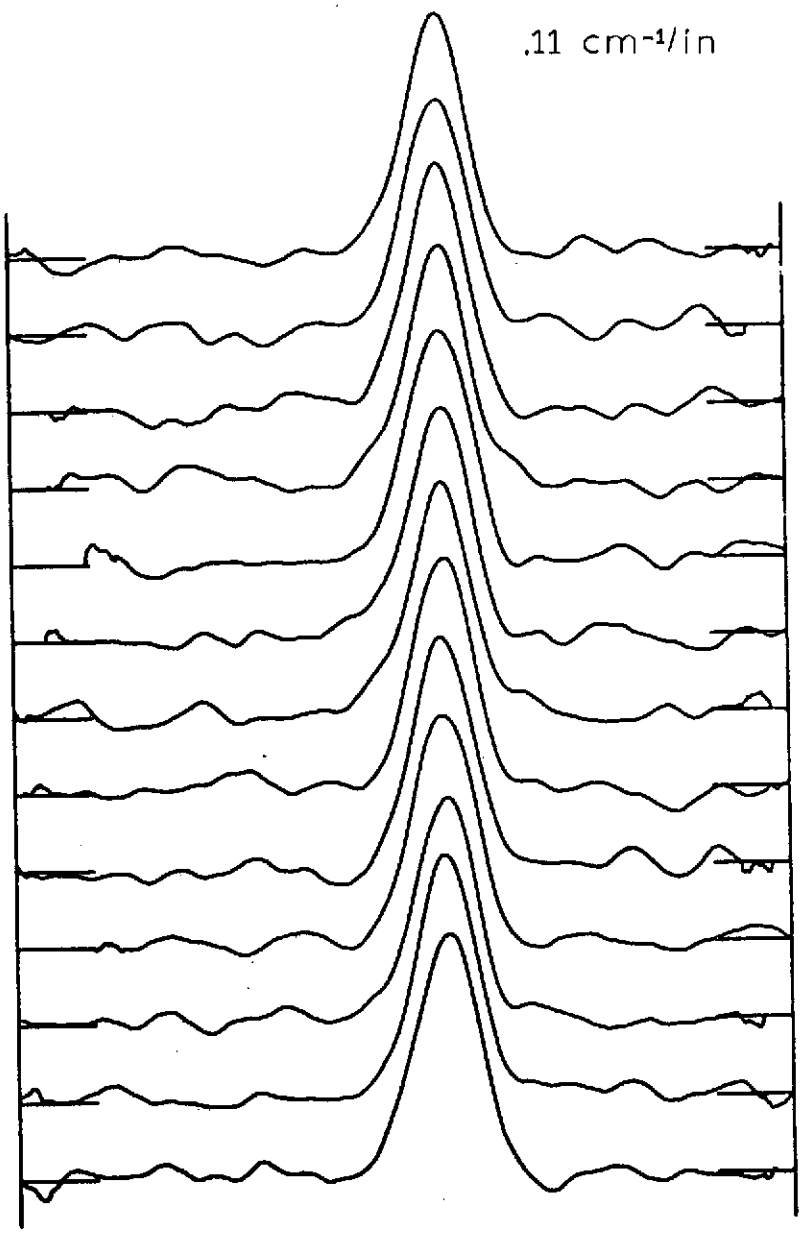

Figure 39. Aligned Data

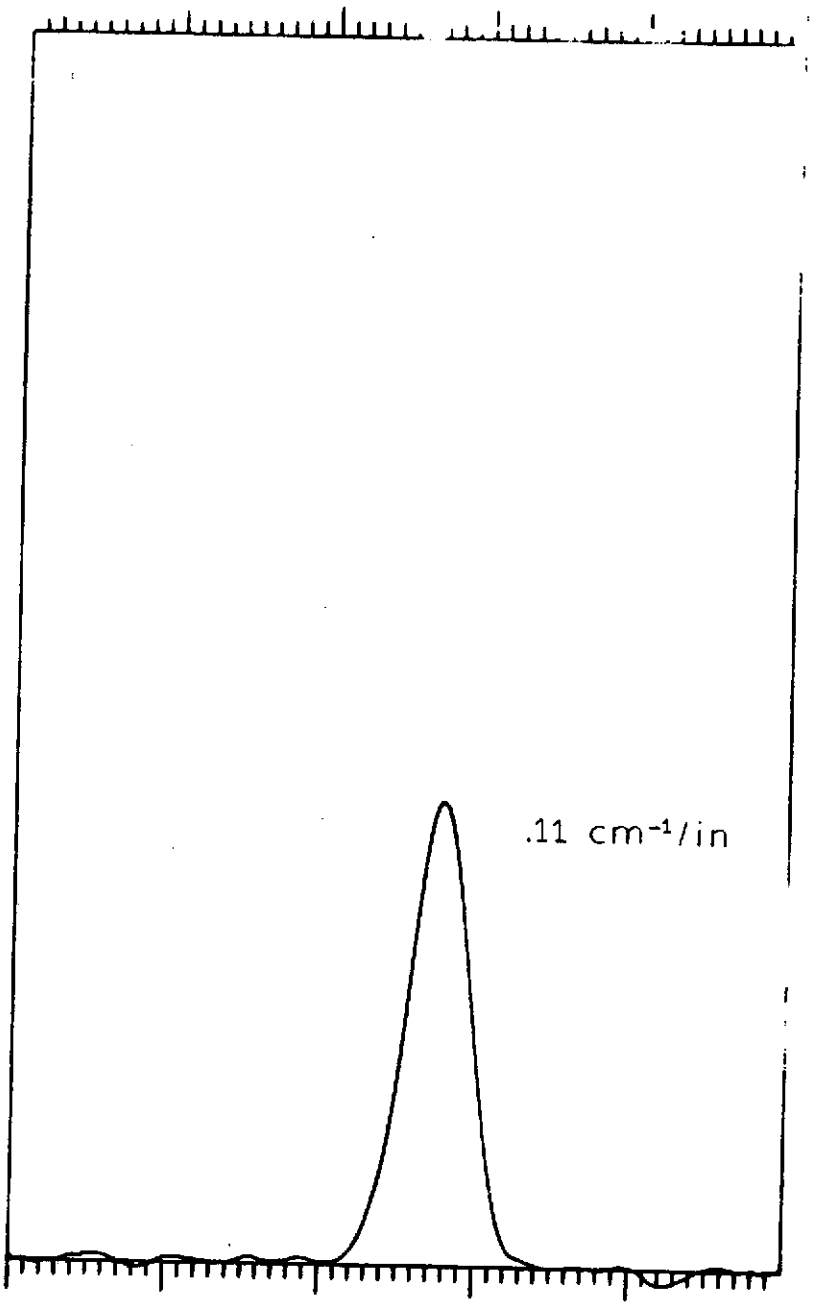

Figure 40. Averaged Response Function

where ν_o is the frequency of the observed line, m is the mass of the CO molecule, K is Boltzmann's constant and c is the speed of light. The deconvolution program may now be used to deconvolute the observed line profile, removing the calculated Doppler contribution and leaving the response function which describes the instrumental broadening. These steps are shown in Figures 41 and 42 where the scale of the response function has been increased to observe more readily the effects of the deconvolution. The excess base line is discarded and then the area under the line profile is computed. Each point was then divided by the area under the response function curve to normalize the area to unity, and the results are punched on cards for use in the deconvolution program. The final response function used for more of the work here contained 352 points. The final response function is compared to a calculated Gaussian of the same half width and height in Figure 43. It is observed that the result is assymetric when compared to the Gaussian. The cause of this assymetry is not known but may possibly be due to abberations in the spectrometer optics or the use of straight entrance and exit slits. Curved slits are being built to replace the straight slits and the effect of the replacement of the slits on the symmetry of spectral lines should be interesting. Appendix B lists the computer program used for the determination of the response function and gives further specific details of the program.

4.9 Width of the H_2, $Q_1(0)$ and $Q_1(1)$ Lines

The widths of the H_2, Q branch lines have been measured and calculated by Hunt et al. (20). The paper gives references to the

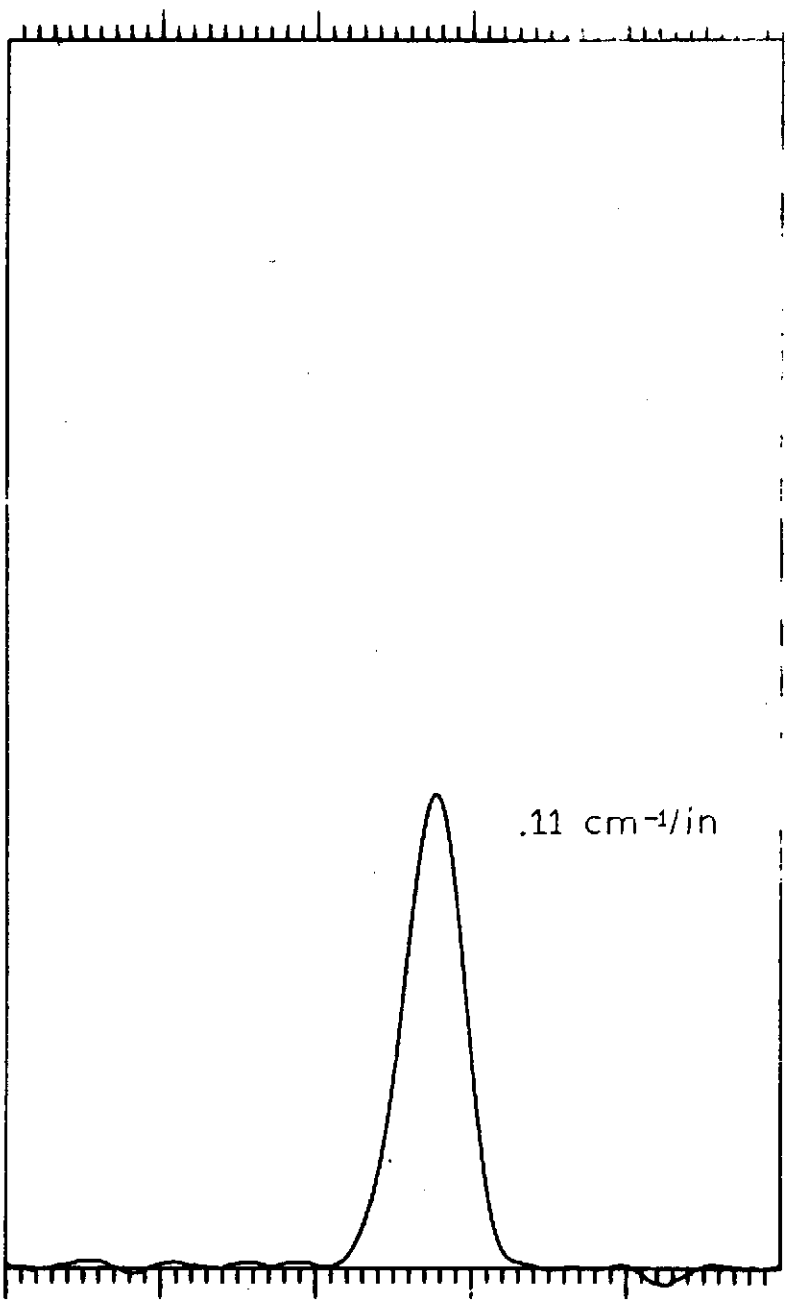

Figure 41. Deconvoluted Response Function

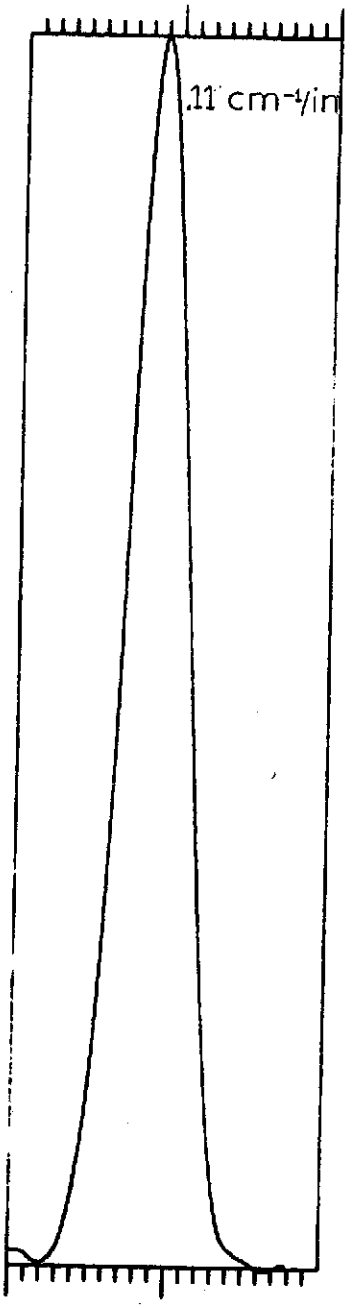

Figure 42. Final Response Function

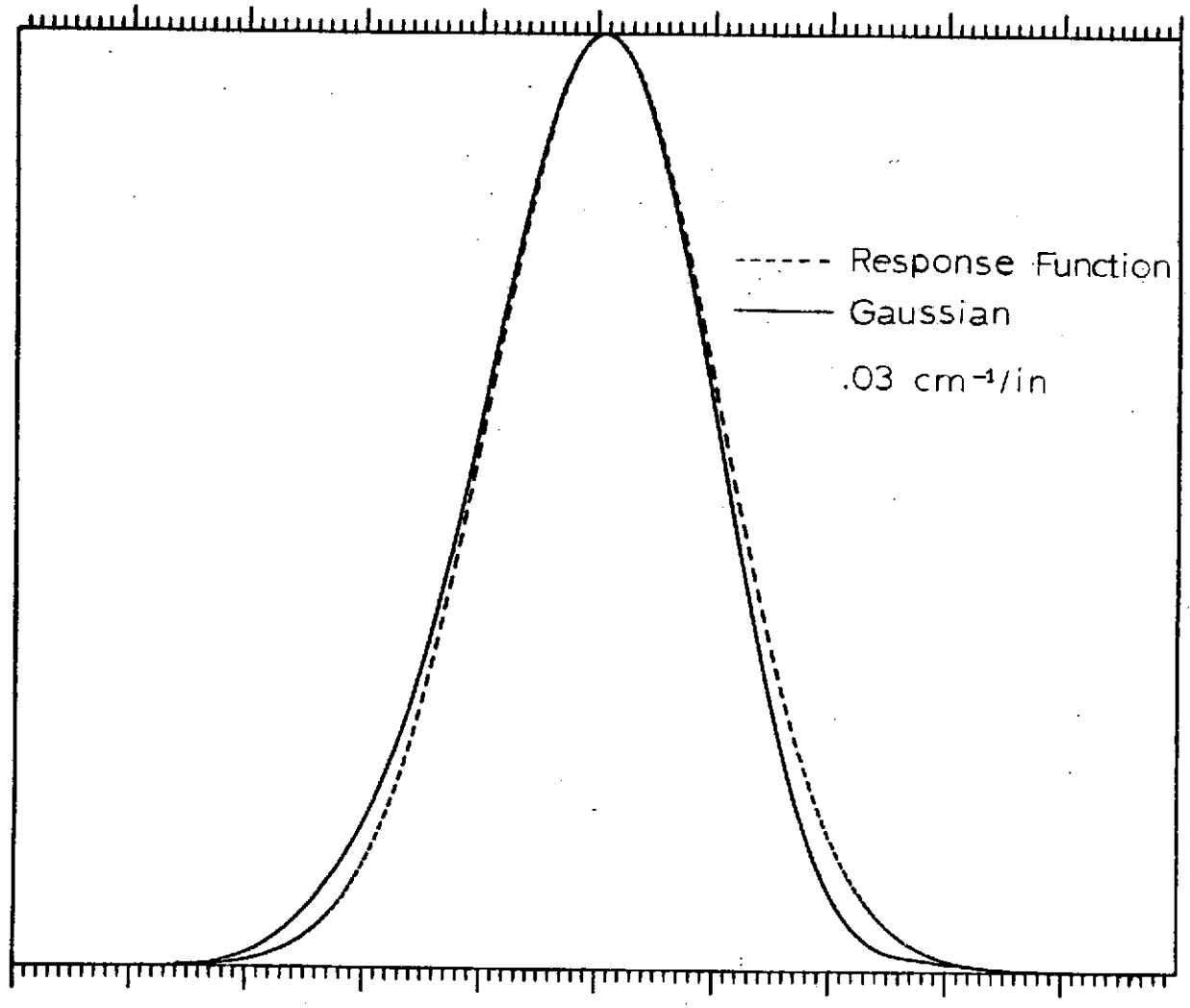

Figure 43. Response Function Compared to a Gaussian

theory of Van Kranendonk (21) and other later expositions pertinent to the H_2 line widths. Brannon (5) observed a possible dependence of the line width on the electric field intensity. Hunt et al. observed no field dependence on the width but offered no data on that effect. For this reason two of the stronger Q branch lines, the $Q_1(0)$ and $Q_1(1)$ were observed at a constant density of 28.21 amagat and varying field intensities. Table XXII and Figure 44 show the data taken for this experiment and show no field dependence of the width of the line to within experimental error. The half widths are measured from the absorption coefficient curves produced by the deconvolution program described in Section 4.7.

The absorption coefficient curve is approximately Lorentzian in shape as it should be for pressure broadened lines. This is observed in Figure 45 where the $Q_1(0)$, H_2 line is compared to a Lorentz function of the same height and half width. The broadening coefficients as a function of density of these two lines were measured and compared to those measured by Hunt et al. (20). Table XXIII and Figures 16 and 17 show the width of the $Q_1(0)$ and $Q_1(1)$ line as a function of density. The broadening coefficients measured in this experiment agree to within experimental error to those observed previously despite the relatively fewer points used in this determination.

4.10 The Response Function at Wider Slits

Figure 48 shows a comparison of two response functions, one obtained at the slit width used for the deconvolution of the lines discussed in

TABLE XXII

WIDTH OF H_2 LINES AS A FUNCTION OF THE ELECTRIC FIELD INTENSITY AT CONSTANT PRESSURE[1]

$Q_1(1)$ Field (volts/cm)	$Q_1(1)$ Width[2] (cm^{-1})	$Q_1(0)$ Field (volts/cm)	$Q_1(0)$ Width[3] (cm^{-1})
179,000	.068	179,000	.085
160,000	.079	160,000	.083
141,000	.060	141,000	.076
122,000	.073	122,000	.089
103,000	.065		
84,000	.059		
65,800	.078		
47,000	.076		

[1]Density = 28.21 Amagat

[2]Average Width = .070 ± .008 cm^{-1}

[3]Average Width = .083 ± .005 cm^{-1}

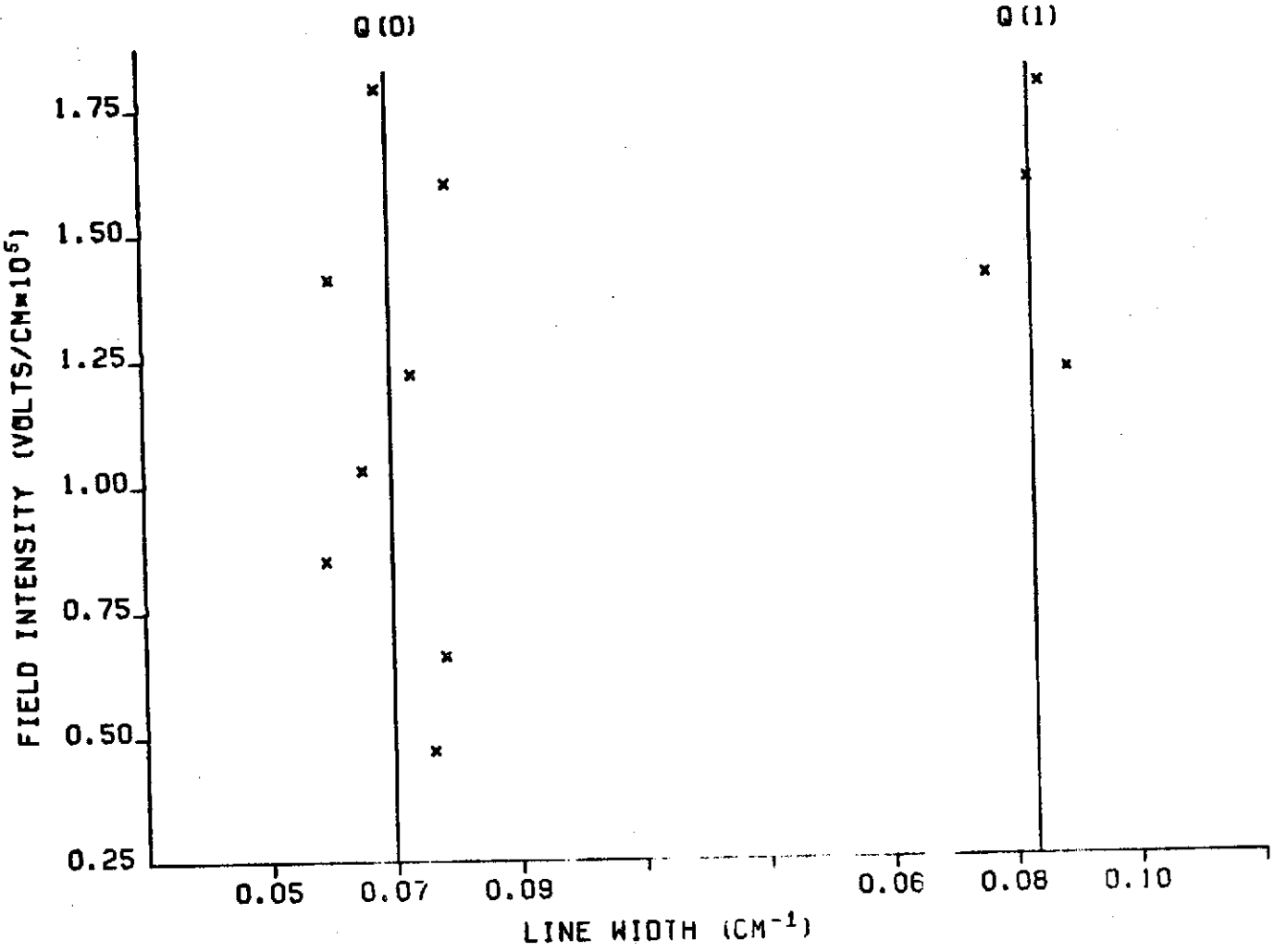

Figure 44. H_2 Line Width versus Electric Field Intensity

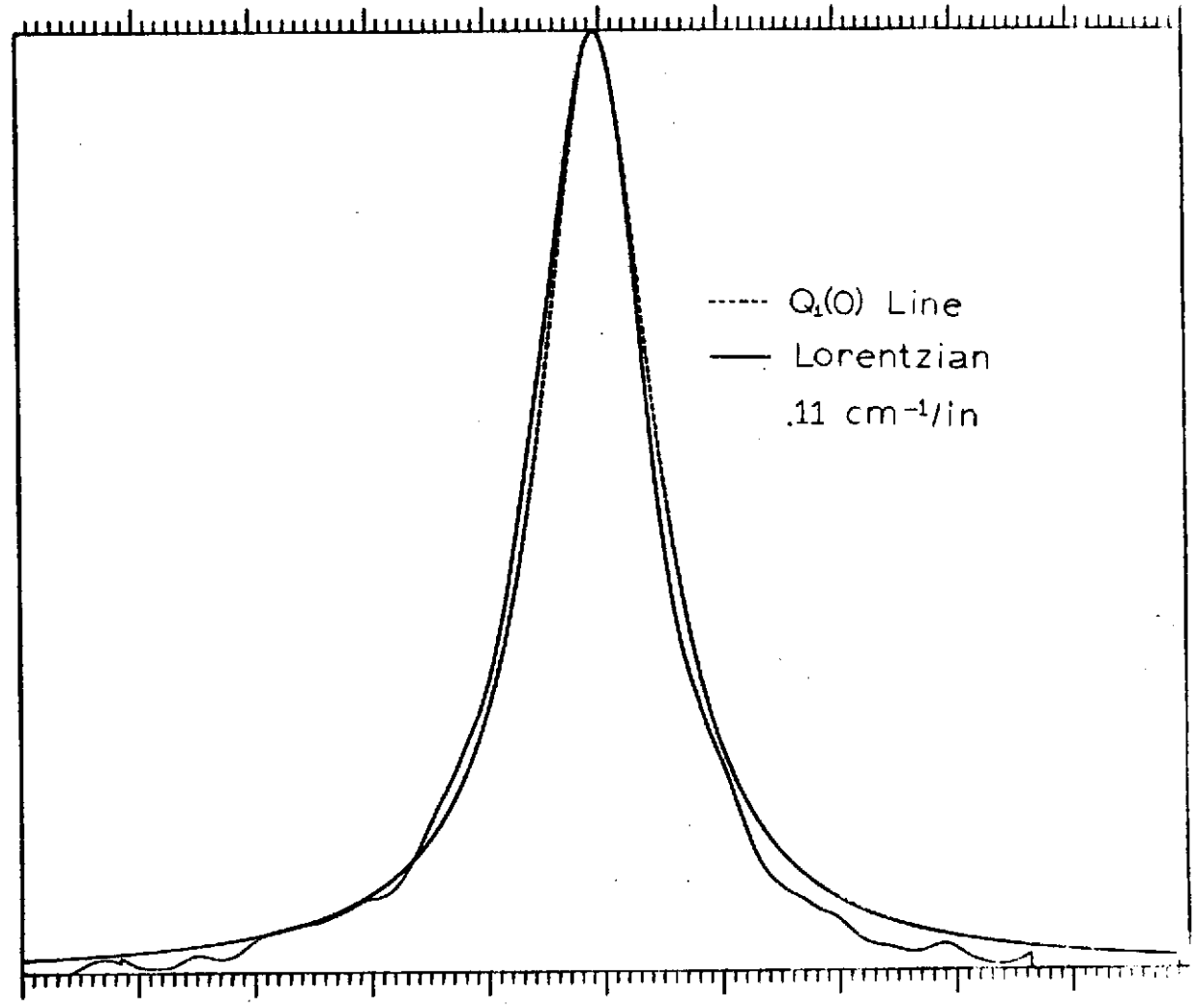

Figure 45. $Q_1(0)$, H_2 Absorption Coefficient Curve Compared to a Lorentzian

TABLE XXIII

WIDTH OF H_2 LINES AS A FUNCTION OF DENSITY

$Q_1(0)$ Density (Amagat)	$Q_1(0)$ Width (cm^{-1})	$Q_1(0)$ Density (Amagat)	$Q_1(0)$ Width (cm^{-1})
28.21	.083	28.21	.070
25.23	.087	23.73	.051
22.23	.075	19.22	.045
19.22	.061	14.69	.046
		10.12	.041

Broadening Coefficient Measured this Experiment (cm^{-1}/Amagat)	Broadening Coefficient Measured this Experiment (cm^{-1}/Amagat)
.0026 ± .0010	.0014 ± .0005

Broadening Coefficient Measured by Hunt et al. (cm^{-1}/Amagat)	Broadening Coefficient Measured by Hunt et al. (cm^{-1}/Amagat)
.00278	.00183

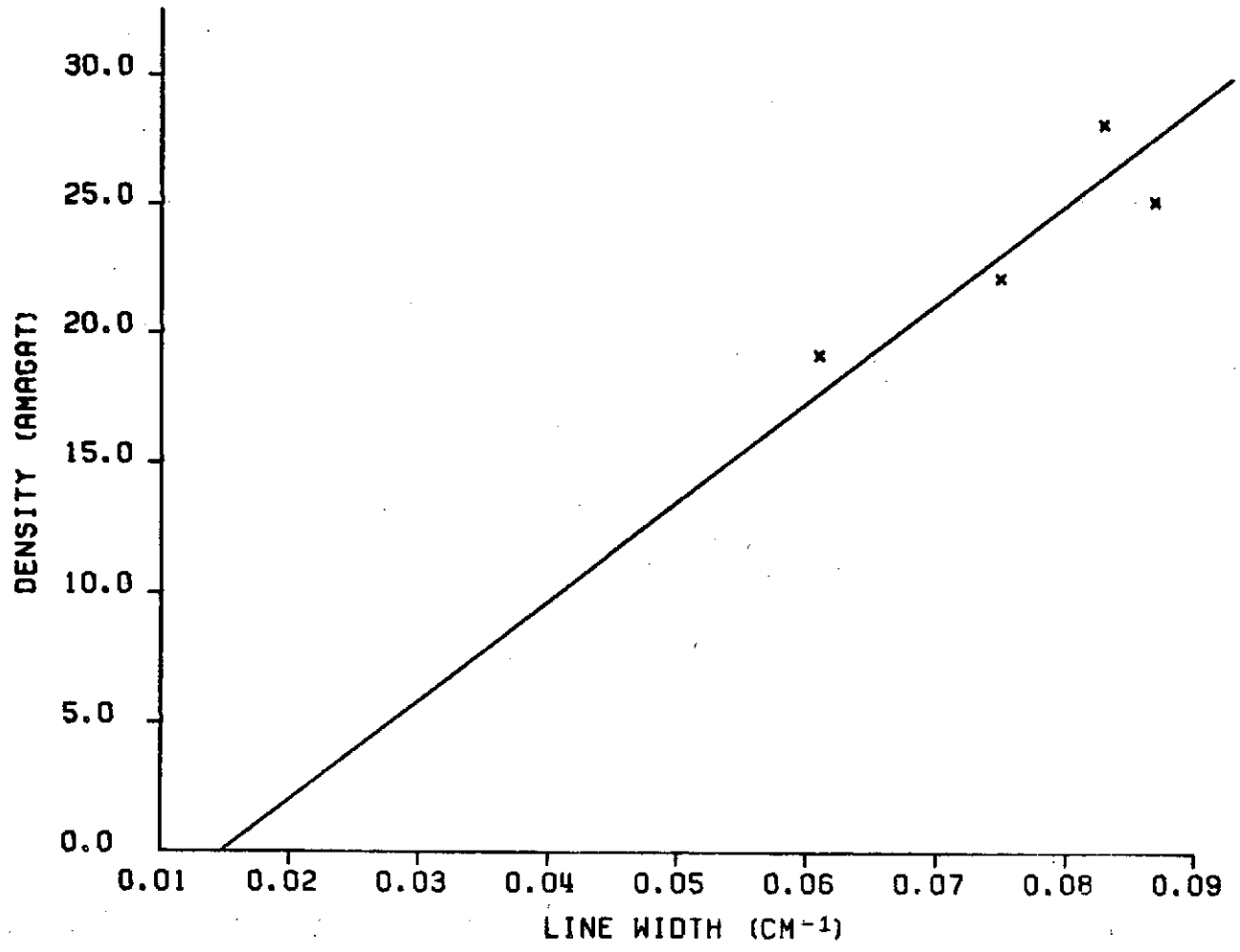

Figure 46. $Q_1(0)$, H_2 Line Width versus Density

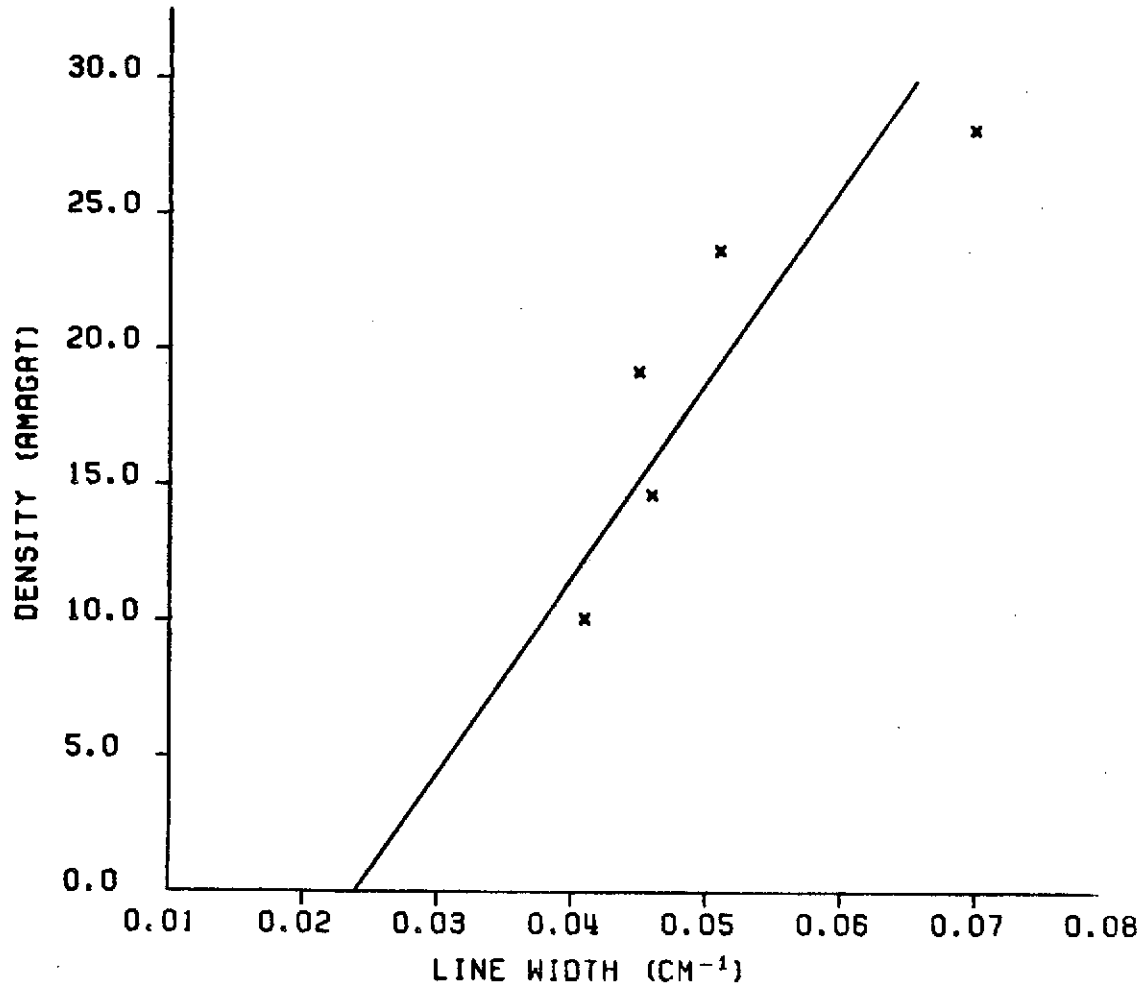

Figure 47. $Q_1(1)$, H_2 Line Width versus Density

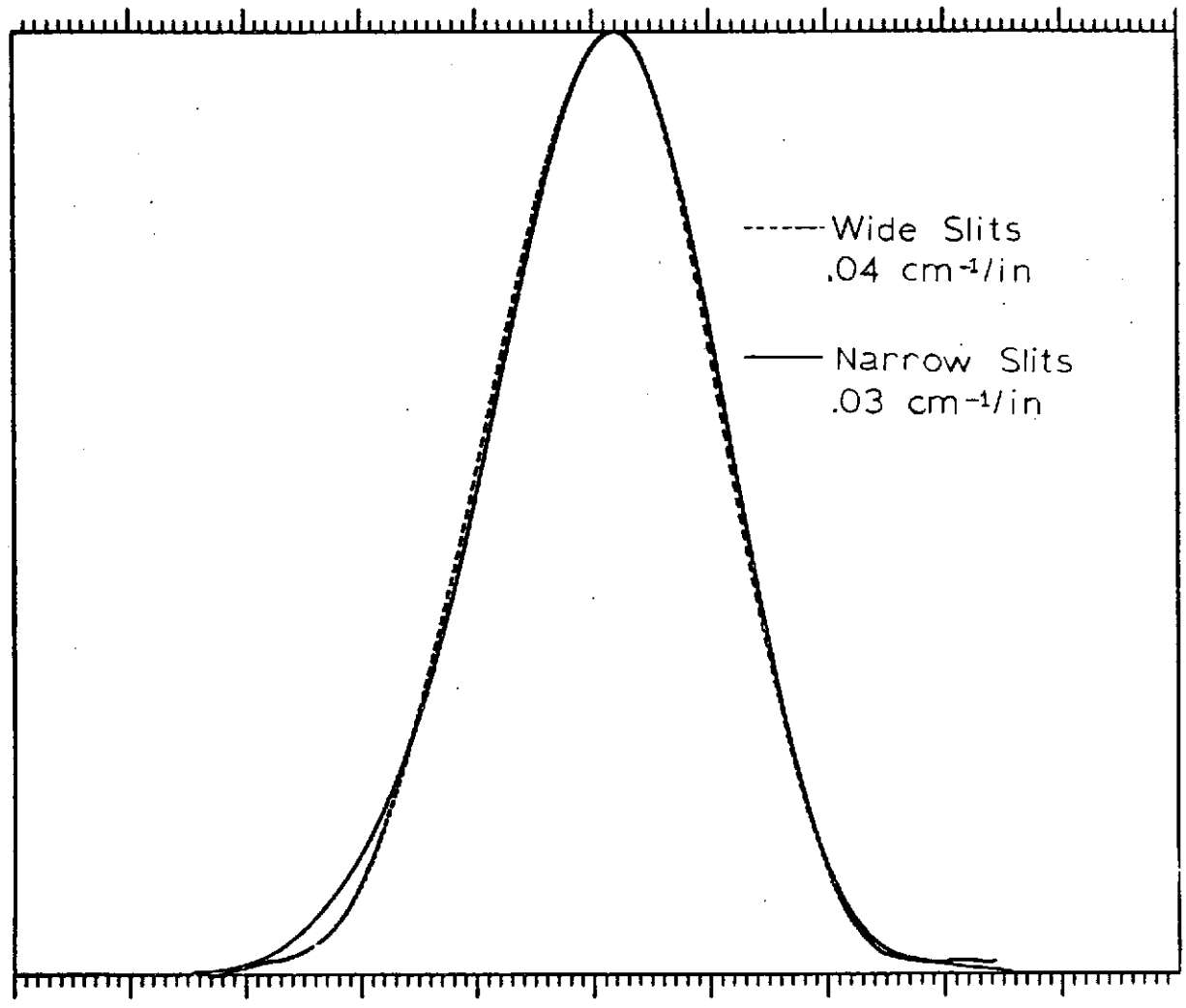

Figure 48. Comparison of Response Functions

Section 4.8 and the other obtained using wider slits. The full half width of the narrow response function is .041 cm^{-1}. The wider response function obtained at the wider slit setting has a full half width of .060 cm^{-1} and has been rescaled to the same half width as that of the narrow response function and aligned at the maximum absorption point. This was done to compare the shapes of the two functions. It is readily observed that the response function observed at wider slits is still assymetric in the same manner as before. However the wing on the low frequency side of the line has dropped somewhat and appears to be more gaussian.

The response function taken at the wider slit width was used to deconvolute the $Q_1(1)$, H_2 line observed at the same wider slit width. The width of the absorption coefficient curve measured at the wide slit width was .065 cm^{-1} as compared to .059 cm^{-1} at the narrower slit width. The electric field and pressure were the same for the two observations. The measured area at the smaller slit width was 7 percent larger than that measured at the wider slit setting. The total number of deconvolution iterations was increased from 12, which was used routinely in most of this work using the narrow response function, to 18 iterations using the wider response function. The result using 12 total iterations was essentially the same as for 18.

The difference between the two measured widths is within the range of variations which was observed on individual measurements of the line widths. So within the experimental error encountered, the deconvolution program used here yields the same half widths at both slit widths used.

Further tests should be made to make more conclusive statements. If the deconvolution method used here is good enough to allow the sacrifice of some resolution for an improvement of signal to noise ratio then the time and effort expended in the acquisition of data could be reduced and the final results improved by the use of wider slits. The reproducibility of line widths and areas is very much affected by the amount of noise in the data, and the deconvolution process itself works better when less noise is present in the data. An improvement in the signal to noise ratio would be extremely important to work similar to that done here where relatively weak signals are observed at high resolution.

4.11 Molecular Constants of H_2 and D_2

The number of zero pressure frequencies of the Q branch lines determined in this experiment is not enough to determine all of the molecular constants of H_2 and D_2. However the differences in the ground and first excited states could be determined, i.e. B_1-B_0, D_0-D_1 and H_1-H_0. Because the Q branch lines are so close together the term in the difference of H was not large enough to contribute significantly to the equation describing the Q-branch frequencies. The Q branch lines were therefore fitted to the equation (see Section 2.1).

$$\nu = \nu_{0\to1} + (B_1-B_0)J(J+1) + (D_0-D_1)J^2(J+1)^2.$$

The differences in the B and D values and the intercept frequency $\nu_{0\to1}$ were determined using a least squares method. Table XXIV shows the calculated constants for both H_2 and D_2, and the calculated values using

TABLE XXIV

H_2 and D_2 CONSTANTS

$\nu_{0\to1}$	4161.1630	95% confidence interval
B_1-B_0	-2.9570	± .0025
D_0-D_1	1.43 x 10^{-3}	± .20 x 10^{-3}

Observed	Calculated	Obs.-Cal.
4161.1632	4161.1630	+.0002
4155.2543	4155.2547	-.0004
4143.4725	4143.4723	+.0002
4125.8845	4125.8845	.0000

D_2 Constants

$\nu_{0\to1}$	2993.6223	95% confidence interval
B_1-B_0	-1.0559	± .0017
D_0-D_1	+2.95 x 10^{-4}	± .83 x 10^{-4}

Observed	Calculated	Obs.-Cal.
2993.6230	2993.6223	+.0007
2991.5100	2991.5116	-.0016
2987.2990	2987.2974	-.0016
2980.9932	2980.9939	-.0007
2972.6224	2972.6222	+.0002

these coefficients. It should be noted that the residuals are smaller than the experimental error.

The constants determined from the quadratic fit are compared with the appropriate data determined by Brannon (5), Stoicheff (14) and Foltz et al. (18) in Table XXV. The difference in the B values measured here compare favorably with the previous measurements. The difference in the D values measured here is smaller than previous measurements. These previous measurements used a greater number of lines which would possibly increase the value of the D constants to counteract the inclusion of constants involving H.

4.12 Integrated Areas of the H_2, $Q_1(0)$ and $Q_1(1)$ Lines

The absorption lines observed in this experiment are pressure broadened and should therefore be Lorentizian in profile. The equation describing the absorption coefficient is

$$K_\nu = \frac{S}{\pi} \frac{\Delta\nu}{\Delta\nu^2+(\nu-\nu_0)^2} \quad , \tag{59}$$

where $\Delta\nu$ is half of the full line width at half maximum absorption. ν_0 is the central frequency of the line and S is the integrated absorption coefficient defined as

$$S = \int K_\nu d_\nu \quad ,$$

or in other words the area under the absorption coefficient curve. According to these two equations we see that given the half width and

TABLE XXV

H_2 and D_2 CONSTANTS COMPARED TO OTHER MEASUREMENTS

	$\nu_{0\to1}$	B_1-B_0	D_0-D_1
This work	4161.1630	-2.9570	$+1.43 \times 10^{-3}$
Brannon	4161.158	-2.9627	$+1.82 \times 10^{-3}$
Stoicheff	4161.134	-2.9614	$+1.64 \times 10^{-3}$
Foltz et al.	4161.1815	-2.9650	$+2.03 \times 10^{-3}$

D_2

	$\nu_{0\to1}$	$B_1- B_0$	D_0-D_1
This work	2993.6223	-1.0559	$+2.95 \times 10^{-4}$
Brannon	2993.606	-1.0575	$+4.38 \times 10^{-4}$
Stoicheff	2993.548	-1.0623	$+5.9 \times 10^{-4}$

and integrated area of the absorption coefficient curve we should be able to calculate the absorption coefficient profile.

The $Q_1(0)$ and $Q_1(1)$ lines were deconvoluted in this experiment. After the deconvoluted profiles were converted to absorption coefficient curves the half widths and integrated areas were measured. The half widths of these lines were not observed to be a function of the electric field intensity, however the integrated area should, according to equation (57), increase as the square of the electric field intensity. Figure 49 clearly shows this to be the case, where the integrated areas of $Q_1(0)$ and $Q_1(1)$ have been measured as a function of electric field intensity squared at a constant density of 28.21 amagat and fitted with a straight line calculated using a leasts squares method. The integrated area should also, according to equation (57) increase linearly with the pressure, so that the product of the pressure and electric field intensity squared versus the integrated area should yield a straight line. Figure 50 demonstrates the validity of this argument.

It should be emphasized that the area measurements were made on the absorption coefficient curve. This is necessary since nonlinear absorption apparently affects the integrated areas as well as the more obvious effect on the half widths. A measurement of the integrated areas of the strongly absorbing $Q_1(1)$ line before deconvolution versus the product DE^2 did not yield a straight line.

If we assume that the integrated area S is given by the expression

$$S = m_s DE^2 \ ,$$

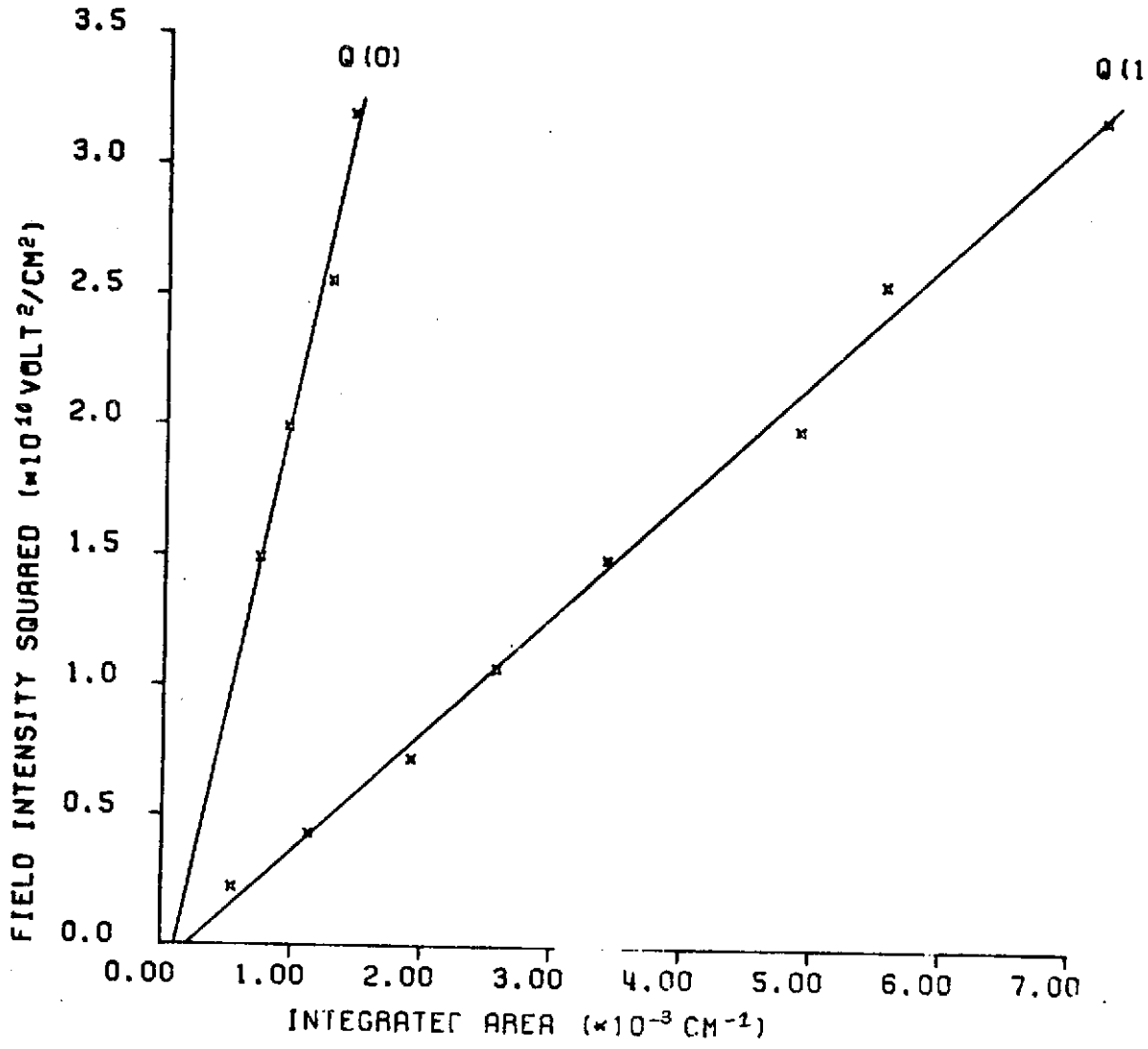

Figure 49. Integrated Area versus E^2

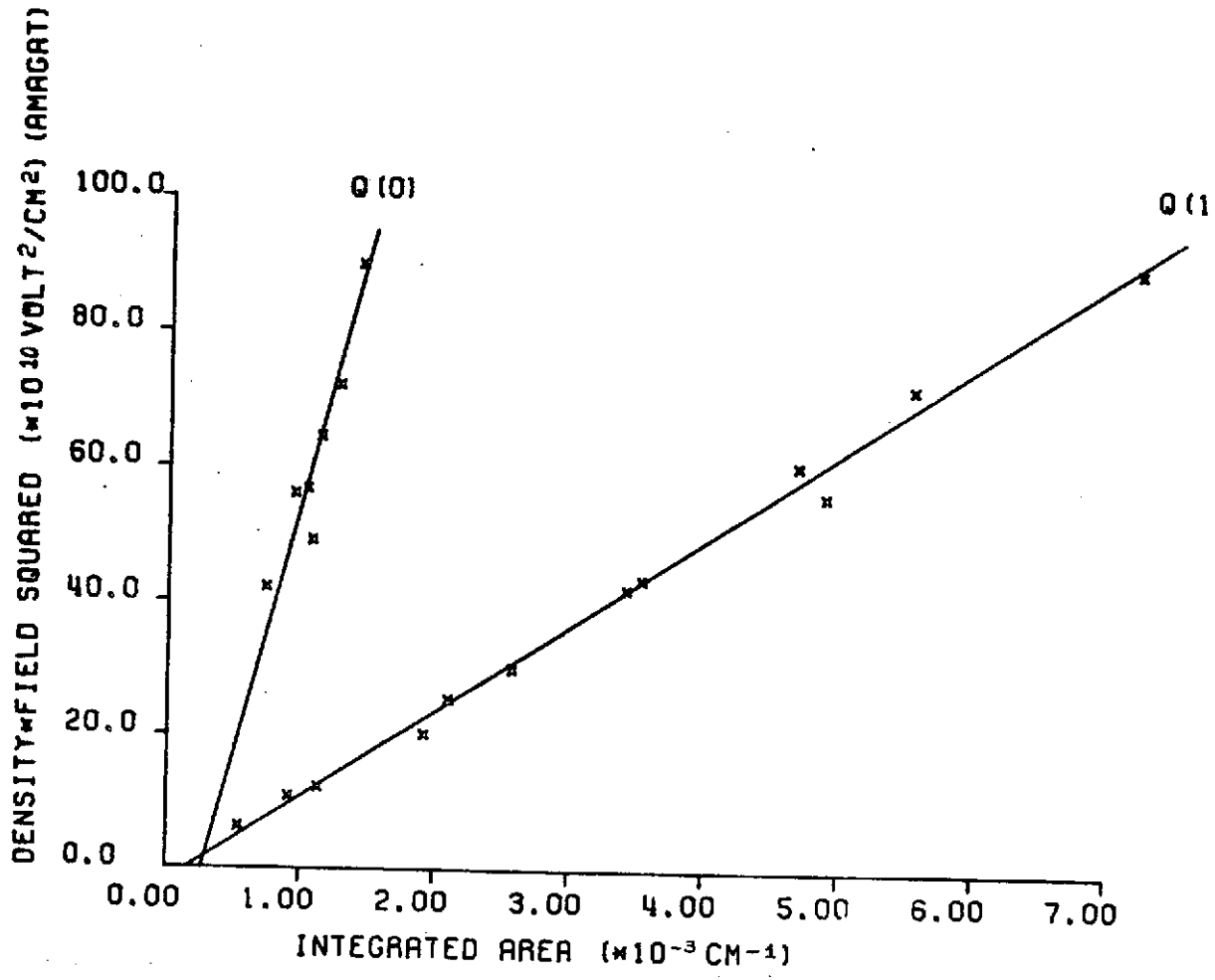

Figure 50. Integrated Area versus DE^2

where D is the gas density, E is the electric field intensity and m_s is the slope of the best fit line shown in Figure 50, then the value of S at an arbitrary density and electric field intensity can be computed for use in equation (59). If we further assume that the half widths $\Delta\nu$ are given by the expression

$$\Delta\nu = m_{\Delta\nu} D \ ,$$

where $m_{\Delta\nu}$ is the broadening coefficient then the half width at an arbitrary pressure can be calculated for use in equation (59). These values can then be used to calculate the absorption coefficient curve at the desired value of D and E. Table XXVI gives the values of the slopes m_s and $m_{\Delta\nu}$ used for this purpose. The value of m_s was obtained from the data shown in Figure 50. The value of $m_{\Delta\nu}$ used is the value measured by Hunt et al. (17) since the present work used only a limited amount of data to observe the broadening coefficient. Table XXVI also compares the calculated absorption coefficient to an experimentally measured coefficient. The values are actual coefficients and are not normalized to the path length. The calculated values compare satisfactorily with the observed values. Therefore for the two lines observed here ($Q_1(1)$ and $Q_1(0)$) we can calculate the absorption coefficient profile at any desired electric field intensity and gas density.

TABLE XXVI

CALCULATION OF ABSORPTION COEFFICIENTS

$m_s \frac{cm^{-1}}{(amagat)\left[\frac{volts}{cm}\right]^2}$	$m^1_{\Delta\nu}$ cm^{-1}/amagat
$Q_1(0)$ 1.32×10^{-15}	2.78×10^{-3}
$Q_1(1)$ 7.08×10^{-15}	1.38×10^{-3}

K_ν Calculated	K_ν Measured
2.333	2.026
1.998	1.831
1.394	1.481
.927	1.151
.631	.857
.447	.624
.330	.455
.252	.335
.197	.264
.159	.224
.130	.184
.109	.145
.097	.110
.083	.080
.072	.069
.063	.060
.055	.048
.048	.042

[1]Measured by Hunt et al. (17)

CHAPTER V

SUMMARY AND SUGGESTIONS FOR FUTURE WORK

5.1 Summary

To summarize the experimental section of this work the following things have been achieved.

1. The $Q_1(0)$ through $Q_1(3)$, H_2 fundamental absorption line frequenices have been measured as a function of density. The shift with pressure in the 7 to 28 amagat range was found to be linear and zero pressure frequencies and shift coefficients are calculated and compared to previous values. The relative and absolute accuracy of the values measured are thought to be better than previous measurements because of the instrumental resolution available and the calibration techniques used.

2. A check on the effect of the electric field on the line position of the $Q_1(0)$ and $Q_1(1)$, H_2 lines showed no shift effects within an experimental error of about .002 cm^{-1}. The field intensities used ranged from about 50,000 to 160,000 volts/cm.

3. The $Q_1(0)$ through $Q_1(4)$, D_2 fundamental absorption line frequencies were measured as a function of density using the same method as for the H_2. The calculated zero pressure frequencies and pressure shifts are thought to be better than the relatively few previous measurements on these lines.

4. The differences in the ground and first excited state molecular constants B and D were found and used to calculate the zero pressure frequencies to less than experimental error. A comparison of these constants to other previously measured values was satisfactory considering the limited number of lines used in this calculation and the exclusion of the H constants which could not be determined from these values due to its small contribution to the closely spaced Q branch lines.

5. The unresolved Q branch of N_2 was observed but was too weak for good quantitative measurements. No S or O lines could be observed.

6. Integrated intensities of the $Q_1(0)$ and $S_1(1)$ lines have been used to calculate the polarizability constants α and γ for H_2. The value for γ agrees with previously measured values. The value for α does not agree as well. The reason for the discrepancy is not known.

7. A highly automated method for measuring the response function of the spectrometer has been developed using some modified techniques described by Jansson (16). The method uses digitized data recorded on magnetic tape. The Fortran coded program will average several determinations of the desired line profile and remove the calculated Doppler contribution by deconvolution methods. The finalized response function is normalized, excess base line is dropped and the results punched on cards for use in the deconvolution of line profiles. Calcomp plots are utilized for visual inspection of the progress of the program.

8. A comparison of the response functions of two slit width settings are compared and show significant although small differences in profile.

9. A program similar in structure has been developed for using the response function calculated by the program above to deconvolute observed spectral lines. The program is again highly automated. The deconvoluted line is converted to an absorption coefficent curve and the half width and area under the curve is calculated by the Fortran coded program.

10. The $Q_1(0)$ and $Q_1(1)$, H_2 absorption coefficient line widths calculated by the program above have been observed as a function of electric field at constant pressure. The experimental error was larger than hoped for but definitely shows that the widths of the electric field induced lines observed do not depend on the electric field intensity. The experimental error is attributed to a poor signal to noise ratio.

11. A comparison of the process of deconvolution on the $Q_1(1)$ H_2 line observed at two different slit widths was made. The observed final widths were different by 9 percent and the integrated areas by 7 percent. The 9 percent variation in the width is about the order of the experimental error encountered in the reproducibility of the line widths.

12. The $Q_1(0)$ and $Q_1(1)$ H_2 line widths were deconvoluted and the widths of the absorption coefficient curves were measured as a function of density. Relatively few points were used in comparison to previous work and the extrapolated lines did not go to zero at zero pressure. The measured broadening coefficients did however compare favorably to previous results within experimental error.

13. A check on the behavior of the integrated area as a function of the electric field intensity squared at constant pressure and on the integrated area as a function of the product of the electric field intensity squared and the pressure was very satisfactory. The integrated areas were taken from the calculated absorption coefficient curves of the $Q_1(0)$ and $Q_1(1)$, H_2 lines, and were found to vary linearly with the field intensity squared as well as with the product of the field intensity squared and the density. The intercepts at zero pressure and zero electric field were very close to zero area. The data obtained from the integrated areas were used to calculate a Lorentzian profile and compared to an experimentally measured profile with satisfactory results.

5.2 Suggestions for Future Studies

Two attempts to study weak electric field induced spectra in this experiment (N_2 and HD) were unsuccessful. The weak N_2 spectra could probably be seen successfully by employing the a.c. electric field technique used by Brannon (5) and others. In this technique a rotating contact is brought into the close proximity of another contact creating a spark gap arrangement which switches the field. If a reference signal is taken off of the rotating shaft in a manner similar to that described for the light chopper built for this experiment then this signal can be used as a reference signal for the lock in amplifiers. In this way only the difference in the absorption with the field on and the field off need be amplified by the electronics and the job of offsetting the

background signal is eliminated. One decided disadvantage of this technique is that it would make intensity measurements difficult. For the detector employed in this laboratory, the chopping rate should ideally be high (1000 c.p.s.) but this would have to be balanced against the rise time of the chopped field. It is felt that the purchase of pure HD and the construction of this electric field chopper would be worth the value of the data obtained.

The flushing cover used could not be completely purged of absorbing atmospheric gases. Since the absorptions which need to be observed in the HD region are small and fall in a region containing H_2D absorption, this problem needs to be solved. The cell could be put into the spectrometer but the high voltage, high pressure and normal maintainance seem to preclude this. A more compact source optics section in an evacuable chamber would solve this problem. Since N_2 lies in a region containing CO_2 atmospheric absorption, this would help in this area also.

LIST OF REFERENCES

LIST OF REFERENCES

1. J. L. Dunham, Phys. Rev. 41, 721 (1932).

2. L. Pauling and E. B. Wilson, Introduction to Quantum Mechanics, McGraw-Hill (1935).

3. G. Herzberg, Spectra of Diatomic Molecules, D. Van Nostrand (1950).

4. H. Goldstein, Classical Mechanics, Addison-Wesley (1965).

5. P. J. Brannon, "Pressure Effects on the Vibrational-Rotational Spectrum of H_2" Thesis, U. of Michigan (1964).

6. C. Manneback, Zs.f. Phys. 62, 244 (1930).

7. C. Manneback, Zs.f. Phys. 65, 574 (1930).

8. E. U. Condon and G. H. Shortley, The Theory of Atomic Spectra, Cambridge University Press (1935).

9. R. H. Dicke, Phys. Rev. 89, (1953).

10. J. L. Gersten and H. M. Foley, J. Opt. Soc. Am. 58, 933 (1968).

11. W. J. Boyd, P. J. Brannon, and N. M. Gailar, App. Phys. Letters 16, 135 (1970).

12. W. J. Boyd, "Electric Field Induced Pure Rotation Spectrum of Hydrogen" Thesis, U. of Tennessee (1969).

13. T. L. Hill, Introduction to Statistical Thermodynamics, Addison-Wesley (1962).

14. D. E. Jennings, (Thesis to be completed 1974), Thesis, U. of Tennessee (1974).

15. K. N. Rao, C. J. Humphreys and D. H. Rank, Wave Length Standards in the Infrared, Academic Press (1966).

16. B. P. Stoicheff, Can. J. Phys. 35, 730, (1957).

17. U. Fink, T. A. Wiggens and D. H. Rank, J. Mol. Spectry. 18, 384, (1965).

18. J. V. Foltz, D. H. Rank and T. A. Wiggens, J. Mol. Spectry. 21, 203 (1966).

19. P. A. Jannson, R. H. Hunt and E. K. Plyler, J. Opt. Soc. Am. 60, 596 (1970).

20. R. H. Hunt, W. L. Barnes and P. J. Brannon, Phys. Rev. 1 (1970).

21. J. Van Kranendonk, Can. J. Phys. 41, 433 (1963).

APPENDICES

APPENDIX A

The program calculates several useful parameters for use in intensity measurements as well as frequencies for homonuclear diatomic molecules. The main program makes some calculations and calls on the various subroutines. Subroutine BOZMAN calculates the relative population of the various J levels discussed in Section 2.4. Subroutine STRONG calculates the strength factors discussed in Section 2.2. Subroutine FREQCY calculates the line positions in the Q, S and O branches discussed in Section 2.1. The frequencies and relative intensities of the strongest lines are plotted by subroutine PLOTTER in a line printer plot. The lines are identified by their frequencies. The necessary input data and format are described in comment cards at the start of the Fortran coded program.

```
C PROGRAM FOR CALCULATING LINE POSITIONS AND RELATIVE INTEN-
C SITIES OF A HOMONUCLEAR MOLECULE WHOSE CONSTANTS ARE KNOWN
C THE PROGRAM GIVES BOLTZMANN FACTORS, STRENGTH FACTORS,
C LINE POSITIONS AND RELATIVE INTENSITIES FOR THE FIRST 26
C LINES IN EACH BRANCH FOR BOTH PARALLEL AND PERPENDICULAR
C POLARIZED RADIATION.  THE STRONGEST LINES ARE PLOTTED OUT
C AS FREQUENCY VS RELATIVE INTENSITY.  ORDER AND DETAIL OF
C DATA CARDS IS AS FOLLOWS.
C         CARD 1....TITLE CARD FOR THE RUN, TYPED ANYWHERE
C                   ON CARD
C         CARD 2....BV   IN COLUMNS  1 TO 15 MOLECULAR CON-
C                        STANT B FOR GROUND STATE V
C                   DV   IN COLUMNS 15 TO 30 MOLECULAR CON-
C                        STANT D FOR GROUND STATE V
C                   HV   IN COLUMNS 30 TO 45 MOLECULAR CON-
C                        STANT H FOR GROUND STATE V
C         CARD 3....T    IN COLUMNS  1 TO 15 KELVIN TEMPERA-
C                        TURE
C                   SO   IN COLUMNS 15 TO 30 SPIN DEGENERACY
C                        FOR ODD J LEVELS
C                   SE   IN COLUMNS 30 TO 45 SPIN DEGENERACY
C                        FOR EVEN J LEVELS
C         CARD 4....AV   IN COLUMNS  1 TO 15 AVERAGE POLARI-
C                        ZIBILITY
C                   GV   IN COLUMNS  1 TO 15 ANISOTROPY OF
C                        POLARIZATION
C         CARD 5....VOI  IN COLUMNS  1 TO 15 VIBRATIONAL CON-
C                  /     STANT
C                   BVP  IN COLUMNS 15 TO 30 MOLECULAR CON-
C                        STANT B OF EXCITED STATE V PRIME
C                   BV   IN COLUMNS 30 TO 45 MOLECULAR CON-
C                        STANT B OF GROUND STATE V
C                   DVP  IN COLUMNS 45 TO 60 MOLECULAR CON-
C                        STANT D OF EXCITED STATE V PRIME
C         CARD 6....DV   IN COLUMNS  1 TO 15 MOLECULAR CON-
C                        STANT D OF GROUND STATE V
C                   HVP  IN COLUMNS 15 TO 30 MOLECULAR CON-
C                        STANT H OF EXCITED STATE V PRIME
C                   HV   IN COLUMNS 30 TO 45 MOLECULAR CON-
C                        STANT H OF GROUND STATE V
C         CARD 7....SCALE OF LINE PLOT IN I5.  SUBTRACT THE
C                   ROUNDED OFF FREQUENCIES OF THE TWO
C                   CLOSEST LINES.  THE SCALE FACTOR TIMES
C                   THIS NUMBER SHOULD BE AT LEAST EQUAL
C                   TO ONE
      DOUBLEPRECISION F(26),S11Q(26),SLQ(26),S11S(26),
     1SLS(26),S11O(26),SLO(26),VQ(26),VS(26),VO(26),
     1A11Q(26),ALQ(26),A11S(26),ALS(26),A11O(26),ALO(26),
     1NA11Q(26),NALQ(26),NA11S(26),NALS(26),NA11O(26),
     1NALO(26),MAX(78),AA(78),VV(78),VVV(78),AAA(78),
     1BIG(6),HUGE
```

```
      INTEGER IMAX,IFLAG,IAM(78)
      CALL BOZMAN(F)
      CALL STRONG(S11Q,SLQ,S11S,SLS,S11O,SLO)
      CALL FREQCY(VQ,VS,VC)
      WRITE(6,100)
  100 FORMAT(1H1,28HBOLTZMANN*STRENGTH*FREQUENCY)
      WRITE(6,101)
  101 FORMAT(1HO,20X,8HQ BRANCH,20X,8HS BRANCH,20X,
     18HO BRANCH)
      WRITE(6,102)
  102 FORMAT(1HO,7X,1HJ,2X,8HPARALLEL,4X,13HPERPENDICULAR,
     14X,8HPARALLEL,4X,13HPERPENDICULAR,4X,8HPARALLEL,4X,
     113HPERPENDICULAR)
      DO2J=1,26
      I=J-1
      A11Q(J)=F(J)*S11Q(J)*VQ(J)
      ALQ(J)=F(J)*SLQ(J)*VQ(J)
      A11S(J)=F(J)*S11S(J)*VS(J)
      ALS(J)=F(J)*SLS(J)*VS(J)
      A11C(J)=F(J)*S11C(J)*VC(J)
      ALC(J)=F(J)*SLC(J)*VC(J)
    2 WRITE(6,106)I,A11Q(J),ALQ(J),A11S(J),ALS(J),A11C(J),
     1ALC(J)
  106 FORMAT(1HO,I5,6D15.6)
      N=1
      M=26
      CALL MAXO1(A11Q,M,IMAX)
      BIG(N)=A11Q(IMAX)
      N=N+1
      CALL MAXO1(ALQ,M,IMAX)
      BIG(N)=ALQ(IMAX)
      N=N+1
      CALL MAXO1(A11S,M,IMAX)
      BIG(N)=A11S(IMAX)
      N=N+1
      CALL MAXO1(ALS,M,IMAX)
      BIG(N)=ALS(IMAX)
      N=N+1
      CALL MAXO1(A11C,M,IMAX)
      BIG(N)=A11C(IMAX)
      N=N+1
      CALL MAXO1(ALC,M,IMAX)
      BIG(N)=ALC(IMAX)
      M=6
      CALL MAXO1(BIG,M,IMAX)
      HUGE=BIG(IMAX)
      DO5 J=1,26
      NA11Q(J)=A11Q(J)/HUGE
      NALQ(J)=ALQ(J)/HUGE
      NA11S(J)=A11S(J)/HUGE
      NALS(J)=ALS(J)/HUGE
```

```
      NA11O(J)=A11O(J)/HUGE
    5 NALO(J)=ALO(J)/HUGE
      WRITE(6,200)
  200 FORMAT(1H1,31HNORMALIZED PRODUCT OF B,S AND V)
      WRITE(6,101)
      WRITE(6,102)
      DO11 J=1,26
      I=J-1
   11 WRITE(6,106)I,NA11Q(J),NALQ(J),NA11S(J),NALS(J),
     1NA11O(J),NALO(J)
      CALL ORDER(NA11Q,NA11S,NA11O,VQ,VS,VO,VV,AA)
      J=1
      M=78
  301 IF(J.EQ.79)GOTO300
      CALL MAXO1(VV,M,IMAX)
      IF(VV(IMAX).EQ.0.0DO)GOTO300
      IF(IMAX.GT.26)GOTO600
      GOTO601
  600 IF(IMAX.GT.52)GOTO602
      GOTO603
  602 IFLAG=3
      GOTO604
  601 IFLAG=1
      GOTO604
  603 IFLAG=2
  604 IAM(J)=IFLAG
      VVV(J)=VV(IMAX)
      VV(IMAX)=0.0DO
      AAA(J)=AA(IMAX)
      J=J+1
      GOTO301
  300 M=J-1
      WRITE(6,304)
  304 FORMAT(1H1,19HLINES TO BE PLOTTED)
      WRITE(6,305)
  305 FORMAT(1HO,2X,4HLINE,6X,9HFREQUENCY,16X,9HINTENSITY)
      DO 302 J=1,M
  302 WRITE(6,303)J,VVV(J),AAA(J)
  303 FORMAT(1HO,I5,2D20.9)
      WRITE(6,1100)
 1100 FORMAT(1H1,31HRELATIVE INTENSITY VS FREQUENCY)
      WRITE(6,1101)
 1101 FORMAT(1HO,38H      FOR PARALLEL POLARIZED RADIATION)
      CALL PLOTER(AAA,VVV,IAM,M)
      STOP
      END
```

```
      SUBROUTINE BOZMAN(F)
      DOUBLEPRECISION FVJ,BOLT,NUM(101),SUM,SPIN,NAME(10),X,
     1CCAL,F(26)
      READ(5,800)NAME
  800 FORMAT(10A8)
      WRITE(6,801)NAME
  801 FORMAT(1H1,35X,10A8)
      WRITE(6,302)
  302 FORMAT(1H0,35X,35H************************************)
  700 READ(5,500)BV,DV,HV
  500 FORMAT(3E15.0)
      WRITE(6,300)
  300 FORMAT(1H0,15HINPUT DATA, BV=,20X,3HDV=,20X,3HHV=)
      WRITE(6,301)BV,DV,HV
  301 FORMAT(1H0,3D25.9)
      READ(5,500) T,SC,SE
      WRITE(6,600)
  600 FORMAT(1H0,14HINPUT DATA, T=,20X,3HSC=,20X,3HSE=)
      WRITE(6,301)T,SC,SE
      WRITE(6,400)
  400 FORMAT(1H0,4X,1HJ,14X,17HBOLTZMANN FACTORS)
      J=0
      IGO=1
    5 K=J+1
      FVJ=J*K*BV-J**2*K**2*DV+J**3*K**3*HV
      CCAL=(1.380622D-16*T)/(6.621960-27*2.997925D+10)
      X=FVJ/CCAL
      BOLT=DEXP(-X)
   13 DEG=2*J+1
      GOTO(10,15),IGO
   10 IGO=2
      SPIN=SE
   11 J=J+1
      IF(J.EQ.102)GOTO20
      NUM(J)=BOLT*DEG*SPIN
      IF(NUM(J).EQ.0.0D0)GOTO5
      IF(NUM(J).LT.1.0D-20)GOTO2
      GOTO5
    2 NUM(J)=0.0D0
      J=J+1
      IF(J.EQ.102)GOTO20
      GOTO2
   15 SPIN=SC
      IGO=1
      GOTO11
   20 SUM=0
      DO25J=1,101
   25 SUM=SUM+NUM(J)
      DO30J=1,26
      F(J)=NUM(J)/SUM
      I=J-1
```

```
 30 WRITE(6,503)I,F(J)
503 FORMAT(1HO,I5,D25.6)
    RETURN
    END
```

```
      SUBROUTINE STRONG(S11Q,SLQ,S11S,SLS,S11C,SLC)
      DOUBLEPRECISION S11Q(26),SLQ(26),S11S(26),SLS(26),
     1S11C(26),SLC(26),A,B,C,D,E,F,G,H,O,GV,R,S,T,U,V,W,AV,
     1P,Q
      READ(5,300)AV,GV
  300 FORMAT(2E15.0)
      WRITE(6,301)
  301 FORMAT(1H1,15HINPUT DATA, AV=,20X,3HGV=)
      WRITE(6,302)AV,GV
  302 FORMAT(1HO,2D25.9)
      WRITE(6,303)
  303 FORMAT(1HO,35X,16HSTRENGTH FACTORS)
      J=0
      R=0.0D0
   18 S=R+1.0D0
      T=2*R-1.0D0
      U=2*R+3.0D0
      V=4.0D0/45.0D0
      W=1.0D0/15.0D0
      J=J+1
      S11Q(J)=(R*S)/(T*U)*V*(GV**2)+(AV**2)
      SLQ(J)=(R*S)/(T*U)*W*(GV**2)
      IF(J.EQ.26)GOTO19
      R=R+1.0D0
      GOTO18
   19 J=0
      A=0.0D0
      P=2.0D0/15.0D0
      Q=0.10DC
    5 B=A+1.0D0
      C=A+2.0D0
      D=2.0D0*A+3.0D0
      E=2.0D0*A+1.0D0
      J=J+1
      S11S(J)=(B*C)/(D*E)*P*(GV**2)
      SLS(J)=(B*C)/(D*E)*Q*(GV**2)
      IF(J.EQ.26)GOTO12
      A=A+1.0D0
      GOTO5
   12 S11C(1)=0.0D0
      SLC(1)=0.0D0
      J=1
      F=1.0D0
   15 G=F-1.0D0
      H=2*F-1.0D0
      O=2*F+1.0D0
      J=J+1
      S11C(J)=(F*G)/(H*O)*P*(GV**2)
      SLC(J)=(F*G)/(H*O)*Q*(GV**2)
      IF(J.EQ.26)GOTO16
      F=F+1.0D0
```

```
      GOTO15
   16 WRITE(6,504)
  504 FORMAT(1HO,20X,8HQ BRANCH,20X,8HS BRANCH,20X,
     18HO BRANCH)
      WRITE(6,505)
  505 FORMAT(1HO,3X,2HJ,4X,8HPARALLEL,6X,13HPERPENDICULAR,
     14X,8HPARALLEL,6X,13HPERPENDICULAR,4X,8HPARALLEL,6X,
     113HPERPENDICULAR)
      DO17J=1,26
      I=J-1
   17 WRITE(6,506)I,S11Q(J),SLQ(J),S11S(J),SLS(J),S11O(J),
     1SLO(J)
  506 FORMAT(1HO,I5,6D15.6)
      RETURN
      END
```

```
      SUBROUTINE FREQCY(VC,VS,VO)
      DOUBLEPRECISION VO(26),VS(26),VC(26),V(26),A,B,C,D
      READ(5,700)VOI,BVP,BV,DVP
  700 FORMAT(4E15.0)
      READ(5,701)DV,HVP,HV
  701 FORMAT(3E15.0)
      WRITE(6,300)
  300 FORMAT(1H1,16HINPUT DATA, VOI=,20X,4HBVP=,20X,3HBV=)
      WRITE(6,301)VOI,BVP,BV
  301 FORMAT(1H0,3D25.9)
      WRITE(6,302)
  302 FORMAT(1H0,16HINPUT DATA, DVP=,20X,3HDV=,20X,4HHVP=,
     120X,3HHV=)
      WRITE(6,303)DVP,DV,HVP,HV
  303 FORMAT(1H0,4D25.9)
      WRITE(6,304)
  304 FORMAT(1H0,35X,14HLINE FREQUENCY)
      J=0
      A=0.0D0
      IGO=1
      IDONE=1
    5 B=A
      C=A+1.0D0
      D=A+1.0D0
   11 J=J+1
      IF(J.EQ.27)GOTO16
      V(J)=VOI+B*D*BVP-A*C*BV-B**2*D**2*DVP+A**2*C**2*DV+
     1B**3*D**3*HVP-A**3*C**3*HV
      A=A+1.0D0
      GOTO(5,18,25),IGO
   16 GOTO(17,19,30),IDONE
   17 DO40J=1,26
   40 VO(J)=V(J)
      J=0
      A=0.0D0
      IGO=2
      IDONE=2
   18 C=A+1.0D0
      B=A+2.0D0
      D=A+3.0D0
      GOTO11
   19 DO41J=1,26
   41 VS(J)=V(J)
      V(1)=0.0D0
      V(2)=0.0D0
      J=2
      A=2.0D0
      IGO=3
      IDONE=3
   25 C=A-1.0D0
      B=A-2.0D0
```

```
      D=A-3.0D0
      GOTO11
   30 DO42J=1,26
   42 VO(J)=V(J)
      WRITE(6,507)
  507 FORMAT(1HO,1HJ,7X,8HQ BRANCH,12X,8HS BRANCH,12X,
     18HO BRANCH)
      DO31J=1,26
      I=J-1
   31 WRITE(6,503)I,VQ(J),VS(J),VO(J)
  503 FORMAT(1HO,I5,3D20.9)
      RETURN
      END
```

```
      SUBROUTINE MAXO1(A,M,IMAX)
      DOUBLE PRECISION GREAT,A(78)
      INTEGER IMAX
      GREAT=0.0D0
      IMAX=1
      DO 1 J=1,M
      IF(A(J).EQ.0.0D0)GOTO1
      IF(A(J).LT.GREAT)GOTO1
      IMAX=J
      GREAT=A(J)
    1 CONTINUE
      RETURN
      END
```

```
      SUBROUTINE ORDER(NA11Q,NA11S,NA11O,VQ,VS,VO,VV,AA)
      DOUBLE PRECISION NA11Q(26),NA11S(26),NA11O(26),VQ(26),
     1VS(26),VO(26),VV(78),AA(78)
      J=1
      DO 3 I=1,26
      VV(I)=VQ(J)
      AA(I)=NA11Q(J)
    3 J=J+1
      J=1
      DO 4 I=27,52
      VV(I)=VS(J)
      AA(I)=NA11S(J)
    4 J=J+1
      J=1
      DO 5 I=53,78
      VV(I)=VO(J)
      AA(I)=NA11O(J)
    5 J=J+1
      I=1
    8 IF(AA(I).EQ.0.0D0)GOTO6
      IF(AA(I).LT.0.1D-3)GOTO6
      GOTO7
    6 VV(I)=0.0D0
      AA(I)=0.000
    7 I=I+1
      IF(I.EQ.79)GOTO9
      GOTO8
    9 RETURN
      END
```

```
      SUBROUTINE PLOTER(A,V,IAM,M)
      DOUBLEPRECISION V(78),A(78),FREQ,R,PQ,SCALE,FIRST
      INTEGER IFREQ,IPQ,J,I,ISTEP,LINE(101),IAM(78)
      READ(5,400)SCALE
  400 FORMAT(1E15.0)
      WRITE(6,406)
  406 FORMAT(1HO,6HSCALE=)
      WRITE(6,402)SCALE
  402 FORMAT(1HO,D20.9)
      DATA IBL,IAST,IMX/2H  ,2H* ,2HX /
      DO910J=1,101
  910 LINE(J)=IAST
  921 WRITE(6,912)LINE
  912 FORMAT(1HO,101A1)
      ISTEP=1
      M=M+1
      J=1
      I=1
  801 IF(V(J).EQ.0.0D0)GOTO800
      GOTO911
  800 J=J+1
      I=I+1
      GOTO801
  911 FIRST=V(J)
  122 R=DABS(V(I)-FIRST)
      FREQ=(R*SCALE)+0.55D+01
      IFREQ=FREQ
      PQ=A(I)*0.10D+03+0.15OD+01
      IPQ=PQ
      DO919 J=1,101
  919 LINE(J)=IBL
      LINE(1)=IAST
  300 IF(IFREQ.EQ.ISTEP)GOTO913
      GOTO918
  913 DO914 J=1,IPQ
  914 LINE(J)=IMX
      IF(IAM(I).EQ.1)GOTO301
      IF(IAM(I).EQ.2)GOTO303
      IF(IAM(I).EQ.3)GOTO305
  301 WRITE(6,302)LINE,V(I)
  302 FORMAT(1H*,101A1,2X,1HQ,D15.6)
      GOTO307
  303 WRITE(6,304)LINE,V(I)
  304 FORMAT(1H ,101A1,2X,1HS,D15.6)
      GOTO307
  305 WRITE(6,306)LINE,V(I)
  306 FORMAT(1H ,101A1,2X,1HO,D15.6)
  307 I=I+1
      IF(I.EQ.M)GOTO917
      ISTEP=ISTEP+1
      IF(ISTEP.EQ.400)GOTO917
```

```
      GOTO122
  918 WRITE(6,916)LINE
  916 FORMAT(1H ,101A1)
      ISTEP=ISTEP+1
      IF(ISTEP.EQ.400)GOTO917
      GOTO300
  917 RETURN
      END
```

APPENDIX B

The program for the response function is coded in Fortran and runs on the IBM 360/65. Two minutes are required with 13 data runs and a total of 15 iterations. Three passes in loop 1, five passes in loop 2, and seven passes in loop 3 are used. The main program manipulates the data and calls on the various subroutines. The program first calls the subroutine READER which reads the first and the second specified base line block for the first data set. These points are averaged and divided by 1024 since the digitized data is recorded as values from 0 to 1024. This determines the base line for the first data set which is then read in by the subroutine READER. The base line value is subtracted from the data and the input value of the 100 percent absorbing point is used to convert the data to a fractional absorption. The data is smoothed once using the subroutine SMTHER which is part of Janssen's (19) deconvolution program. The array is then searched for the maximum value which is the peak absorption and the data points corresponding to the half absorption values are then found. This data is used to calculate the line center. The next steps in the program align the several data runs, with respect to this first computed line center point. The first data set is not moved but subsequent data sets are aligned so that the measured center point of the line lies at this first computed center point. Two separate loops, one for moving the data to the left and one for moving the data to the right, are used. The results for each subsequent data set is added into the array D, for

averaging after all data sets are processed. The subroutine BLOCK is called three times in these steps and plots the raw data, the smoothed data and the aligned data for each data set. After looping back to read each subsequent data set the array D is averaged to give an average line profile. Subroutine GAUSSIAN is used to calculate the doppler profile for use in the deconvolution steps. The doppler profile is normalized and used in calling the subroutines DECONER and DECONVO which are part of Jannson's program which have been modified as discussed in Section 4.7. The half-width of the deconvoluted profile is measured by looping back into the first part of the program which finds the points corresponding to the 50 percent peak absorbing points. All excess base line is then discarded which lies outside four times this computed half width. The area under the curve is then computed and each point normalized to this value so that the area is equal to unity. The final result which is the response function is punched on cards for use in the deconvolution program. Subroutine BBPLOT is called twice in these final steps. This subroutines plots the averaged data and the deconvoluted data with the excess base line dropped. It may be necessary to drop a few more base line points before using the response function in the deconvolution program. The data needed for the program and the format of this data is documented in comment cards listed at the start of the program.

```
C   THE PROGRAM TAKES UP TO 13 RESPONSE FUNCTIONS FROM
C   MAGNETIC TAPE AND AVERAGES THEM AND DECONVOLUTES THE
C   DOPPLER WIDTH FROM THE AVERAGE.  THE PROGRAM FIRST
C   READS IO, THE 100% ABSORBING POINT.  FOR THE FIRST
C   RESPONSE FUNCTION, TWO SPECIFIED BLOCKS ARE READ AND
C   AVERAGED.  THE INPUT DATA IS READ AND SMOOTHED ONCE.
C   THE BASE LINE IS SUBTRACTED AND THE DATA IS CONVERTED
C   TO A FRACTIONAL ABSORBANCE.  SUCESSIVE INPUT DATA IS
C   READ AND THE RESPONSE FUNCTIONS ARE ALIGNED, AVERAGED,
C   DECONVOLUTED, NORMALIZED AND PUNCHED ON CARDS.  THE
C   WIDTH OF THE RESPONSE FUNCTION IS CUT TO 4 HALF
C   WIDTHS IN THE FINAL STEPS.  CALCOMP PLOTS ARE MADE AT
C   INTERMEDIATE STEPS TO CHECK THE PROGRESS OF THE
C   PROGRAM.
C   DATA CARDS AS FOLLOWS:
C   CARD 1, LABEL FOR RUN ANYWHERE ON CARD
C   CARD 2, NUMBER OF RESPONSE FUNCTIONS TO AVERAGE
C   CARD 3, NUMBER OF BLOCKS READ FOR IO(=1) IN 5,
C           STARTING BLOCK IN 10
C   CARD 4, NUMBER OF BLOCKS READ FOR FIRST BASE BLOCK
C           (=1) IN 5, STARTING BLOCK IN 10
C   CARD 5, SAME AS 3 FOR SECOND BASE BLOCK
C   CARD 6, NUMBER OF BLOCKS READ FOR RESPONSE FUNCTION(=5)
C           IN 5, STARTING BLOCK IN 10
C   NEXT CARD, REPEAT 4 TO 6 FOR EACH RESPONSE FUNCTION
C   NEXT CARD, # OF CHARACTERS IN FIRST BBPLOT LABEL IN 5
C   NEXT CARD, LABEL FOR ABOVE STARTING IN ZERO
C   NEXT CARD, DATA TO CALCULATE GAUSSIAN
C           FREQ. OF LINE IN 15, MASS OF MOLECULE IN 30,
C           KELVIN TEMP. IN 45, FREQ. PER DP. IN 60
C   NEXT CARD, DECONVOLUTION DATA
C   NEXT CARD, # OF CHARACTERS IN SECOND BBPLOT LABEL IN 5
C   NEXT CARD, LABEL FOR ABOVE STARTING IN ZERO
C   NEXT CARD, # OF CHARACTERS IN THIRD BBPLOT LABEL IN 5
C   NEXT CARD, LABEL FOR ABOVE STARTING IN ZERO
      REAL*4 IO
      COMMON /A/X(1280),J,SRMS/B/Y(1280),A(150),NA
      DIMENSION IBUF(664),D(1280),NAME(20)
      INTEGER IMID(15)
      CALL PLOTS(IBUF,664,80.0,'BCYD#','REMOTE2#')
      CALL PLOT(0.0,0.5,-3)
      READ(5,723)NAME
  723 FORMAT(20A4)
      WRITE(6,724)NAME
  724 FORMAT(1H1,20A4)
  900 FORMAT(1H ,10F12.5)
  132 FORMAT(2I5)
  618 FORMAT(1HO,15X,3HNB=,I3,10X,4HNB1=,I3)
  725 FORMAT(1HO,25H**********************)
      DO 800 I=1,1280
  800 D(I)=0.0
```

```
      READ(5,139)ITEST
  139 FORMAT(I5)
C   READ IC
      READ(5,122)NB,NB1
      WRITE(6,618)NB,NB1
      CALL READER(NB,NB1,0,&15)
      TOTAL=0.0
      DO 702 I=1,256
  702 TOTAL=TOTAL+X(I)
      IC=TOTAL/(0.256E+03*0.1024E+04)
      WRITE(6,502)IC
      WRITE(6,725)
  502 FORMAT(1H0,20X,3HIC=,F10.6)
C   READ BASE LINE FROM TWO SEPARATE BLOCKS
      IAM=1
  714 IGO=1
      BASE=0.0
  245 READ(5,132)NB,NB1
      WRITE(6,618)NB,NB1
      CALL READER(NB,NB1,0,&15)
      DO 712 I=1,256
  712 BASE=BASE+X(I)
      IF(IGO.EQ.2)GO TO 247
      IGO=2
      GO TO 245
  247 BASE=BASE/(512.0*1024.0)
      WRITE(6,838)BASE
  838 FORMAT(1H0,20X,5HBASE=,F10.6)
C   READ INPUT DATA
      READ(5,132)NB,NB1
      J=NB*256
      WRITE(6,619)NB,NB1
  619 FORMAT(1H0,15X,3HNB=,I3,10X,4HNB1=,I3)
      WRITE(6,701)
  701 FORMAT(1H0,17HINPUT INTENSITIES)
      CALL READER(NB,NB1,0,&15)
      DO 938 I=1,J
  938 X(I)=X(I)/0.1024E+04
C   PLOT RAW DATA
      CALL PBLOCK(X,J)
      CALL PLOT(6.0,0.0,-3)
C   SMOOTH INPUT DATA
      CALL SMTHER(99)
C   SUBTRACT BASE LINE AND CONVERT TO FRACTIONAL ABSORPTION
      RIC=IC-BASE
  870 DO 788 I=1,J
  788 X(I)=(X(I)-BASE)/RIC
C   WRITE INPUT INTENSITIES
  901 WRITE(6,900)(X(I),I=1,J,10)
C   PLOT SMOOTHED DATA
      CALL BBLOCK(X,J)
```

```
      CALL PLOT(6.0,0.0,-3)
C  FIND MID POINT
  885 GREAT=0.0
      DO 718 I=1,J
      IF(X(I).LT.GREAT)GO TO 718
      GREAT=X(I)
      IGREAT=I
  718 CONTINUE
      IF(IGO.EQ.4)GO TO 884
      HALF=GREAT/2.0
      I=IGREAT
  768 I=I+1
      IF(X(I)-HALF) 770,770,768
  770 IHALF2=I
      I=IGREAT
  769 I=I-1
      IF(X(I)-HALF) 771,771,769
  771 IHALF1=I
      IMID(IAM)=(IHALF1+IHALF2)/2
      WRITE(6,772)IGREAT,IHALF1,IHALF2,IMID(IAM)
  772 FORMAT(1HO,7HIGREAT=,I5,10X,7HIHALF1=,I5,10X,
     1      7HIHALF2=,I7,10X,5HIMID=I7)
      WRITE(6,725)
      IREDO=IMID(1)-IMID(IAM)
  888 IF(IREDO) 70,71,72
   70 DO 969 I=1,J
      K=I-IREDO
      IF(K.LT.1.OR.K.GT.J)GO TO 697
      X(I)=X(K)
      GO TO 969
  697 X(I)=0.0E0
  969 CONTINUE
      GO TO 71
   72 DO 698 L=1,J
      I=J-L+1
      K=I-IREDO
      IF(K.LT.1.OR.K.GT.J)GO TO 699
      X(I)=X(K)
      GO TO 698
  699 X(I)=0.0E0
  698 CONTINUE
   71 IF(IGO.EQ.3)GO TO 999
C  PLOT ALIGNED DATA
      CALL BBLOCK(X,J)
      CALL PLOT(-12.0,0.5,-3)
C  ADD RESPONSE FUNCTIONS
      DO 970 I=1,J
  970 C(I)=C(I)+X(I)
      IF(IAM.EQ.ITEST)GO TO 713
      IAM=IAM+1
C  RESTART FOR NEXT RESPONSE FUNCTION
```

```
      GO TO 714
C   AVERAGE RESPONSE FUNCTION
  713 CALL PLOT(18.0,-FLOAT(ITEST-2)*0.5,-3)
      C=ITEST
      DO 971 I=1,J
  971 X(I)=D(I)/C
      WRITE(6,782)
  782 FORMAT(1HO,26HAVERAGED RESPONSE FUNCTION)
      WRITE(6,900)(X(I),I=1,J,10)
C   PLOT RESPONSE FUNCTION
      CALL BBPLOT(256.0)
C   CALCULATE GAUSSIAN FOR DECONVOLUTION
      CALL GAUSS(A,NA)
C   WRITE OUT GAUSSIAN
      WRITE(6,726)
  726 FORMAT(1HO,15HDOPPLER PROFILE)
      WRITE(6,900)(A(I),I=1,NA)
C   DECONVOLUTE RESPONSE FUNCTION
      CALL DCONVO
C   PLOT DECONVOLUTED RESPONSE FUNCTION
      CALL BBPLOT(256.0)
C   DROP EXCESS BASE LINE
      LENGTH=2*(IHALF2-IHALF1)
      IREDO=-(IMID(1)-LENGTH)
      IGO=3
      GO TO 888
C   NORMALIZE RESPONSE FUNCTION
  999 AREA=0.0
      J=2*LENGTH
      DO 778 I=1,J
  778 AREA=AREA+X(I)
      DO 779 I=1,J
  779 X(I)=X(I)/AREA
      WRITE(6,780)
  780 FORMAT(1H1,23HFINAL RESPONSE FUNCTION)
      WRITE(6,781)(X(I),I=1,J)
  781 FORMAT(1H ,10F12.5)
C   PUNCH RESPONSE FUNCTION
      WRITE(7,777)(X(I),I=1,J)
  777 FORMAT(8E10.4)
C   CHANGE SCALE AND REPLOT
      IGO=4
      GO TO 885
  884 DO 886 I=1,J
  886 X(I)=X(I)/GREAT
      CALL BBPLOT(256.0)
      CALL PLOT(0.0,0.0,999)
   15 CALL EXIT
      END
```

```
      SUBROUTINE READER(NX,NB1,KODE,*)
C-----NX BLOCKS OF DATA FROM UNIT 9 (TAPE) -- 256 I*2 FORM
C-----READ INTO X STARTING WITH BLOCK # NB1
C------IF KODE NE 0  UNIT 9 ENDED
C-----LOC = NEXT BLOCK ON TAPE, #0 = LABEL
      COMMON  /A/X(1280),KKK,SRMS
      INTEGER*2 INPUT(256),LI
      LOGICAL*1 LABEL(14),LK,L(2)
      EQUIVALENCE (L(1),LI)
      DATA LOC/0/
      IF(LOC.EQ.0)  GO TO 6
      IF(NB1-LOC)  3,2,1
    3 REWIND 9
      LOC=0
    6 ID=1
      READ(9,101,END=7,ERR=7)  LABEL
      LOC=1
  100 FORMAT(128(2A2))
  101 FORMAT(14A1)
    1 ND=NB1-LOC
      ID=2
      DO  5  I=1,ND
      LOC=LOC+1
    5 READ(9,100,END=7,ERR=7)  M
    2 CONTINUE
      NXX=-256
      ID=3
      DO  4  I=1,NX
      NXX=NXX+256
      READ(9,100,END=7,ERR=7)  INPUT
      LOC=LOC+1
      DO  4  J=1,256
      LI=INPUT(J)
      LK=L(1)
      L(1)=L(2)
      L(2)=LK
    4 X(NXX+J)=LI
      IF(KODE.EQ.0)  RETURN
C------END FILE---
      ID=4
    8 READ(9,100,END=9,ERR=7)  M
      LOC=LOC+1
      GO TO 8
    9 LOC=0
      RETURN
    7 WRITE(6,200)  ID,LOC
  200 FORMAT(5X3HID=I3,5X4HLOC=I5,5X,
     1       'READER ERROR PROGRAM REROUTED')
      RETURN 1
      END
```

```
      SUBROUTINE GAUSS(A,NA)
      DIMENSION A(150)
      READ(5,331)VO,W,T,FPERDP
  331 FORMAT(4E15.0)
      C=2.997925E+10
      B=1.38622E-16
      WRITE(6,330)
  330 FORMAT(1H1,23HINPUT DATA FOR GAUSSIAN)
      WRITE(6,332)VO,W,T,FPERDP
  332 FORMAT(1H0,6HFREQ.=,E15.7,5X,5HMASS=,E15.7,5X,
     1       6HTEMP.=,E15.7,5X,10HFREQ./DP.=,E15.7)
      Q=(W*C*C)/(2.*VO*VO*B*T)*FPERDP*FPERDP
      R=-ALOG(0.1E-3)
      IMID=SQRT(R)/SQRT(Q)+1.0
      NA=2*IMID-1
      S=SQRT(Q/3.1415)
      A(IMID)=S
      MID=IMID-1
      DO 1 I=1,MID
      J=IMID+I
      K=IMID-I
      X=I
      Y=EXP(-X*X*Q)*S
      A(J)=Y
    1 A(K)=Y
      RETURN
      END
```

```
      SUBROUTINE SMTHER(NSM)
      COMMON /A/DATA(1280),ND,SRMS
      DIMENSION S(99),T(200)
      DATA KSM/0/
    7 IF(NSM.EQ.KSM)GOTO8
      K=(NSM-1)/2
      R=NSM
      K3=NSM+1
      A2=K*(K+1)*(2*K+1)/6
      A=3*K*(K+1)-1
      XNORM=R*A-10.*A2
      DO  1  I=1,K
      R=I
    1 S(I)=(A-5.*R*R)/XNORM
      SO=A/XNORM
      K1=K+1
    8 SK=0.
      DO  2  I=1,NSM
    2 T(I)=DATA(I)
      I=K
    3 I=I+1
      T(NSM+1)=DATA(I+K1)
      ST=SO*T(K1)
      DO  5  L=1,K
    5 ST=ST+S(L)*(T(K1+L)+T(K1-L) )
      DO  6  L=1,NSM
    6 T(L)=T(L+1)
      SK=SK+(DATA(I)-ST)**2
      DATA(I)=ST
      IF(I+K1.LT.ND)  GO TO 3
      Z=I-K
      SRMS=SQRT(SK/Z)
      KSM=NSM
      RETURN
      END
```

```
      SUBROUTINE BBLOCK(X,NX)
      DIMENSION X(1),S(4),T(4)
      DATA S,T/3*0.0,0.5,0.3,-0.3,2*0.0/
      CALL PLOT(0.0,0.0,3)
      DO 1 I=1,4
    1 CALL PLOT(S(I),T(I),2)
      CALL PLOT(0.0,X(1)*4.0,3)
      DO 2 I=2,NX
    2 CALL PLOT(FLOAT(I)/256.0,X(I)*4.0,2)
      CALL PLOT(5.0,0.0,3)
      DO 3 I=1,4
    3 CALL PLOT(5.0-S(I),T(I),2)
      RETURN
      END
```

```
      SUBROUTINE BBPLOT(PPN)
C-----BBPLOT ASSUMES THE DATA "X" HAS THE RANGE 0.0 TO 1.0.
      COMMON  /A/X(1280),NX,SRMS
      DIMENSION F(31),G(31),LABEL(20)
C-----F AND G CONTAIN INFORMATION USED TO PRODUCE SCALES---
C-----LABEL WILL BE USED TO LABEL THE PLOT
      DATA F,G/0.,.2,2*0.,.1,2*0.,.1,2*0.,.1,2*0.,.1,2*0.,
     1   .1,2*0.,.1,2*0.,.1,2*0.,.1,2*0.,.1,5*0.,3*.1,3*.2,
     2   3*.3,3*.4,3*.5,3*.6,3*.7,3*.8,3*.9,1.0/
      CALL PLOT(0.0,8.0*X(1),3)
      DO  1  I=2,NX
    1 CALL PLOT(FLOAT(I)/PPN,8.0*X(I),2)
      CALL PLOT(0.0,0.0,3)
      IPPN=PPN
      K=(NX-1)/IPPN+1
      DO  2  J=1,K
      B=J-1
      DO  2  L=1,31
    2 CALL PLOT(B+G(L),-F(L),2)
      XL=B+1.0
      CALL PLOT(XL,8.0,2)
      DO  3  J=1,K
      B=J-1
      B=XL-B
      DO  3 L=1,31
    3 CALL PLOT(B-G(L),8.0+F(L),2)
      CALL PLOT(0.0,0.0,2)
      READ(5,100)  N
      READ(5,101)  LABEL
  100 FORMAT(I5)
  101 FORMAT(20A4)
      SL=.14*FLOAT(N)
      T=(XL-SL)/2.0
      CALL SYMBOL(T,-.5,.14,LABEL,0.0,N)
      T=(XL-2.94)/2.0
      CALL NUMBER(T,-1.0,.14,PPN,0.0,-1)
      CALL SYMBOL(999.0,-1.0,.14,' POINTS PER INCH',0.0,16)
      CALL PLOT(XL+1.0,0.0,-3)
C-----MOVE PEN AND ORIGIN 1 INCH BEYOND LEFT LIMIT OF PLOT.
      RETURN
      END
```

```
      SUBROUTINE DCCNVC
      COMMON IX,RMSD,DMAX,IDMAX,NOUTSD/A/RES(1280),NS,SRMS
      COMMON /B/SPEC(1280),RESP(150),NF
      READ(5,100)   LOOPC,NSMO,LOOP1,NSM1,ALPHA1,LOOP2,
     2    ALPHA2,LOOP3,ALPHA3
  100 FORMAT(4I5,F5.2,2(I5,F5.2))
      WRITE(6,217)
  217 FORMAT(1H1,20X,18HDECCNVOLUTION DATA)
      WRITE(6,199)  LOOPC,NSMO,LOOP1,NSM1,ALPHA1,LOOP2,
     1    ALPHA2,LOOP3,ALPHA3
  199 FORMAT(5X6HLOOPO=I5/6X5HNSMO=I5/5X6HLOOP1=I5/
     1    6X5HNSM1=I5/4X7HALPHA1=F5.2/5X6HLOOP2=I5/
     2    4X7HALPHA2=F5.2/5X6HLOOP3=I5/4X7HALPHA3=F5.2///)
      X=0.
      DO  1  I=1,NF
      IF(RESP(I).LT.X) GO TO 1
      X=RESP(I)
      IX=I
    1 CONTINUE
    3 IF(LOOPC.EQ.0)  GO TO 5
      DO  4  I=1,LOOPO
      CALL SMTHER(NSMO)
    4 WRITE(6,200)  I,SRMS
  200 FORMAT(/5X7HILOOPO=I5,5X,22HRMS SMOOTH CORRECTION=,
     1       E12.5)
    5 DO  50  I=1,NS
   50 SPEC(I)=RES(I)
      IF(LOOP1.EQ.0)  GO TO 7
      DO  6  I=1,LOOP1
      CALL DCONER(ALPHA1,7)
      WRITE(6,201)  I,RMSD,DMAX,IDMAX,NOUTSD
  201 FORMAT(/4X7HILOOP1=I5,5X14HRMS DEVIATION=E12.5,
     1    5X18HMAXIMUM DEVIATION=E12.5,9H AT POINTI5,
     2    5X27HNUMBER OF POINTS >1 OR <0 =I5)
      CALL SMTHER(NSM1)
    6 WRITE(6,202)  I,SRMS
  202 FORMAT(/5X7HILOOP1=I5,5X,22HRMS SMOOTH CORRECTION=,
     1       E12.5)
    7 IF(LOOP2.EQ.0)  GO TO 9
      DO  8  I=1,LOOP2
      CALL DCONER(ALPHA2,4)
    8 WRITE(6,203)  I,RMSD,DMAX,IDMAX,NOUTSD
  203 FORMAT(/4X7HILOOP2=I5,5X14HRMS DEVIATION=E12.5,
     1    5X18HMAXIMUM DEVIATION=E12.5,9H AT POINTI5,
     2    5X27HNUMBER OF POINTS >1 OR <0 =I5)
    9 IF(LOOP3.EQ.0)  GO TO 11
      DO  10  I=1,LOOP3
      CALL DCONER(ALPHA3,1)
   10 WRITE(6,204)  I,RMSD,DMAX,IDMAX,NOUTSD
  204 FORMAT(/4X7HILOOP3=I5,5X14HRMS DEVIATION=E12.5,
     1    5X18HMAXIMUM DEVIATION=E12.5,9H AT POINTI5,
```

```
  2     5X27HNUMBER OF POINTS >1 OR <0 =15)
11 RETURN
   END
```

```
      SUBROUTINE DCONER(PARAM,KDELT)
      COMMON IX,RMSD,DMAX,IDMAX,NOUTSD/A/RES(1280),NS,SRMS
      COMMON  /B/SPEC(1280),RESP(150),NF
      RMSD=0.
      DMAX=0.
      NOUTSD=0
      M=NF-KDELT
      I=IX-KDELT
   12 I=I+KDELT
      M=M+KDELT
      PROX=0.
      DO  3  J=1,NF
      JJ=J+I-IX
    3 PROX=PROX+RESP(J)*RES(JJ)
      D=SPEC(I)-PROX
      IF(ABS(D).LE.ABS(DMAX))  GO TO 77
      DMAX=D
      IDMAX=I
   77 RMSD=RMSD+D*D
      D=D*PARAM
      RES(I)=RES(I)+D
      IF(KDELT.EQ.1)  GO TO 78
      KK=KDELT-1
      DO  6  J=1,KK
      Q=FLOAT(KDELT-J)/FLOAT(KDELT)*D
      RES(I+J)=RES(I+J)+Q
    6 RES(I-J)=RES(I-J)+Q
   78 IF(M+KDELT.LE.NS)  GO TO 12
      Z=(I-IX)/KDELT+1
      RMSD=SQRT(RMSD/Z)
      DO  7  J=IX,I
      IF(RES(J)*RES(J).GT.RES(J))  NOUTSD=NOUTSD+1
    7 CONTINUE
      RETURN
      END
```

APPENDIX C

The program for the deconvolution of the H_2 lines follows essentially the same procedure as the program for determining the Response function described in Appendix B. The same subroutines are used with the exception of GAUSSIAN and therefore only the main program is listed. Within the main program the base line is read, averaged and subtracted from each line used. After converting to a fractional absorption, using the value of the 100 percent absorbing point and the polarizer efficiency, the data is aligned and averaged as before. The response function is then read from cards produced by the response function program and the line is deconvoluted. The data is then converted to an absorption coefficient curve using equation (57) given in Section 2.5. The width at half maximum of this curve is measured in units of data points by the portion of the program which locates the 50 percent peak absorption points for the alignment of the data. The total area under the curve is data point units is also measured in 100 data point intervals and totaled.

```
C   THE PROGRAM TAKES UP TO 10 RUNS OF EACH LINE FROM
C   MAGNETIC TAPE AND AVERAGES THEM AND DECONVOLUTES THE
C   RESPONSE FUNCTION FROM THE AVERAGE.  FOR THE FIRST
C   LINE, TWO SPECIFIED BLOCKS ARE READ AND AVERAGED
C   FOR THE BASE LINE.  THE INPUT DATA IS READ AND SMOOTHED
C   ONCE.  THE BASE LINE IS SUBTRACTED AND THE DATA IS
C   CONVERTED TO A FRACTIONAL ABSORBANCE.  SUCESSIVE DATA
C   IS TREATED IN THE SAME WAY AND THE LINES ARE ALIGNED,
C   AVERAGED,AND DECONVOLUTED.  THE FINAL PROFILE IS
C   CONVERTED TO AN ABSORPTION COEFFICIENT CURVE.  THE
C   HALF WIDTH AND THE AREA OF THE CURVE IS MEASURED BY
C   THE PROGRAM.  CALCOMP PLOTS ARE MADE AT INTERMEDIATE
C   STEPS TO CHECK THE PROGRESS OF THE PROGRAM.
C   DATA CARDS AS FOLLOWS:
C   CARD 1, LABEL FOR RUN ANYWHERE ON CARD
C   CARD 2, # OF LINES TO AVERAGE IN 5, # OF POINTS IN
C           RESPONSE FUNCTION IN 10
C   CARD 3, IO THE 100% ABSORBING POINT IN 15, EFF THE
C           POLARIZER EFFICIENCY IN 30
C   CARD 4, NUMBER OF BLOCKS READ FOR FIRST BASE BLOCK
C           (=1) IN 5, STARTING BLOCK IN 10
C   CARD 5, SAME AS 3 FOR SECOND BASE BLOCK
C   CARD 6, # OF BLOCKS READ FOR LINE(=10) IN 5, STARTING
C           BLOCK IN 10
C   NEXT CARD, REPEAT 3 TO 5 FOR EACH LINE
C   NEXT CARD, # OF CHARACTERS IN FIRST BBPLOT LABEL IN 5
C   NEXT CARD, LABEL FOR ABOVE STARTING IN ZERO
C   NEXT CARDS, RESPONSE FUNCTION
C   NEXT CARD, DECONVOLUTION DATA AS FOLLOWS:
C      # OF PASSES IN LOOP 0 IN 5, SMOOTHING INTERVAL IN 10
C      EXPRESSED IN DATA POINTS(ODD # ONLY), # OF PASSES IN
C      LOOP 1 IN 15, SMOOTHING INTERVAL IN 20, DECONVOLUTION
C      PARAMETER IN 25, # OF PASSES IN LOOP 2 IN 30,
C      DECONVOLUTION PARAMETER IN 35, # OF PASSES IN LOOP
C      3 IN 40, DECONVOLUTION PARAMETER IN 45.
C   NEXT CARD, # OF CHARACTERS IN SECOND BBPLOT LABEL IN 5
C   NEXT CARD, LABEL FOR ABOVE STARTING IN ZERO
C   NEXT CARD, # OF CHARACTERS IN THIRD BBPLOT LABEL IN 5
C   NEXT CARD, LABEL FOR ABOVE STARTING IN ZERO
      REAL*4 IO
      COMMON /A/X(2560),J,SRMS/B/Y(2560),RESP(536),NF
      DIMENSION IBUF(664),D(2560),NAME(20),AREA(20)
      INTEGER IMID(10)
      CALL PLOTS(IBUF,664,80.0,'BOYD#','REMOTE2#')
      CALL PLOT(0.0,0.5,-3)
      READ(5,723)NAME
  723 FORMAT(20A4)
      WRITE(6,724)NAME
  724 FORMAT(1H1,20A4)
  900 FORMAT(1H ,10F12.5)
  132 FORMAT(2I5)
```

```
  618 FORMAT(1HC,15X,3HNB=,I3,10X,4HNB1=,I3)
  725 FORMAT(1H0,25H**************************)
      J=2560
      DO 800 I=1,J
  800 C(I)=0.0
      READ(5,132)ITEST,NF
      READ(5,133)IO,EFF
  133 FORMAT(2F15.0)
      WRITE(6,502)IO,EFF
  502 FORMAT(1HC,20X,3HIC=,F10.6,5X,4HEFF=,F10.6)
      WRITE(6,725)
C  READ BASE LINE FROM TWO SEPARATE BLOCKS
      IAM=1
  714 IGO=1
      BASE=0.0
  245 READ(5,132)NB,NB1
      WRITE(6,618)NB,NB1
      CALL READER(NB,NB1,0,&15)
      DO 712 I=1,256
  712 BASE=BASE+X(I)
      IF(IGO.EQ.2)GO TO 247
      IGO=2
      GO TO 245
  247 BASE=BASE/(512.0*1024.0)
      WRITE(6,838)BASE
  838 FORMAT(1H0,20X,5HBASE=,F10.6)
C  READ INPUT DATA
      READ(5,132)NB,NB1
      J=NB*256
      WRITE(6,619)NB,NB1
  619 FORMAT(1HC,15X,3HNB=,I3,10X,4HNB1=,I3)
      WRITE(6,701)
  701 FORMAT(1H0,17HINPUT INTENSITIES)
      CALL READER(NB,NB1,0,&15)
      DO 938 I=1,J
  938 X(I)=X(I)/0.1024E+04
C  PLOT RAW DATA
      CALL BBLOCK(X,J)
      CALL PLOT(6.0,0.0,-3)
C  SMOOTH INPUT DATA
      CALL SMTHER(199)
C  SUBTRACT BASE LINE AND CONVERT TO FRACTIONAL ABSORPTION
      RIC=(IO-BASE)*EFF
  870 DO 788 I=1,J
  788 X(I)=(X(I)-BASE)/RIC
C  WRITE INPUT INTENSITIES
  901 WRITE(6,900)(X(I),I=1,J,20)
C  PLOT SMOOTHED DATA
      CALL BBLOCK(X,J)
      CALL PLOT(6.0,0.0,-3)
C  FIND MID POINT
```

```
  884 GREAT=0.0
      DO 718 I=1,J
      IF(X(I).LT.GREAT)GO TO 718
      GREAT=X(I)
      IGREAT=I
  718 CONTINUE
      HALF=GREAT/2.0
      I=IGREAT
  768 I=I+1
      IF(X(I)-HALF) 770,770,768
  770 IHALF2=I
      I=IGREAT
  769 I=I-1
      IF(X(I)-HALF) 771,771,769
  771 IHALF1=I
      IF(IGO.EQ.3)GO TO 885
      IMID(IAM)=(IHALF1+IHALF2)/2
      WRITE(6,772)IGREAT,IHALF1,IHALF2,IMID(IAM)
  772 FORMAT(1H0,7HIGREAT=,I5,10X,7HIHALF1=,I5,10X,
     1      7HIHALF2=,I7,10X,5HIMID=I7)
      WRITE(6,725)
      IREDO=IMID(1)-IMID(IAM)
      IF(IREDO) 70,71,72
   70 DO 969 I=1,J
      K=I-IREDO
      IF(K.LT.1.OR.K.GT.J)GO TO 697
      X(I)=X(K)
      GO TO 969
  697 X(I)=0.0E0
  969 CONTINUE
      GO TO 71
   72 DO 698 L=1,J
      I=J-L+1
      K=I-IREDO
      IF(K.LT.1.OR.K.GT.J)GO TO 699
      X(I)=X(K)
      GO TO 698
  699 X(I)=0.0E0
  698 CONTINUE
C   PLOT ALIGNED DATA
   71 CALL BBLOCK(X,J)
      CALL PLOT(-12.0,0.5,-3)
C   ADD LINE PROFILES
      DO 970 I=1,J
  970 D(I)=D(I)+X(I)
      IF(IAM.EQ.ITEST)GO TO 713
      IAM=IAM+1
C   RESTART FOR NEXT LINE
      GO TO 714
C   AVERAGE LINE PROFILES
  713 CALL PLOT(18.0,-FLOAT(ITEST-2)*0.5,-3)
```

```
      C=ITEST
      DO 971 I=1,J
  971 X(I)=D(I)/C
      WRITE(6,782)
  782 FORMAT(1HO,21HAVERAGED LINE PROFILE)
      WRITE(6,900)(X(I),I=1,J,20)
C  PLOT AVERAGE LINE PROFILE
      CALL BBPLOT(512.0)
C  READ RESPONSE FUNCTION
      READ(5,139)(RESP(I),I=1,NF)
  139 FORMAT(8E10.4)
      WRITE(6,726)
  726 FORMAT(1HO,17HRESPONSE FUNCTION)
      WRITE(6,900)(RESP(I),I=1,NF,10)
C  DECONVOLUTE LINE PROFILE
      CALL DCONVO
C  PLOT DECONVOLUTED LINE PROFILE
      CALL BBPLOT(512.0)
      WRITE(6,780)
  780 FORMAT(1H1,25HDECONVOLUTED LINE PROFILE)
      WRITE(6,900)(X(I),I=1,J,20)
C  CALCULATE ABSORPTION COEFFICIENT
  871 DO 110 I=1,J
  110 X(I)=-(ALOG(1.0-X(I)))
      WRITE(6,505)
  505 FORMAT(1H1,22HABSORPTION COEFFICIENT)
  102 WRITE(6,900)(X(I),I=1,J)
C  CALCULATE AREA
      DO 201 M=1,20
  201 AREA(M)=0.0
      N=20
      M=1
      K=1
      L=128
      WRITE(6,372)
  372 FORMAT(1H1,39HCALCULATED AREAS IN HALF BLOCK SEGMENTS)
  200 DO 300 I=K,L
  300 AREA(M)=AREA(M)+X(I)
      WRITE(6,302)M,AREA(M)
  302 FORMAT(1H ,5HAREA(,I2,2H)=,F15.5)
      M=M+1
      K=L
      L=K+128
      IF(M.EQ.N+1)GO TO 202
      GO TO 200
  202 BIGA=0.0
      DO 400 M=1,20
  400 BIGA=BIGA+AREA(M)
      WRITE(6,401)BIGA
  401 FORMAT(1HO,5X,11HTOTAL AREA=,F15.5)
C  FIND HALF WIDTH
```

```
      IGO=3
      GO TO 884
  885 IDIFF=IHALF2-IHALF1
      WRITE(6,932)IGREAT,IHALF1,IHALF2
  932 FORMAT(1H1,7HIGREAT=,I5,10X,7HIHALF1=,I5,10X,
     1      7HIHALF2=,I5)
      WRITE(6,773)IDIFF
  773 FORMAT(1H0,26HHALF WIDTH IN DATA POINTS=,I5)
      IF(GREAT.LT.1.0)GO TO 764
      DO 719 I=1,J
  719 X(I)=X(I)/GREAT
  764 WRITE(6,720)
  720 FORMAT(1H0,20HRESCALED ABS. COEFF.)
      WRITE(6,900)(X(I),I=1,J,20)
C  PLOT ABSORPTION COEFFICIENT
      CALL BBPLOT(512.0)
      CALL PLOT(0.0,0.0,999)
   15 CALL EXIT
      END
```

VITA

William Joseph Boyd III was born in [redacted].

The majority of his preliminary education was received in Dyersburg, Tennessee, where he graduated from Dyersburg High School in 1961. He attended Southwestern at Memphis for two years and after transferring to The University of Tennessee received a Bachelor of Science degree there in 1965. He received his Master of Science degree in 1969 and his Doctor of Philosophy degree in 1974 from The University of Tennessee both with a major in Physics. Three summers were taken from his graduate studies to work in the Fiber Surface Research Section at E. I. DuPont de Nemours in Kinston, North Carolina. After graduation he accepted a research position at the Pioneering Research Laboratory of E. I. DuPont de Nemours in Wilmington, Delaware.

He is married to the former Jeanne Lavonne Humphreys of Memphis, Tennessee.